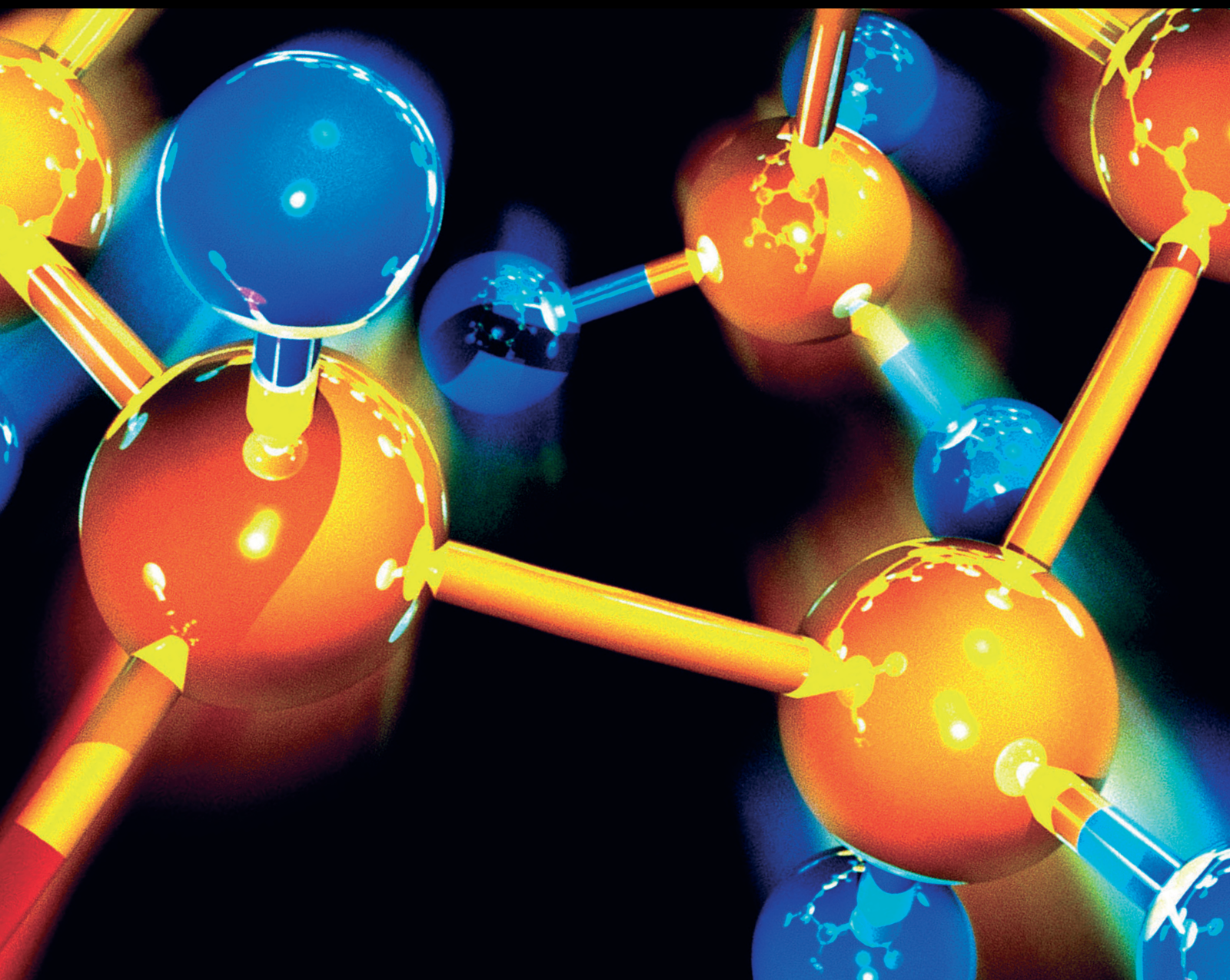# Flotation Colloid Chemistry: Inter-particle, Inter-bubble and Bubble-particle Interactions

Lead Guest Editor: Yaowen Xing
Guest Editors: Jinhong Zhang, Xiahui Gui, and Lei Pan

# Flotation Colloid Chemistry: Inter-particle, Inter-bubble and Bubble-particle Interactions

# Flotation Colloid Chemistry: Inter-particle, Inter-bubble and Bubble-particle Interactions

Lead Guest Editor: Yaowen Xing
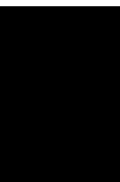Guest Editors: Jinhong Zhang, Xiahui Gui, and Lei Pan

# Chief Editor

Kaustubha Mohanty, India

# Associate Editors

Mohammad Al-Ghouti, Qatar
Tingyue Gu ⬤, USA
Teodorico C. Ramalho ⬤, Brazil
Artur M. S. Silva ⬤, Portugal

# Contents

*Research Article*

# The Interaction Force between Scheelite and Scheelite/Fluorite/Calcite Measured Using Atomic Force Microscopy

**Junyan Yang** [ID],[1,2,3,4] **Shen Qi** [ID],[1,3,4] **Bo Song** [ID],[2] **Qi Zheng** [ID],[1,3,4] **Xiaokui Che** [ID],[1,3,4] **and Lijun Wang** [ID][1,3,4]

[1]*National Engineering Laboratory of Biohydrometallurgy, GRINM Group Corp., Ltd., Beijing 100088, China*
[2]*School of Metallurgical and Ecological Engineering, University of Science and Technology Beijing, 100083 Beijing, China*
[3]*GRINM Resources and Environment Tech. Co., Ltd., 100088 Beijing, China*
[4]*General Research Institute for Nonferrous Metal, Beijing 100088, China*

Correspondence should be addressed to Junyan Yang; yang8865139@163.com and Lijun Wang; gold@grinm.com

The mechanism of the formation of the hydrophobic agglomerate in fine scheelite flotation was studied using zeta potential measurement, contact angle measurement, optical microscope measurement, and atomic force microscopy (AFM) colloid probe technology. Zeta potential measurement results confirmed the adsorption of sodium oleate on scheelite, fluorite, and calcite surface and surface potential difference at different pH values of ultrapure water. Contact angle measurement results confirmed the surface of nature scheelite, fluorite, and calcite was hydrophilic, and the surface after thread by sodium oleate solution was hydrophobic. The optical microscope measurement results confirmed the agglomerates could really form in ultrapure water of pH 8 or 10 and in 1 mM sodium oleate solution of pH 10. The agglomerations were empty and not tight in ultrapure water. On the contrary, the hydrophobic agglomerations were larger and denser after treated with sodium oleate solution than that of in ultrapure water. According to the AFM experiment results, the interaction forces on hydrophilic scheelite-scheelite and scheelite-fluorite were repulsive at pH 5.6 and attractive at pH 8 or 10. However, the interaction forces on hydrophilic scheelite-calcite were attractive at pH 5.6, 8 or 10. The interaction forces on hydrophobic scheelite-scheelite, scheelite-fluorite, and scheelite-calcite were attractive strongly due to the existence of hydrophobic force. The measurement results of the interaction forces were in good agreement with the changes of zeta potential and contact angle at different conditions. The combined results could be beneficial to understand the interaction force in fine scheelite flotation.

## 1. Introduction

Froth flotation has been considered as one of the most widely used methods for the separation of minerals [1]. It is the most efficient when the mineral particle sizes are between $10\,\mu$m and $100\,\mu$m. However, the flotation of fine mineral particles of less than $10\,\mu$m is still a technical challenge [2–4]. Scheelite is a kind of easily slimed mineral. In the grinding process of scheelite, a large number of fine slimes can be produced, which seriously affects the flotation efficiency of scheelite [1]; this is because many calcium-bearing minerals (fluorite and calcite) exhibit similar surface properties to scheelite. In order to solve this problem, many works

including shear flocculation flotation [5], carrier flotation [6], selective flocculation flotation [7], and density functional theory calculation [8] had been researched by a large number of researchers, which had achieved remarkable achievements. Flotation agents can improve effectively the separation effect of calcium-bearing minerals in flotation processing. The Pb-BHA complexes were used in flotation separate scheelite from fluorite and calcite [9, 10], increasing the recovery of scheelite. The rheological control of the flotation pulp by using garnet makes a significant improvement in fine scheelite flotation [11]. There exists strong correlation among the flotation rate, pulp rheology, froth, and floc morphology in the cleaning flotation, so the

formation of aggregates is very important for fine scheelite flotation.

The formation mechanism of hydrophobic agglomerates had been widely studied. The hydrophobic association between collector molecules and mineral surface and the hydrophobic interaction energy between mineral particles were the reasons for the formation of hydrophobic agglomerates [5, 12], and the capillary condensation of collector and the bridge chain were conducive to the formation of agglomerations [13]. The DLVO and EDLVO theory were also used to describe the agglomeration and dispersion of fine particles in solution. The phenomenon of adsorption, collision, and adhesion on the mineral's surface after adding collector could not be described very well by DLVO theory [14], but the EDLVO theory explained that hydrophobic force [15] was the original cause of agglomeration of mineral particles [16].

The formation mechanism of hydrophobic agglomerates was explained from the aspects of adsorption, colloidal interface, and theoretical calculation. However, the mechanism was still unclear at the micro-nano scale because of the complexity of experimental verification. Surface and interface forces (van der Waals force, electrical double layer force, hydration force, hydrophobic force, etc.) are significant for understanding the interaction between particles in the flotation system [17, 18]. Atomic force microscopy (AFM), as a surface and interface force measuring technology [19, 20], is used widely at the micro-nano scale. The hydrophilic/hydrophobic force had been studied by researchers since the AFM was developed [21–23], especially with the colloid probe technology [24, 25]. Ducker et al. [26] directly measured the colloidal force between silica microspheres and substrate in sodium chloride solution using AFM firstly; meanwhile, Butt [27] measured the colloidal force in different concentrations of potassium chloride and magnesium chloride electrolyte solutions with colloidal probes. All the microspheres used in the above studies were surface smooth, spherical particles of defined radius, which is conducive to the direct measurement and quantitative analysis of force curves [19]. However, the actual shape of mineral particles cannot be spherical and the surface is rough, so it is difficult to analyse quantitatively the interaction force between actual particle and surface. Gui et al. [25] studied the interaction between coal and coal, kaolinite and kaolinite, and coal and kaolinite in deionized aqueous solution by colloidal probe technology. The repulsion between kaolinite and kaolinite made it difficult for fine kaolinite to sedimentation at natural pH, which was harmful in coal flotation. The interaction between fluorite particles and scheelite surface was measured at the condition of different pH values and various concentration of calcium ion [28]. The adhesion between fluorite and scheelite surface was enhanced remarkably after adding calcium ion, while the adhesion between fluorite and scheelite surface was reduced significantly by using sodium silicate as inhibitor.

In this study, the interaction forces between scheelite particle and scheelite surface, scheelite particle and fluorite surface, and scheelite particle and calcite surface in ultrapure aqueous solution and sodium oleate solution system were studied by using the AFM colloidal probe technique. However, it must be pointed out that the irregularity of the scheelite particles and the nano-heterogeneity [29] of the mineral surface make it difficult to measure the surface force quantitatively. The force curve obtained in the experiment is also difficult to fit quantitatively with DLVO theory and EDLVO theory, but it can still be described qualitatively [25]. The experimental results contribute to understanding the formation mechanism of agglomerations in the flotation process of fine scheelite and provide guidance for the separation of scheelite from calcite and fluorite.

## 2. Materials and Methods

*2.1. Minerals and Reagents.* Pure minerals of scheelite, fluorite, and calcite were bought from Taobao; the three minerals samples were crushed by a hand hammer, and several pieces were cut to obtain cuboid of 1 cm length, 0.8 cm width, and 0.5 cm high for contact angle and AFM measurements. The rest of the scheelite sample was further purified using an optical microscope and then was milled into 38–75 $\mu$m powder particle using an agate mortar. Chemical analysis showed that the purity of calcite, fluorite, and calcite was 94.56%, 98.17%, and 98.29%, respectively. X-ray diffraction (XRD) analysis of the scheelite power revealed that the mineral was pure scheelite (Figure 1). The collector sodium oleate (analytical grade, Sinopharm Chemical Reagent Co., Ltd) was used for soaking three minerals. NaOH (analytical grade, Sinopharm Chemical Reagent Co., Ltd) was used to adjust the pH of the solutions; ultrapure water was used in the all experiments (resistivity of 18.2 M$\Omega$·cm; conductivity of 0.054 $\mu$s).

*2.2. Zeta Potential Measurements.* Zeta potential measurements were carried out on dilute dispersions of three minerals of particle size less than 5 $\mu$m using a Malvern Zeta sizer ZS90. Steps are as follows: weigh three minerals 0.005 g into a beaker and then add 50 ml of ultrapure water/1 mM sodium oleate solution. Suspensions of the minerals were dispersed by magnetic stirring for 10 min at room temperature; after 30 min, the specific pH value was then adjusted by HCl or NaOH solution; the pH was measured and liquid supernatant was used for zeta potential measurement. Repeat determination at least three times for each sample.

*2.3. Preparation of Surface.* The sample is usually a basal plane with a planar, nano-level smooth surface in the AFM experiment [30]. Surface of natural minerals are generally rough, so scheelite, fluorite, and calcite were lapped using 800 mesh, 1200 mesh, 1500 mesh sandpaper in turn, polished with aluminium oxide powder (0.02 $\mu$m) using a metallographic polishing machine (MP-1), and then washed with ultrapure water five times and dried with high-pure N$_2$ (Figure 2). The Scanasyst-air probe (elastic coefficient 0.4 N/m) was used for roughness measurement of the three mineral substrates by atomic force microscopy (Dimension FastScan Bruker, Germany). The roughness of scheelite, fluorite, and calcite substrates was 11.9 nm, 14.3 nm, and
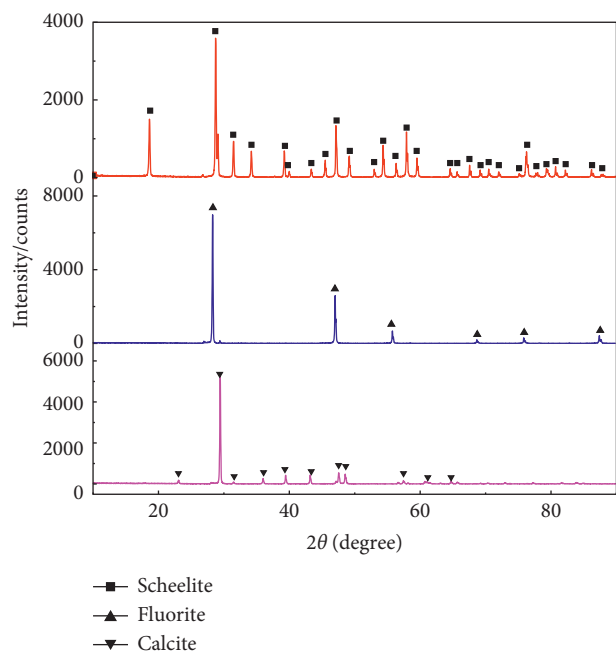
FIGURE 1: XRD patterns of powder scheelite, fluorite, and calcite for the AFM experiments and zeta potential measurements.
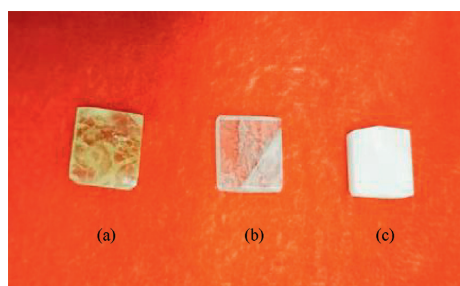


FIGURE 2: The surface of minerals: (a) scheelite, (b) fluorite, and (c) calcite.

12.3 nm in turn. The three mineral substrates were soaked in ultrapure water (pH = 5.6, 8, 10) and 0.1 mM/1 mM sodium oleate solution of pH 10 for 30 minutes, which were used for AFM experiments and contact angle measurements.

*2.4. Contact Angle Measurements.* The sessile drop method was carried out using a dynamic contact angle meter (DSA 100, Krüss GmbH, Germany) between ultrapure water drop (pH 5.6) and mineral substrates. Three mineral substrates prepared in section 2.3 were used for contact angle measurements. The average angle of three different area measurements was recorded as the final contact angle. This method is consistent with the literature [31].

*2.5. Optical Microscope Measurements.* Scheelite-scheelite, scheelite-fluorite, and scheelite-calcite powders (1 g) were put into a beaker and then 50 ml of ultrapure water was added. After 10 minutes of stirring using a magnetic stirrer, a drop was sucked onto the slide and a metallographic microscope (9XB-PC, Shanghai China) was used to see if the agglomerates had formed.

*2.6. AFM Experiments and Tip Modification.* Surface force measurements on scheelite particle and three mineral substrates (scheelite, fluorite, and calcite) were carried out in aqueous solutions at various pH values (5.6, 8, and 10) using a Multimode 8 AFM instrument (Bruker, Germany) in contact mode. The N-type silicon AFM probe (CSC37/Tipless/No Al, MikroMasch, Estonia) was used to prepare the scheelite colloid probe for interaction force measurements. Scheelite powders of 38–75 $\mu$m were selected evenly dispersed on the silicon chip, and then the sphere particle was selected under the light microscope; after that, the epoxy resin AB blue was coated around the target particle. The probe was moved over the target particle, put down slowly until contacting with epoxy resin AB glue, and lifted quickly. Then the target particle was glued by the tip of probe within 10 min. The scheelite colloid probe is shown in Figure 3. In the schematic diagram of AFM (Figure 4), the sample was scanned by a scheelite colloid probe, which was mounted to a cantilever spring. The forces between the scheelite colloid probe and the samples were measured by monitoring the deflection of the cantilever. The cantilever will swing after the tip touches the sample, the laser shines on the end of the cantilever, and the position of the reflected light will also change, which will cause the offset. The photodetector records offset and converts them into electrical signals, which were converted to force-versus-distance curves. Before the force curve measurement, the mineral substrate was put into the sample chamber. One or two drops of ultrapure water were dropped on the substrate, and the scheelite colloidal probe was moved into the water drop. The cantilever elastic coefficient was corrected by the Sader method, and the elastic coefficient was 0.3060–0.3794 N/m. After the setpoint, ramp size (1 $\mu$m), and ramp rate (0.01 Hz) were set, the force curve measurements was started, and four different points were selected for each condition. The force curve was analysed using the offline software NanoScope analysis 1.8.

AFM force-displacement curves are shown in Figure 5. At position 1, the tip is far away from the sample, and there is no interaction force between the tip and the sample. As the tip moves downward, the tip is attracted to the surface of the sample at position 2; this phenomenon is called "jump-in" in the experiment. As tip continued down, the cantilever begins to change deformation, and then the tip began to press the surface of the sample, as shown at position 3, and the force was repulsive. When the deformation of the cantilever reaches the set limit, the tip starts to go up at position 4. Due to the adhesive effect of the sample on the tip, the tip will not rise synchronously with the rise of the cantilever. Until the detachment force generated by the bending deformation of the cantilever and the adhesion force reach equilibrium, the tip will be separated from the sample at position 5. This phenomenon is called "jump-out" in the experiment. There is no interaction force between tip and surface along with the separation distance increases.
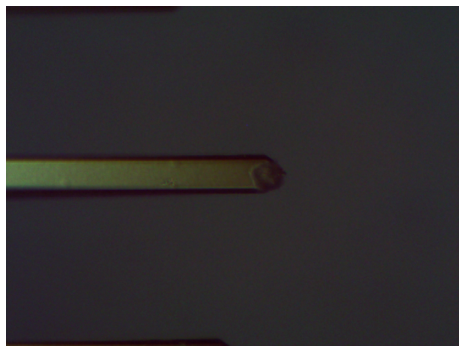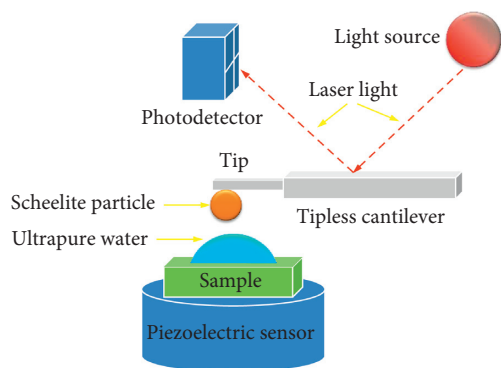
FIGURE 3: The photo of scheelite particle probe.



FIGURE 4: Schematic diagram of AFM.

## 3. Results and Discussion

*3.1. Zeta Potential Measurements.* Figure 6 shows the zeta potentials of scheelite, fluorite, and calcite at different pH values in aqueous solutions (Figure 6(a)) and 1 mM sodium oleate solution (Figure 6(b)). The zeta potentials of scheelite were negatively charged from pH 2 to pH 12 and −30.87 mv at pH 9. An isoelectric point (IEP) of scheelite was not observed, which was consistent with the literature [32]. The isoelectric point (IEP) of fluorite and calcite, respectively, was about at pH $8.4 \pm 0.1$ and pH $9.4 \pm 0.1$, which was also consistent with the previous reports [33]. When the three minerals were treated with 1 mM sodium oleate solution, the zeta potentials become more negative at various pH values; it is probably due to the adsorption of the sodium oleate on the surface of minerals [34, 35]. To contrast the adsorption effect of three minerals surface, contract angles were measured in the next section.

*3.2. Contact Angle Measurements.* As shown in Figure 7, natural minerals of scheelite, fluorite, and calcite had strong hydrophilicity [36]; contact angles were, respectively, scheelite—27.30° (Figure 7(a)), fluorite—36.90° (Figure 7(c)), and calcite—38.80° (Figure 7(e)), so the natural floatability of the three minerals were calcite > fluorite > scheelite. Contact angles suddenly increased significantly to scheelite—93.60° (Figure 7(b)), fluorite—91.00° (Figure 7(d)), and calcite—80.90° (Figure 7(f)). Therefore,

the hydrophobicity of three minerals obviously increased, and scheelite had best floatability than other minerals. The adsorption of sodium oleate on the mineral surface was also confirmed, which was in agreement with zeta potential measurement results .

*3.3. Optical Microscope Measurements.* As shown in Figures 8–10, scheelite and scheelite, scheelite and fluorite, and scheelite and calcite particles could attract each other to form agglomeration in the ultrapure water solution of pH 8 and 10, but the agglomerations were empty and not tight. As shown in Figure 11, the agglomerations were larger and denser when the particles of scheelite, fluorite, and calcite were soaked by sodium oleate.

*3.4. AFM Experiments.*
Derjaguin–Landau–Verwey–Overbeek (DLVO) theory [37, 38] was used to predict the dispersion and aggregation of colloidal particles in colloidal chemistry. DLVO forces are composed of van der Waals force ($F_{vdm}$) and double electrical layer force ($F_{edl}$), and the total interaction forces are the sum of two forces. Therefore, the total interaction forces are given by equation (1). According to the DLVO theory, the stability of the dispersion system depends on the relative relationship between the van der Waals force and the electrical double layer force. The van der Waals attraction force occupies the dominant role when the separation distance is long. As the separation distance decreases, the repulsive force of the electrical double layer increases gradually to prevent the particles from attracting each other. In the flotation process, the hydrophobic force overcomes the repulsion of the electrical double layer after the collector is added. Usually, when the distance between particles is less than 20 nm [39], the hydrophobic particles attract each other and form agglomerates.

$$F_t = F_{edl} + F_{vdm}. \tag{1}$$

The electrical double layer structure is a common phenomenon in the solid-liquid interface. The mineral surface will be charged when the mineral surface contacted the solution, which may be originated from the dissolution of surface groups [18], the adsorption of ions, or the charge exchange mechanism. The opposite charge of ions is balanced by counterions to sustain the colloidal system electrically neutral. Therefore, the electric double layer structure is formed at the solid-liquid interface. The electrical double-layer force exhibits a repulsive interaction on the condition of the unique surface charge. On the contrary, an attractive force is produced in situation of the opposite surface charge. The electrical double-layer force between a sphere with radius $R$ and a plane can be described by the following equations [18]:

$$F_{edl} = \gamma RZe^{-kD}, \tag{2}$$

$$Z = 64\pi\varepsilon_0\varepsilon\left(\frac{kT}{e}\right)^2 \tanh^2\left(\frac{ze\Psi_0}{4kT}\right) = \left(9.22 * 10^{-11}\right)\tanh^2\left(\frac{\Psi_0}{103}\right), \tag{3}$$
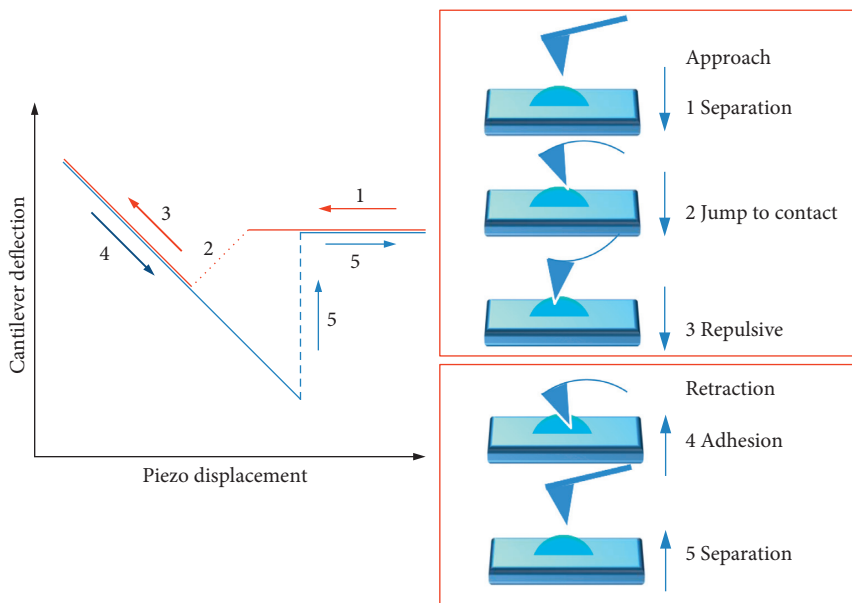
FIGURE 5: AFM force-displacement curves (left) and the related cantilever (right).



(a)

(b)
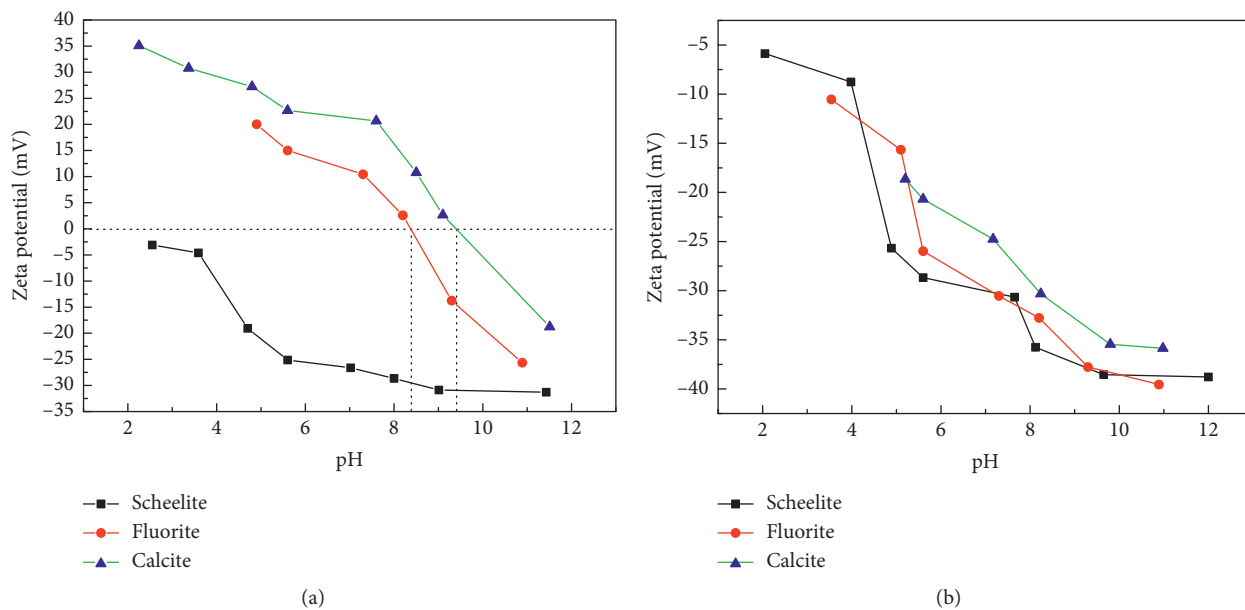
FIGURE 6: Zeta potentials of scheelite, fluorite, and calcite in (a) aqueous solution and (b) 1 mM sodium oleate solution.

$$\gamma^{-1} = \frac{0.304 * 10^{-9}}{\sqrt{M}m}, \tag{4}$$

where $\gamma^{-1}$ is the Debye length, $M$ is the electrolyte concentration, $R$ is the scheelite sphere radius, $Z$ is the interaction coefficient, $D$ is the separation distance between scheelite sphere and mineral flat substrate, $\varepsilon$ is the relative permittivity of the medium, $\varepsilon_0$ is the vacuum permittivity, $k$ is the Boltzmann constant, and $\Psi_0$ is the surface potential of minerals.

van der Waals force is a common surface force, which consists of three forces: dispersion force, induction force, and orientation force. All of these three forces decay with the seventh power of the distance between molecules. At a larger distance ($H > 10$ nm), due to the electromagnetic delay effect, the dispersion force decays 10 times faster. The resultant force of van der Waals interaction is dominated by dispersion force in aqueous solution. van der Waals force is calculated mainly by Hamaker approximation and/or Lifshitz approximation. It can be described by the following equation [18]:

(a)                                                    (b)                                                    (c)



(d)                                                    (e)                                                    (f)
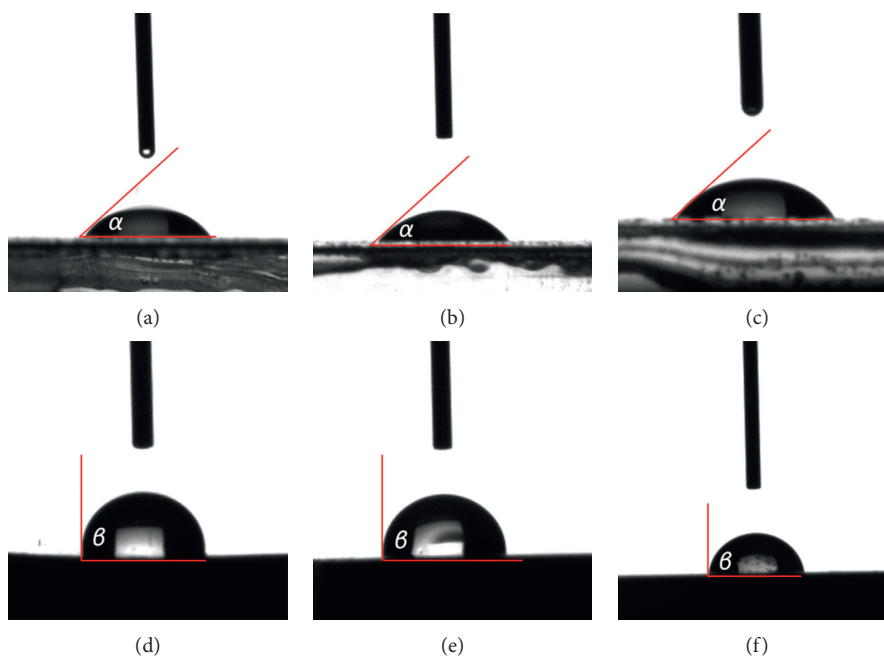
FIGURE 7: Contact angle of freshly exfoliated minerals substrates ((a) scheelite, (c) fluorite, and (e) calcite) and 1 mM sodium oleate solution soaked minerals substrates ((b) scheelite, (d) fluorite, and (e) calcite). (a) scheelite 27.30° (b) scheelite 93.60° (c) fluorite 36.90° (d) fluorite 80.90° (e) calcite 38.80° (f) calcite 91.00°.



(a)                                                                                          (b)
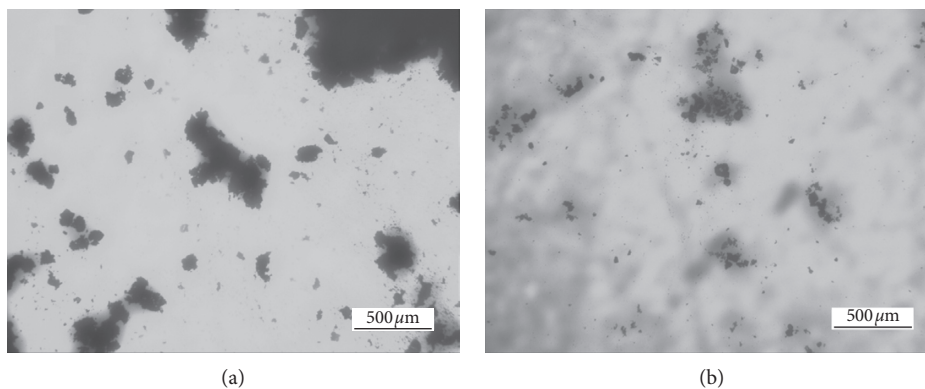
FIGURE 8: Scheelite particles ($-10\,\mu$m) in ultrapure water: (a) pH 8; (b) pH 10.



(a)                                                                                          (b)
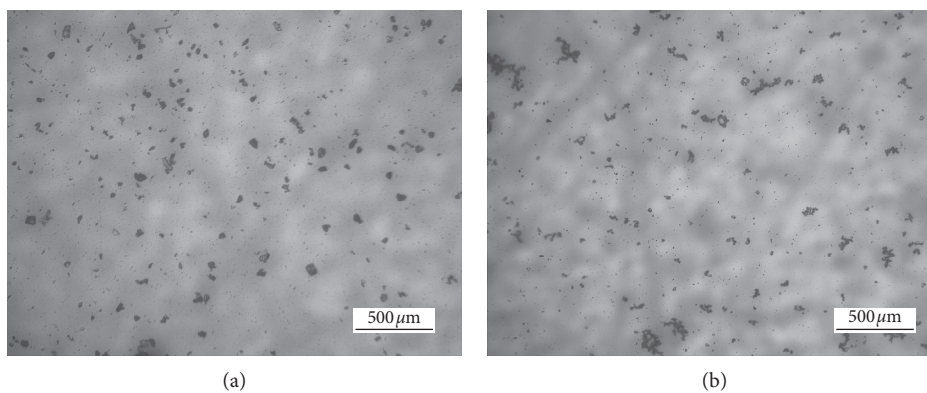
FIGURE 9: Scheelite and fluorite particles ($-10\,\mu$m) in ultrapure water: (a) pH 8; (b) pH 10.

(a)



(b)
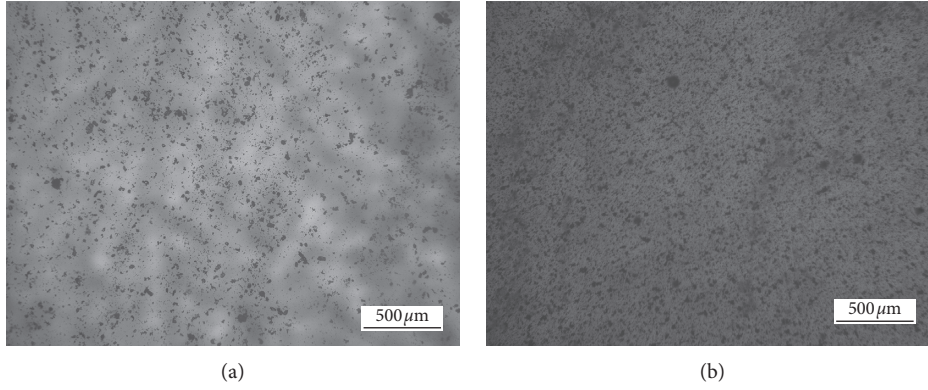
FIGURE 10: Scheelite and calcite particles ($-10\,\mu$m) in ultrapure water: (a) pH 8; (b) pH 10.



(a)



(b)



(c)
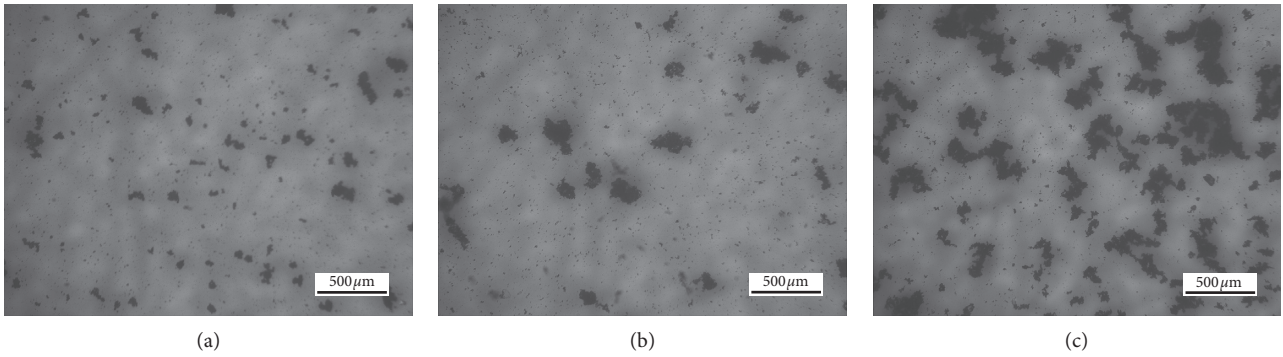
FIGURE 11: Particles ($-10\,\mu$m) in 1 mM sodium oleate solution at pH 10: (a) scheelite-scheelite and scheelite-calcite; (b) scheelite-fluorite; (c) scheelite-calcite.

$$F_{\text{vdw}} = -\frac{AR}{6D^2}, \tag{5}$$

$$A_{132} = \left(\sqrt{A_{11}} - \sqrt{A_{33}}\right)\left(\sqrt{A_{22}} - \sqrt{A_{33}}\right), \tag{6}$$

where $A$ is the Hamaker constant, $R$ is the scheelite sphere radius, $D$ is the separation distance between scheelite sphere and mineral flat substrate, $A_{132}$ is the Hamaker constant between mineral 1 and mineral 2 immersed in medium 3, and $A_{11}$, $A_{22}$, and $A_{33}$ are the Hamaker constants for the interactions between two identical media containing minerals 1, 2, or 3 in vacuum. However, there were still non-DLVO forces at complex conditions, which could be described with the EDLVO theory. Hydration force ($F_{\text{hydration}}$) and hydrophobic force ($F_{\text{hydrophobic}}$) were two typical non-DLVO forces [17].

$$F_t = F_{\text{edl}} + F_{\text{vdm}} + F_{\text{Hydration}}, \tag{7}$$

$$F_t = F_{\text{edl}} + F_{\text{vdm}} + F_{\text{hydrophobic}}, \tag{8}$$

$$F_{\text{hydration}} = 2\pi \frac{R_1 R_2}{R_1 + R_2} K_{\text{hydration}} \exp\left(\frac{-D}{\gamma^{-1}}\right), \tag{9}$$

$$F_{\text{hydrophobic}} = K_{\text{hydrophobic}} \exp\left(\frac{-D}{\gamma^{-1}}\right), \tag{10}$$

where $R_1$ and $R_2$ are the scheelite sphere radii, $\gamma - 1$ is the Debye length, $K_{\text{hydration}}$ is the hydrophilic force constant, $K_{\text{hydrophobic}}$ is the hydrophobic force constant, and $D$ is the separation distance between scheelite sphere and mineral flat substrate.

According to equation (6), the Hamaker constant on scheelite-scheelite, scheelite-fluorite, and scheelite-calcite in pure water is calculated using the Hamaker constant of Table 1, and the results are $1.35E-20$, $6.50E-21$, and $1.77E-20$. Similarly, the Hamaker constant between scheelite and scheelite, scheelite and fluorite, and scheelite and calcite immersed in sodium oleate is $9.89E-21$, $3.89E-21$, and $1.35E-20$. According to equation (5), the van der Waals forces between scheelite and scheelite, scheelite and fluorite, and scheelite and calcite are all negative in pure water and sodium oleate solution. Combining equations (1)–(4), DLVO and EDLVO forces on scheelite-scheelite, scheelite-fluorite, and scheelite-calcite were calculated. As shown in Figure 12, the DLVO and EDLVO forces on scheelite-scheelite, scheelite-fluorite, and scheelite-calcite were all negative in pure water of pH 8 or 10 and 1 mM sodium oleate solution of pH 10, which means that agglomerates on scheelite-scheelite, scheelite-fluorite, and scheelite-calcite could be formed easily in pure water of pH 8 or 10. The EDLVO forces were more negative because of the existence of hydrophilic force. This is consistent with the results of the optical microscope experiments.

Table 1: Hamaker constant for two identical media in vacuum.

| Medium | Hamaker constant | References |
| --- | --- | --- |
| Pure water | $4.00E - 20$ | [15] |
| Sodium oleate | $4.70E - 20$ | [40] |
| Scheelite | $1.00E - 19$ | [41] |
| Fluorite | $6.55E - 20$ | [42] |
| Calcite | $1.24E - 19$ | [40] |

*3.4.1. Interaction Forces on Scheelite-Scheelite, Scheelite-Fluorite, and Scheelite-Calcite in Ultrapure Water.* The interaction forces were measured on scheelite-scheelite, scheelite-fluorite, and scheelite-calcite in ultrapure water. As shown in Figure 13(a). The measured forces as a function of separation distance showed repulsion during approach at natural pH 5.6 between scheelite particle and scheelite substrate. It was illustrated that scheelite particles were dispersed in ultrapure water at natural pH 5.6 because no attraction force appeared. Classical DLVO theoretical model (the green solid line) could not be well fitted with the curves, as strong repulsive forces were observed at less than a separation distance of 5 nm. The repulsive force had been proved by Israelachvili and Adams [43] between mica surfaces in aqueous $KNO_3$ solution. This non-DLVO force was named hydration force, which acts on hydrophilic particles when the separation distance is less than about 4 nm [19]. The interaction force between scheelite and scheelite could be explained by the EDLVO theoretical model (the red solid line). Although the red line could not perfectly match the approach curves, the trend was clear. A slight jump-in was observed between scheelite and scheelite in ultrapure water of pH 8 or pH 10 when approaching. These results indicated that van der Waals forces overcame electrical double layer repulsion force to attract scheelite particles to the surface at pH 8 or pH 10, and scheelite particles could be attracted to each other in ultrapure water, which had been proved by the photo of optical microscope in Figure 8(b). An adhesion force of 1 nN at 15 nm separation distance was obtained between scheelite and scheelite at natural pH 5.6 as shown in Figure 13(b). With the increase of pH, the adhesion force greatly enhanced, which was 5 nN at 40 nm separation distance at pH 10 and 8 nN at 100 nm separation distance at pH 8. This may be because scheelite surface was negatively charged at the range of pH from 5.6 to 10 and the addition of Na ions reduced the electric double layer repulsive force [27], so scheelite particles were easy to attract together at pH 10.

As demonstrated in Figure 14(a), a jump-in was not observed between scheelite and fluorite when measured in natural ultrapure water (pH 5.6) in the approach curves. According to the results in the curves, scheelite and fluorite particles in ultrapure water (pH 5.6) could not attract each other obviously due to repulsive force. With the increase of pH, a light jump-in was observed at the separation distance of 30 nm at pH 8 and 10. Here, van der Waals force contributed the main force by overcoming the electrical double layer force, indicating that scheelite and calcite could agglomerate, but the attraction force (less than 1nN) may lead to fracture easily of the agglomeration. As shown in Figure 14(b), the adhesion force reached the lowest at natural pH 5.6, and the separation distance of jump-out was 25 nm. The adhesion force increased with the increase of pH and reached 6 nN of separation distance 50 nm at pH 8. It should be pointed out that the adhesion force reduced obviously on scheelite-fluorite compared with that on scheelite-scheelite under the same condition. The retraction curve results indicated that the separation of fluorite from scheelite would be easier than scheelite from scheelite in flotation. This was because isoelectric point (IEP) of fluorite was pH 8.5 as shown in Figure 6. When the solution pH was greater than 8.5, the surface of fluorite was negatively charged [44]. When the solution pH was less than 8.5, the fluorite surface charged positively, while the scheelite surface charged negatively when the solution pH was from pH 8 to pH 10. Therefore, the electrical double-layer force between scheelite and fluorite was an attraction interaction at pH 8 and repulsive interaction at pH 10. So, the adhesion force reduced in the ultrapure water of pH 8, which was consistent with the retraction curves. The force curve results in Figure 14 indicated that the agglomeration could occur between scheelite and fluorite particles in the ultrapure water of pH 8 or 10, but it was easier to be separated because of tiny adhesion force.

The interaction force curves between scheelite and calcite are shown in Figure 15(a). In the ultrapure water of pH 5.6 or 8, an obvious jump-in was found at 20 nm separation distance. This was because the surface of calcite was positively charged at pH 5.6 or 8, while the surface of scheelite was negatively charged with pH range of 5.6 to 8, so the electrical double layer force between scheelite and calcite exhibited an attraction force, and van der Waals force also exhibited an attraction force. The interaction force curves could be well described by the DLVO theory when the separation distance was away from 10 nm at pH 10. Under this condition, the zeta potential of calcite was close to 0 mv, which led to the minimum electrical double layer force between scheelite and calcite, and the interaction force on scheelite-calcite was also minimum, so an adhesion force of 3 nN at 18 nm separation distance at pH 10 is shown in Figure 10(b).

In a word, scheelite-scheelite and scheelite-fluorite particles were all dispersed in natural ultrapure water (pH 5.6), while scheelite-calcite particles could attract each other. With the increase of pH, scheelite-scheelite, scheelite-fluorite, and scheelite-calcite particles could attract each other to form agglomerates at pH 10, which would affect the flotation of fine scheelite.

*3.4.2. Interaction Forces on Scheelite-Scheelite, Scheelite-Fluorite, and Scheelite-Calcite in Sodium Oleate Solution.* As shown in Figure 16, a strong jump-in was observed on scheelite-scheelite, scheelite-fluorite, and scheelite-calcite from interaction force curves after the scheelite, fluorite, and calcite substrates had been soaked in 0.1 mM/1 mM sodium oleate solution of pH 8 or 10 for 30 minutes. It should be noted that there is no force curve data of scheelite-scheelite in 1 mM sodium oleate solution (pH
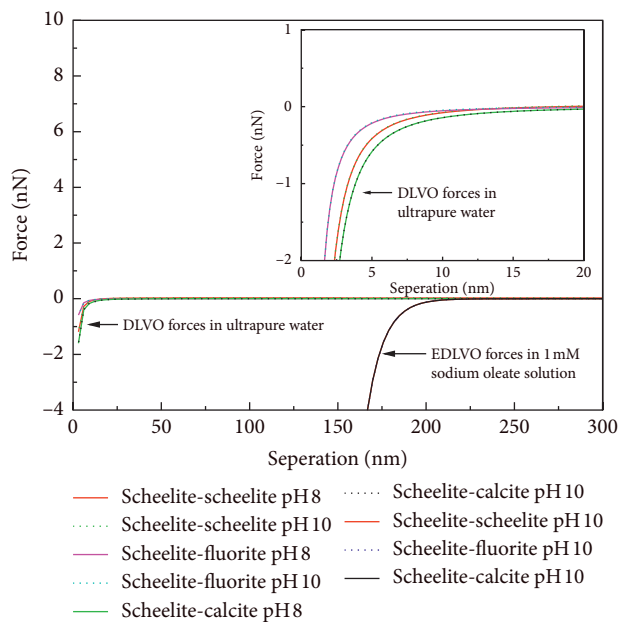
FIGURE 12: DLVO and EDLVO forces on scheelite-scheelite, scheelite-fluorite, and scheelite-calcite (in pure water of pH 8 or 10, $\gamma^{-1} = 960$ nm [18], and $R = 5 * 10^{-9}$ m; in 1 mM sodium oleate solution of pH 10, $\gamma^{-1} = 9.6$ nm [18], and $K_{hydrophobic} = -1.4 * 10^{8}$ nN/m [15]).
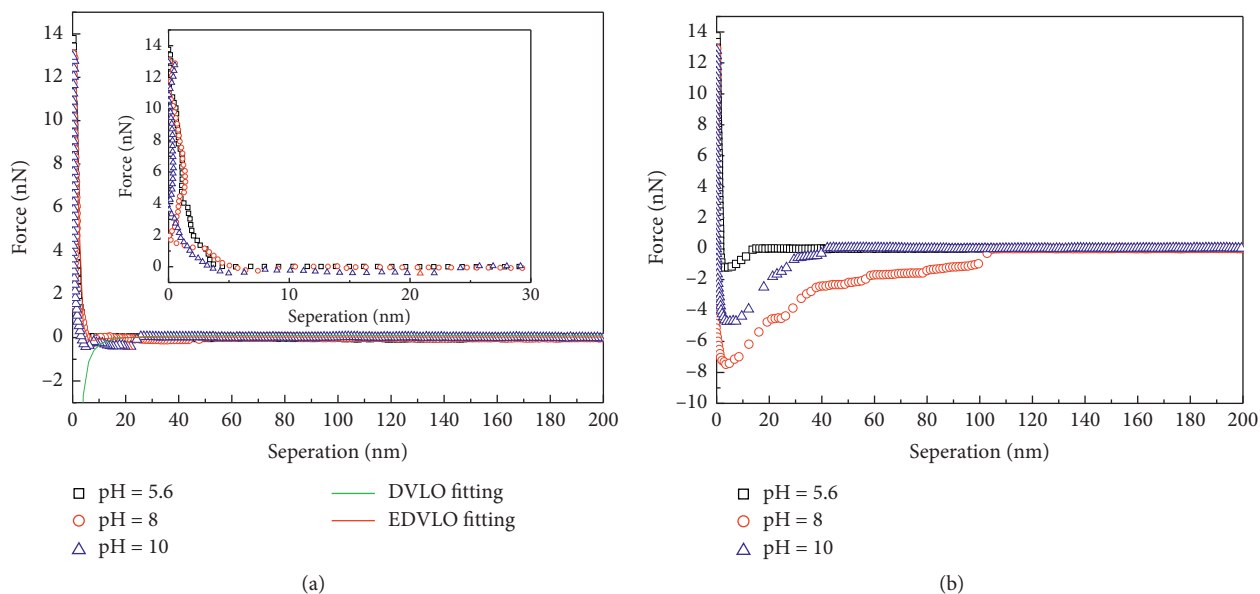


FIGURE 13: The interaction forces between scheelite particle and scheelite substrate in ultrapure water solution: (a) approach curves; (b) retraction curves.

10); this may be because the force exceeds the elastic constant of the colloidal probe, so the force curve is not obtained using AFM. These results indicated that the hydrophobic forces exhibited attractive between particles and surfaces. Previous studies manifested that the hydrophobic attraction force was several orders of magnitude larger than van der Waals force and electrical double layer force, so the hydrophobic force contributed to the main interaction. It could be found from Figure 16(a) that the hydrophobic force increased with the increase of pH. At

pH 10, the interaction force between scheelite and scheelite was greater than that at pH 8, which indicated that the adsorption effect of sodium oleate on scheelite surface was better at pH 10. This result was consistent with the previous research [45]. When the concentration of sodium oleate is 0.1 mM, according to species distribution diagram [46] of the oleic acid solution, the maximum pH of ion-molecular association concentration is 8.21. Accordingly, the sodium oleate mainly existed in the form of $RCOO^-$ and $RCOO_2^{2-}$ at pH 10, and the surface of scheelite

(a)

(b)
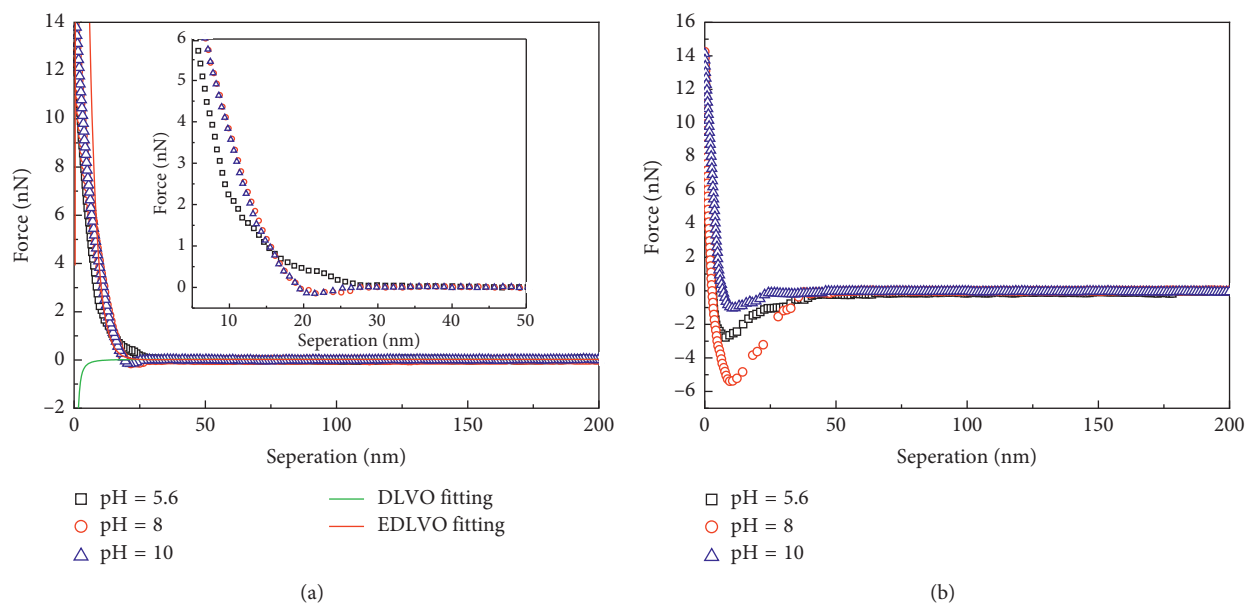
FIGURE 14: The interaction forces between scheelite particle and fluorite substrate in ultrapure water solution: (a) approach curves; (b) retraction curves.



(a)

(b)
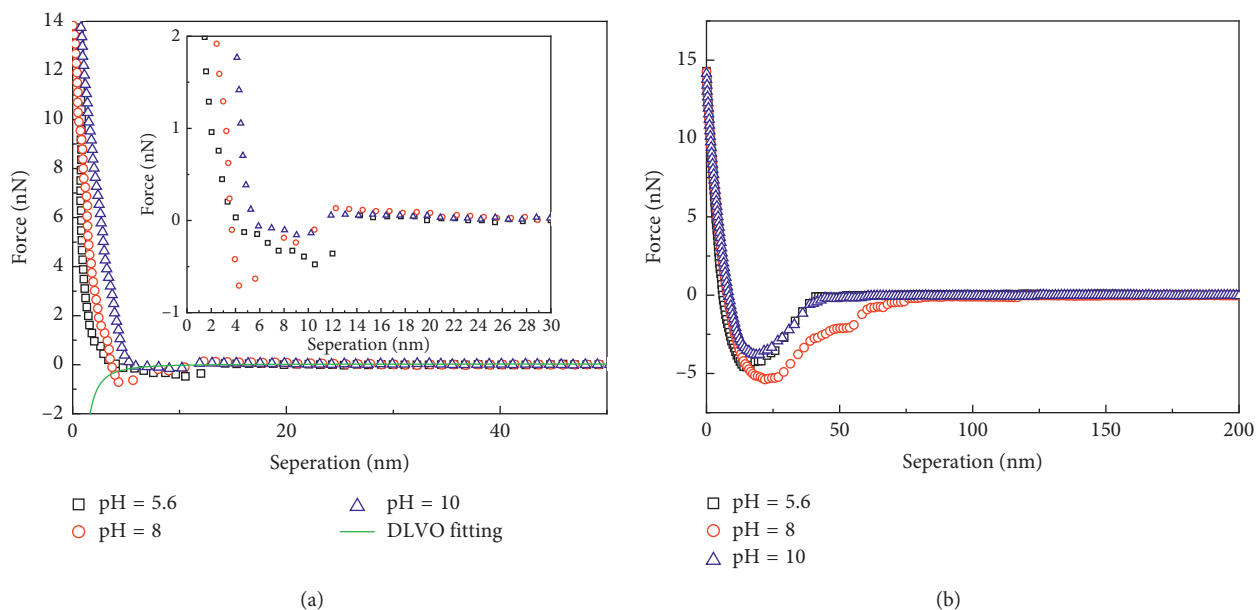
FIGURE 15: The interaction forces between scheelite particle and calcite substrate in ultrapure water solution: (a) approach curves; (b) retraction curves.

charged negatively under the same condition is shown in Figure 6. Therefore, the sodium oleate was adsorbed on the surface of scheelite by chemisorption. However, at pH 8, the sodium oleate mainly existed in the form of oleic acid molecule RCOOH [47]; consequently, the sodium oleate was adsorbed on the surface of scheelite by physical absorption. The approach curves could be well described by EDLVO theoretical model (red and blank solid line) in Figure 16(a). However, the EDLVO fitting line did not appear in Figures 16(b) and 16(c) due to irregularity of the

approach curves. It may be caused by mineral surface heterogeneity and limitation of elastic coefficient on the scheelite colloid probe. The same phenomenon was also found on scheelite-fluorite and scheelite-calcite after treating with 0.1 mM/1 mM sodium oleate solution as shown in Figures 16(b) and 16(c). The hydrophobic force increased obviously in 1 mM sodium oleate solution compared to that in 0.1 mM sodium oleate solution. An attractive force of 8 nN at 28 nm separation distance was obtained between scheelite and fluorite after treating with 1 mM sodium oleate as shown

(a)



(b)



(c)

Figure 16: The approach curves in sodium oleate solution: (a) scheelite-scheelite in 0.1 mM sodium oleate solution; (b) scheelite-fluorite; (c) scheelite-calcite.

in Figure 16(b), and an attraction force of 33 nN at 195 nm separation distance was obtained between scheelite and calcite in the same experiment condition as shown in Figure 16(c). All the results above indicated that the main formation reason of hydrophobic agglomeration was the existence of hydrophobic force after the minerals were treated with the sodium oleate solution .

As shown in Figures 17 and 18, the jump-in distance and force on scheelite-scheelite, scheelite-fluorite, and scheelite-calcite in approach curves at pH 10 were compared. The jump-in distance and force were almost similar in ultrapure water, but increased obviously in 0.1 mM and 1 mM sodium oleate solution, which fully showed that agglomerations were easier to form in higher concentration of sodium oleate. After treated with 0.1 mM sodium oleate, the jump-in distance and force were ordered as follows: scheelite-

scheelite > scheelite-calcite > scheelite-fluorite, which was consistent with the result of adhesion force in Figure 19. These results indicated that the agglomerations on scheelite-scheelite were easiest to be formed, and hardest to fracture.

Previous studies [21] reported a simplified model (equation (11)) for calculating the adhesion between a particle and a surface with nanoscale roughness. The increase of adhesion force may be related to $R_q$.

$$\frac{F_{ad}}{R} = \frac{A_{12}}{6Z_0^2\left[\left(1.485R_q/1.485R_q + R\right) + \left(1/\left(1 + 1.485R_q\right)/Z_0\right)^2\right]},$$

(11)

where $Z_0$ is the equilibrium distance (closest approach) between two surfaces, which is usually taken as 0.3 nm [48], $A_{12}$ is the Hamaker constant for mineral 1 interacting with
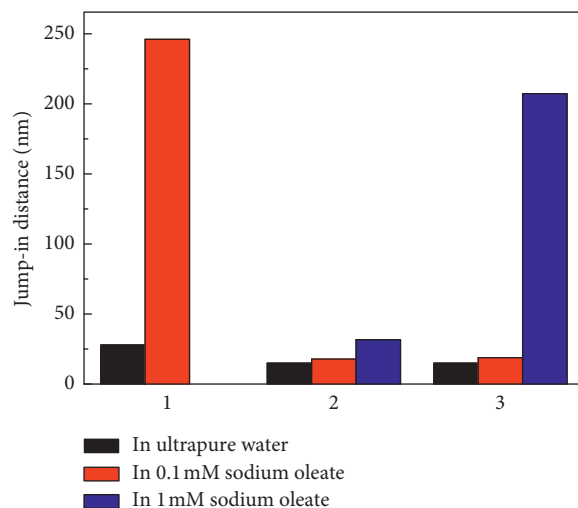
FIGURE 17: The jump-in distance on scheelite-scheelite, scheelite-fluorite, and scheelite-calcite in approach curves at pH 10.
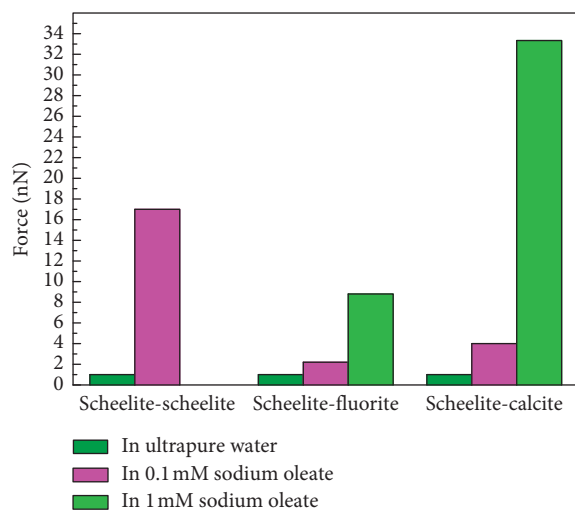


FIGURE 18: The force on scheelite-scheelite, scheelite-fluorite, and scheelite-calcite in approach curves at pH 10.
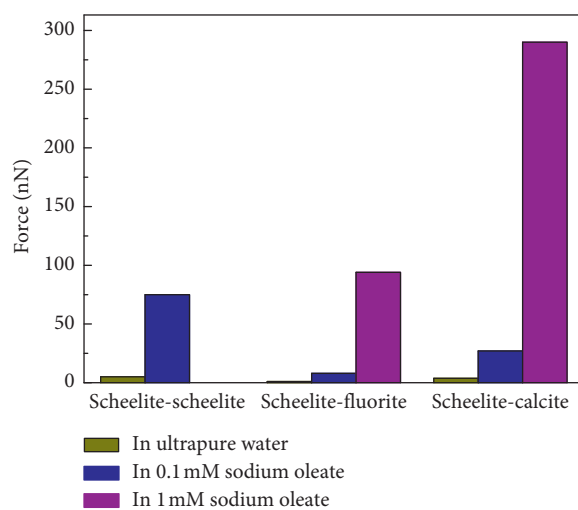


FIGURE 19: The adhesion force on scheelite-scheelite, scheelite-fluorite, and scheelite-calcite in retraction curves at pH 10.
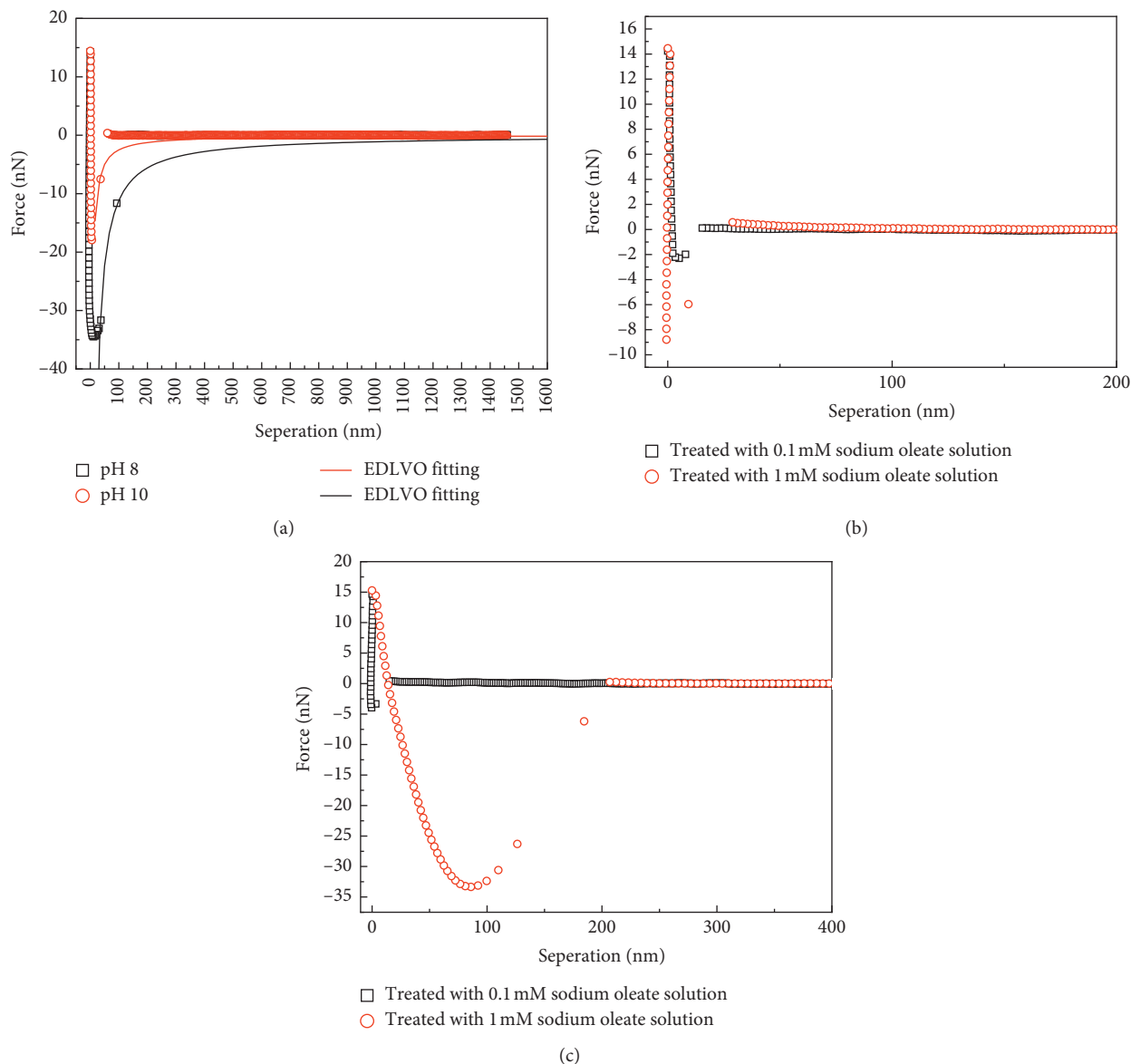
(a)



(b)



(c)
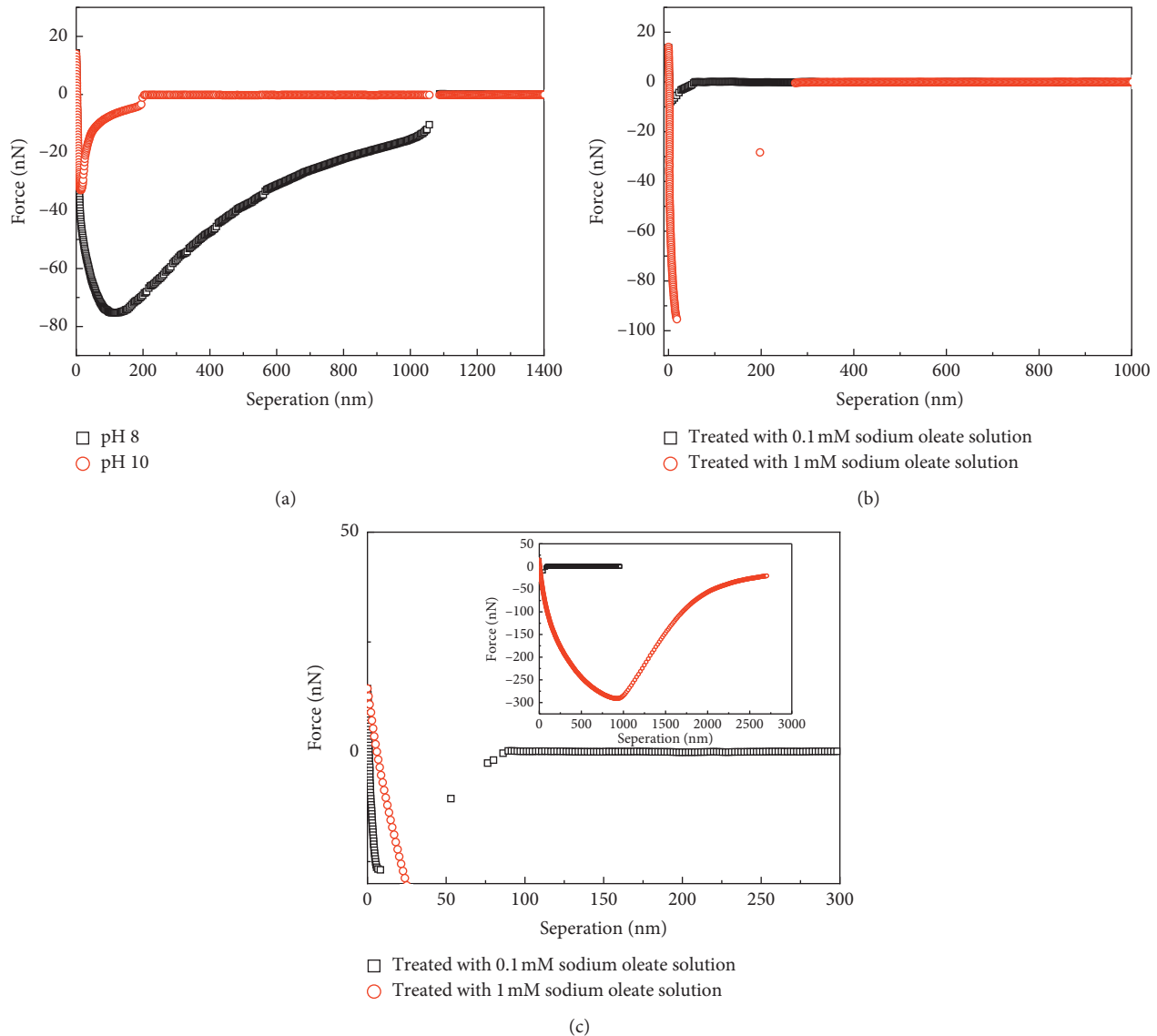
FIGURE 20: The retraction curves in sodium oleate solution: (a) scheelite-scheelite in 0.1 mM sodium oleate solution; (b) scheelite-fluorite; (c) scheelite-calcite.

mineral 2 in vacuum or air, and $R_q$ is the roughness of mineral surface.

As shown in Figures 19 and 20, the adhesion forces of scheelite-scheelite, scheelite-fluorite, and scheelite-calcite increased obviously after treating with 0.1 mM/1 mM sodium oleate solution and increased with the increase of sodium oleate concentration and so did the corresponding separation distance. The adhesion force of scheelite-scheelite was strongest after treated with 0.1 mM sodium oleate solution (pH 10) compared with adhesion forces in Figures20(b) and 20(c). This may be because the roughness when sodium oleate was adsorbed on scheelite particle had been changed due to equation (11).

All the above results indicated hydrophobic force played a key role in the formation of agglomerates. The agglomerates were attracted by hydrophobic force pushing hydration layer out. The interaction forces

changed to strong adhesion forces, and the long separation distance also verified these results. The agglomeration formed between scheelite and scheelite made the fine scheelite particles grow, which was conducive to improving the efficiency of scheelite flotation. The agglomeration formed between scheelite and fluorite and scheelite and calcite seriously affected the grade and recovery of scheelite concentrate. Therefore, effective inhibitors of fluorite and calcite must be used to prevent the formation of agglomerations in the flotation process of fine scheelite.

## 4. Conclusions

Hydrophobic aggregation flotation is a typical process in fine scheelite flotation. The interaction forces on scheelite-scheelite, scheelite-fluorite, and scheelite-calcite in ultrapure

water and sodium oleate solution were examined by using the AFM colloid probe technique. The corresponding optical microscope measurements, zeta potential measurements, and contact angle measurements were also carried out to verify the AFM results in this paper.

(1) The surface of natural scheelite, fluorite, and calcite was hydrophilic according to contact angle measurements results. A strong hydration force existed in the interaction force curves on hydrophilic scheelite-scheelite and scheelite-fluorite in ultrapure water (pH 5.6). The results implied that on scheelite-scheelite, scheelite-fluorite particles were dispersed in scheelite flotation. However, scheelite-calcite may be easy to attract each other at pH 5.6 because of the weak attractive force. With the increase of pH, a slight jump-in was found in the interaction force curves on scheelite-scheelite, scheelite-fluorite, and scheelite-calcite at pH 8 or 10. The formation of agglomerates on scheelite-scheelite, scheelite-fluorite, and scheelite-calcite was proved by optical microscope measurements results, but the agglomerations were empty and not tight.

(2) The adsorption of the sodium oleate on the surface of scheelite, fluorite, and calcite was proved by zeta potential measurements results. Furthermore, the surface of scheelite, fluorite, and calcite treated by sodium oleate solution was hydrophobic according to contact angle measurements results. The interaction force increased obviously because of the existing hydrophobic force, which could be well described by EDLVO theory, which was verified by the corresponding optical microscope measurements. Hydrophobic agglomerations could form on scheelite-scheelite, scheelite-fluorite, and scheelite-calcite treated by sodium oleate solution, which were proved by optical microscope measurements results. Furthermore, optical microscope measurements results indicated the hydrophobic agglomerations were larger and more dense when the particles of scheelite, fluorite, and calcite were soaked by sodium oleate, which was proved by the adhesion force curves.

(3) All results show that fluorite and calcite must be effectively restrained to prevent them from agglomerating with scheelite in the flotation process, which can reduce the grade and recovery of scheelite concentrate. The interaction on scheelite-scheelite, scheelite-fluorite, and scheelite-calcite still needs to be further studied after treated by inhibitor using AFM.

## Data Availability

All data included in this study are available upon request by contacting the corresponding author.

## Conflicts of Interest

The authors declare no conflicts of interest.

## Acknowledgments

## References

[1] N. Kupka and M. Rudolph, "Froth flotation of scheelite-a review," *International Journal of Mining Science and Technology*, vol. 28, no. 3, pp. 373–384, 2018.

[2] T. V. Subrahmanyam and K. S. E. Forssberg, "Fine particles processing: shear-flocculation and carrier flotation-a review," *International Journal of Mineral Processing*, vol. 30, no. 3-4, pp. 265–286, 1990.

[3] A. Ozkan, "Determination of the critical surface tension of wetting of minerals treated with surfactants by shear flocculation approach," *Journal of Colloid and Interface Science*, vol. 277, no. 2, pp. 437–442, 2004.

[4] W. Zhou, H. Chen, L. Ou, and Q. Shi, "Aggregation of ultrafine scheelite particles induced by hydrodynamic cavitation," *International Journal of Mineral Processing*, vol. 157, pp. 236–240, 2016.

[5] L. J. Warren, "Shear-flocculation of ultrafine scheelite in sodium oleate solutions," *Journal of Colloid and Interface Science*, vol. 50, no. 2, pp. 307–318, 1975.

[6] L. Valderrama and J. Rubio, "High intensity conditioning and the carrier flotation of gold fine particles," *International Journal of Mineral Processing*, vol. 52, no. 4, pp. 273–285, 1998.

[7] S. Song, A. Lopez-Valdivieso, J. L. Reyes-Bahena, H. I. Bermejo-Perez, and O. Trass, "Hydrophobic flocculation of galena fines in aqueous suspensions," *Journal of Colloid and Interface Science*, vol. 227, no. 2, pp. 272–281, 2000.

[8] C. Zhang, L. Li, Z. Yuan, X. Xu, Z. Song, and Y. R. Zhang, "Mechanical properties of siderite and hematite from DFT calculation," *Minerals Engineering*, vol. 146, Article ID 106107, 2020.

[9] R. Wang, Z. Wei, H. Han et al., "Fluorite particles as a novel calcite recovery depressant in scheelite flotation using Pb-BHA complexes as collectors," *Minerals Engineering*, vol. 132, pp. 84–91, 2019.

[10] H. Han, Y. Xiao, Y. Hu et al., "Replacing Petrov's process with atmospheric flotation using Pb-BHA complexes for separating scheelite from fluorite," *Minerals Engineering*, vol. 145, Article ID 106053, 2020.

[11] W. Chen, F. Chen, X. Bu, G. Zhang, C. Zhang, and Y. Song, "A significant improvement of fine scheelite flotation through rheological control of flotation pulp by using garnet," *Minerals Engineering*, vol. 138, pp. 257–266, 2019.

[12] L. J. Warren, "Flocculation of stirred suspensions of cassiterite and tourmaline," *Colloids and Surfaces*, vol. 5, no. 4, pp. 301–319, 1982.

[13] P. Koh and L. Warren, "A pilot plant test of the shear-flocculation of ultrafine scheelite," in *Proceedings of the Chemeca 80: Process Industries in the 80's; 8th Australian Chemical*

*Engineering Conference*, p. 90, Melbourne, Australia, August 1980.

[14] Y. Xing, M. Xu, X. Gui et al., "The application of atomic force microscopy in mineral flotation," *Advances in Colloid and Interface Science*, vol. 256, pp. 373–392, 2018.

[15] J. Israelachvili and R. Pashley, "The hydrophobic interaction is long range, decaying exponentially with distance," *Nature*, vol. 300, no. 5890, pp. 341-342, 1982.

[16] R. M. Pashley and J. N. Israelachvili, "A comparison of surface forces and interfacial properties of mica in purified surfactant solutions," *Colloids and Surfaces*, vol. 2, no. 2, pp. 169–187, 1981.

[17] A. Nguyen and H. J. Schulze, *Colloidal Science of Flotation*, CRC Press, Boca Raton, FL, USA, 2003.

[18] J. N. Israelachvili, *Intermolecular and Surface Forces*, Academic Press, Cambridge, MA, USA, 2015.

[19] H.-J. Butt, B. Cappella, and M. Kappl, "Force measurements with the atomic force microscope: technique, interpretation and applications," *Surface Science Reports*, vol. 59, no. 1–6, pp. 1–152, 2005.

[20] B. Cappella and G. Dietler, "Force-distance curves by atomic force microscopy," *Surface Science Reports*, vol. 34, no. 1–3, pp. 1–104, 1999.

[21] J. Wang, J. Li, L. Xie, C. Shi, Q. Liu, and H. Zeng, "Interactions between elemental selenium and hydrophilic/hydrophobic surfaces: direct force measurements using AFM," *Chemical Engineering Journal*, vol. 303, pp. 646–654, 2016.

[22] J. Drelich, J. Nalaskowski, A. Gosiewska, E. Beach, and J. D. Miller, "Long-range attractive forces and energy barriers in de-inking flotation: AFM studies of interactions between polyethylene and toner," *Journal of Adhesion Science and Technology*, vol. 14, no. 14, pp. 1829–1843, 2000.

[23] Y. Xing, C. Li, and Y. Cao, "Interaction forces between paraffin/stearic acid and fresh/oxidized coal particles measured by atomic force microscopy," *Energy & Fuels*, vol. 31, no. 3, pp. 3305–3312, 2017.

[24] E. Rohem Peçanha, M. D. da Fonseca de Albuquerque, R. A. Simão, L. de Salles Leal Filho, and M. B. de Mello Monte, "Interaction forces between colloidal starch and quartz and hematite particles in mineral flotation," *Colloids and Surfaces A: Physicochemical and Engineering Aspects*, vol. 562, pp. 79–85, 2019.

[25] X. Gui, Y. Xing, G. Rong, Y. Cao, and J. Liu, "Interaction forces between coal and kaolinite particles measured by atomic force microscopy," *Powder Technology*, vol. 301, pp. 349–355, 2016.

[26] W. A. Ducker, T. J. Senden, and R. M. Pashley, "Direct measurement of colloidal forces using an atomic force microscope," *Nature*, vol. 353, no. 6341, pp. 239–241, 1991.

[27] H.-J. Butt, "Measuring electrostatic, Van der Waals, and hydration forces in electrolyte solutions with an atomic force microscope," *Biophysical Journal*, vol. 60, no. 6, pp. 1438–1444, 1991.

[28] Z. Zhang, Y. Cao, L. Sun, Z. Ma, and Y. Liao, "Interaction forces between scheelite and fluorite in calcium solution measured by atomic force microscopy," *Applied Surface Science*, vol. 486, pp. 323–336, 2019.

[29] L. Xie, J. Wang, C. Shi et al., "Mapping the nanoscale heterogeneity of surface hydrophobicity on the sphalerite mineral," *The Journal of Physical Chemistry C*, vol. 121, no. 10, pp. 5620–5628, 2017.

[30] Z. Lu, Q. Liu, Z. Xu, and H. Zeng, "Probing anisotropic surface properties of molybdenite by direct force measurements," *Langmuir*, vol. 31, no. 42, pp. 11409–11418, 2015.

[31] A. Beaussart, L. Parkinson, A. Mierczynska-Vasilev, and D. A. Beattie, "Adsorption of modified dextrins on molybdenite: AFM imaging, contact angle, and flotation studies," *Journal of Colloid and Interface Science*, vol. 368, no. 1, pp. 608–615, 2012.

[32] Z. Gao, Y. Hu, W. Sun, and J. W. Drelich, "Surface-charge anisotropy of scheelite crystals," *Langmuir*, vol. 32, no. 25, pp. 6282–6288, 2016.

[33] S. Assemi, J. Nalaskowski, J. D. Miller, and W. P. Johnson, "Isoelectric point of fluorite by direct force measurements using atomic force microscopy," *Langmuir*, vol. 22, no. 4, pp. 1403–1405, 2006.

[34] W. Chen, Q. Feng, G. Zhang, L. Li, and S. Jin, "Effect of energy input on flocculation process and flotation performance of fine scheelite using sodium oleate," *Minerals Engineering*, vol. 112, pp. 27–35, 2017.

[35] J. Wang, Y. Mao, Y. Cheng, Y. Xiao, Y. Zhang, and J. Bai, "Effect of Pb(II) on the flotation behavior of scheelite using sodium oleate as collector," *Minerals Engineering*, vol. 136, pp. 161–167, 2019.

[36] B. A. Wills, *Chapter 12-Froth Flotation*, B. A. Wills, Ed., O'Reilly Media, Inc., Newton, MA, USA, 1985.

[37] B. Derjaguin and L. Landau, "Theory of the stability of strongly charged lyophobic sols and of the adhesion of strongly charged particles in solutions of electrolytes," *Progress in Surface Science*, vol. 43, no. 1–4, pp. 30–59, 1993.

[38] E. J. W. Verwey, "Theory of the stability of lyophobic colloids," *The Journal of Physical and Colloid Chemistry*, vol. 51, no. 3, pp. 631–636, 1947.

[39] X.-T. Huang, W. Xiao, H.-B. Zhao et al., "Hydrophobic flocculation flotation of rutile fines in presence of styryl phosphonic acid," *Transactions of Nonferrous Metals Society of China*, vol. 28, no. 7, pp. 1424–1432, 2018.

[40] G. Qiu, Y. Hu, and D. Wang, *Particle Interaction and Fine Particle Flotation*, Central South University Press, Changsha, China, 1993.

[41] X. Liu, *Study on Flotation Behavior of Fine-Grained Scheelite Study on Flotation Behavior of Fine-Grained Scheelite*, Central South University, Changsha, China, 2010.

[42] J. Visser, "On Hamaker constants: a comparison between Hamaker constants and Lifshitz-Van der Waals constants," *Advances in Colloid and Interface Science*, vol. 3, no. 4, pp. 331–363, 1972.

[43] J. N. Israelachvili and G. E. Adams, "Direct measurement of long range forces between two mica surfaces in aqueous $KNO_3$ solutions," *Nature*, vol. 262, no. 5571, pp. 774–776, 1976.

[44] J. D. Miller, K. Fa, J. V. Calara, and V. K. Paruchuri, "The surface charge of fluorite in the absence of surface carbonation," *Colloids and Surfaces A: Physicochemical and Engineering Aspects*, vol. 238, no. 1–3, pp. 91–97, 2004.

[45] W.-Z. Yin and J.-Z. Wang, "Effects of particle size and particle interactions on scheelite flotation," *Transactions of Nonferrous Metals Society of China*, vol. 24, no. 11, pp. 3682–3687, 2014.

[46] P. Somasundaran and D. Wang, *Solution Chemistry: Minerals and Reagents*, Elsevier, Amsterdam, Netherlands, 2006.

[47] P. Somasundaran, K. P. Ananthapadmanabhan, and I. B. Ivanov, "Dimerization of oleate in aqueous solutions," *Journal of Colloid and Interface Science*, vol. 99, no. 1, pp. 128–135, 1984.

[48] Y. I. Rabinovich, J. J. Adler, A. Ata, R. K. Singh, and B. M. Moudgil, "Adhesion between nanoscale rough surfaces," *Journal of Colloid and Interface Science*, vol. 232, no. 1, pp. 17–24, 2000.

*Research Article*

# Adsorption of Thymol onto Natural Clays of Morocco: Kinetic and Isotherm Studies

**Hamid Ziyat** [1], **Mohammed Naciri Bennani,**[1] **Hassan Hajjaj,**[2] **Omar Qabaqous,**[1] **Said Arhzaf,**[1] **Soumiya Mekdad,**[1] **and Safae Allaoui** [1]

*[1]Laboratory of Chemistry-Biology Applied to the Environment,*
*Research Team "Applied Materials and Catalyses" Chemistry Department, Faculty of Sciences, Moulay-Ismail University,*
*BP. 11201 Zitoune, Meknes, Morocco*
*[2]Laboratory of Plant Biotechnology and Molecular Biology, Applied Mycology Team, Faculty of Sciences,*
*Moulay-Ismail University, BP. 11201 Zitoune, Meknes, Morocco*

Correspondence should be addressed to Hamid Ziyat; ziyat.hamid@gmail.com

The present work aims to study the affinity of a component of the thyme essential oil "thymol" to natural Moroccan clay "Rhassoul" using the adsorption technique. The physicochemical characterizations of the purified and modified clay were carried out by X-ray diffraction (XRD), Fourier transform infrared spectroscopy (FTIR), DTA/TGA, and SEM-EDX. Thymol adsorption tests on the purified Rhassoul (Rh-P) and the modified one by CTAB (Rh-CTAB) were followed by UV-visible spectroscopy. They show that the adsorption isotherms can be described by the Freundlich model and that the kinetics of adsorption is in accordance with the pseudo-second-order model for the two clays. Adsorption capacities obtained were of the order of 6 mg/g for the purified Rhassoul and 16 mg/g for the modified Rhassoul by cetyltrimethylammonium bromide (CTAB). These values show that the modified Rhassoul has a better adsorption capacity compared to the purified Rhassoul.

## 1. Introduction

Rhassoul is a natural clay soil of Moroccan origin, traditionally used for centuries in cosmetics (soap, shampoo, masks,...) by all the populations of North Africa and even in some regions of the Middle East. The Rhassoul deposits, unique in the world, are located on the edge of the southeast of the tertiary sector of Missour in the Moulouya valley 200 km from the Fes city. Rhassoul is a natural mineral product composed mainly of stevensite and other minerals such as quartz, gypsum, dolomite, or sepiolite but in low proportions [1]. The use of Rhassoul as an adsorbent is justified by its low cost, natural abundance, and high surface area. Rhassoul has been the subject of some recent studies which concerned the adsorption of fungicides [2], adsorption of textile dyes such as methylene blue [3, 4], basic yellow

cationic dye [5], and methyl violet [6], and also other applications in water treatment [7–11].

The use of essential oils in antifungal applications for the preservation of foodstuffs is limited by the volatile nature of their constituents. Indeed, the essential oils are mainly formed of terpenoids that have high vaporization pressure at 25°C [12]. Because of the high volatility of essential oils or their constituents, the duration of their activities is very short. So, to increase their activities and to control their release, they can be encapsulated in clays or modified clays [13, 14]. The development of clay-essential oil compounds should remedy this disadvantage. The adsorption of essential oils onto a support such as clays is a technique that will immobilize volatile compounds, stabilize the essential oil and protect it against light, and modulate its release over time. Similar studies were done; montmorillonite and

kaolinite have been tested as effective materials for the adsorption of terpenic compounds, and the use of loaded clays as new natural insecticides has been proposed [13, 15, 16]; especially, the adsorption of thymol onto the purified bentonite and its counterpart modifies part CTAB [14].

In this context, we are interested in testing the affinity of thymol to Rhassoul by studying its adsorption kinetics to determine the relative adsorption capacity of each clay and specify the kinetic model and the adsorption isotherm.

## 2. Materials and Methods

### 2.1. Raw Material.
The clay used in this study is from a commercial Rhassoul named "Rhassoul Chorafa Al Akhdar." It corresponds to the natural product crushed without any treatment and dried at 100°C to remove weakly bound water and then crushed and sieved. Only aggregates smaller than 63 $\mu$m in diameter were retained.

Thymol of 99% purity and sodium chloride (NaCl) of 98% purity were provided by Sigma-Aldrich; cetyltrimethylammonium bromide (CTAB) of 98% purity was provided by LOBA Chemie. NaOH and HCl were provided by Fisher.

### 2.2. Purification of Rhassoul.
Rhassoul, previously crushed and sieved to a size less than 63 $\mu$m, is suspended in a solution of NaCl (1M concentration) to replace all the exchangeable cations ($Ca^{2+}$, $Mg^{2+}$, $K^+$,...) of the natural clay with the $Na^+$ ions. For this purpose, the mass $m$ of clay is introduced into a beaker containing 100 ml of an NaCl solution (1M). After 4 hours of stirring, the clay particles are separated from the aqueous phase by centrifugation at a speed of 3400 rpm/min during 10 min. After 4 successive treatments (saturation-centrifugation), the suspension is subsequently centrifuged and washed several times with distilled water until complete elimination of chloride ions (until the silver nitrate test is negative). The suspension obtained is dried at 70°C overnight, and the purified compound (Rh-P) is crushed using a porcelain mortar.

### 2.3. Preparation of Rhassoul-CTAB (Rh-CTAB).
A suitable amount of cationic surfactant bromide, cetyltrimethylammonium bromide (CTAB), with purity >96% and the chemical formula $CH_3(CH_2)_{15}N(CH_3)_3^+ Br^-$, was dissociated in distilled water previously heated to 40°C in order to increase the solubility of CTAB.

Rhassoul interposed by the surfactant cetyltrimethylammonium bromide (denoted Rh-CTAB) is obtained by dispersing 2.4 g of the Rh-P, decarbonated by HCl, and treated with $H_2O_2$ at 30% in 100 ml of distilled water (at a ratio of CTAB/Rhassoul equal to 1.14 mmol/g) to which a solution of cetyltrimethylammonium bromide (1 g of CTAB in 100 ml of distilled water) is added dropwise [10]. The mixture was stirred for 24 h, recovered by centrifugation, washed three times with distilled water, and dried at 60°C for 12 hours.

### 2.4. Characterization Techniques.
The purified Rhassoul and modified one obtained were characterized by physicochemical techniques (XRD, FTIR, DTA/TGA, and SEM-EDX).

The X-ray diffraction analysis was carried out on powder using a Philips PW 1800 apparatus (K$\alpha$ copper line $\lambda = 1.5418$ Å, 40 kV, 20 mA). The spectra of the different samples were recorded in a $2\theta$ range between 1° and 80° with an angular increment of 0.02°. Infrared spectra were obtained using a Fourier transform spectrometer (FTIR) of Shimadzu IRAffinity-1S type. The samples were packaged as pellets with 12 mm diameter. The absorption spectra were recorded in the range of 400 to 4000 $cm^{-1}$ in absorbance with a resolution of 2 $cm^{-1}$. The textural was examined by the BET method using a Micromeritics ASAP 2010 device. The samples were degassed beforehand at 100°C under vacuum overnight. The DTA and TGA were carried out by using a Shimadzu TA-60 type apparatus operating under air with a linear heating rate of 10°C/min from room temperature up to 600°C. The morphology of the clay powder was observed using a scanning electron microscope TESCAN Vega3-EDAX instrument with an accelerating voltage of 20 kV. The elemental composition of our materials was determined by energy-dispersive X-ray spectroscopy (EDX).

### 2.5. Methods.
Experiment adsorption was carried out in closed bottles protected from light. 20 ml of the aqueous solution of thymol, with an initial concentration of 80 mg/L, was brought into contact with 100 mg sample of Rhassoul. The adsorption kinetics of thymol on the different solids at room temperature was monitored at regular times (30 min, 1 h, 2 h, 4 h, 6 h, and 8 h) at a pH equal to 9. The mixture was passed through a filtration system with a 0.45 $\mu$m membrane before analysis. The filtrate was then analyzed by UV-visible spectroscopy, and the residual concentration was determined by measuring the absorbance at the wavelength of 273 nm.

The amount of thymol adsorbed (mg/g) was calculated using the following equation [17]:

$$q_e = \frac{(C_0 - C_e) \cdot V}{m},\tag{1}$$

where $C_0$ and $C_e$ are, respectively, the initial and equilibrium concentrations of thymol in mg/L; $m$ is the mass of the adsorbent in g; $V$ is the volume of the thymol solution in mL; and $q_e$ is the amount adsorbed per gram of the adsorbent in mg/g.

The adsorption isotherms were carried out under the same conditions as those of the adsorption kinetics using the increasing concentration of thymol from 0 to 200 mg/L. The contents of the flasks were stirred for 5 hours until reaching the equilibrium time and then centrifuged. Residual concentrations and adsorbed quantities were determined as previously by (1).

## 3. Results and Discussion

### 3.1. Characterization of Rhassoul

#### 3.1.1. XRD Analysis.
The XRD patterns of raw Ghassoul clay ((a) in Figure 1) and the purified Rhassoul ((b) in Figure 1)
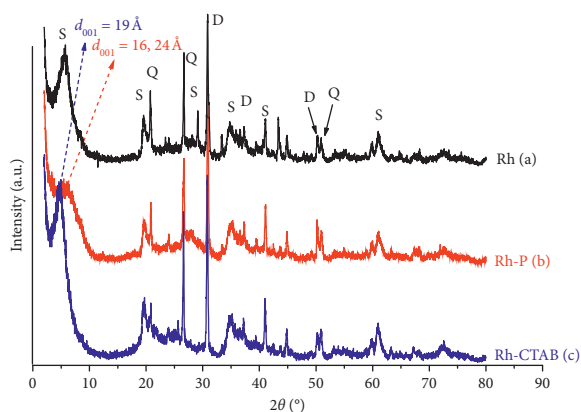
Figure 1: XRD patterns of Rh (a), Rh-P (b), and Rh-CTAB (c).

Table 1: Basal distance of the diffraction peak (001) of the Rh-P and Rh-CTAB.

| Clay | $2\theta$ (°) | $d_{001}$ (Å) |
| --- | --- | --- |
| Rh-P | 5.44 | 16.24 |
| Rh-CTAB | 4.65 | 19.00 |

are similar, which shows that the dominant phase is stevensite with the presence of quartz and dolomite. The XRD patterns reveal the presence of the diffraction peak characteristic of stevensite (S) at $2\theta = 5.36°$, $19.65°$, $29.13°$, $34.73°$, $40.91°$, and $60.6°$ which is the majority phase of Rhassoul. The presence of the dolomite phase (D) is confirmed by the diffraction peak at $2\theta = 30.67°$, $37.24°$, and $50.18°$. The quartz phase (Q) in small quantity as an impurity is manifested by the diffraction peak at $2\theta = 20.81°$, $26.62°$, and $50.95°$. These results are similar to those reported previously by Benhammou et al. [18].

The diffractogram of Rhassoul modified with cetyltrimethylammonium bromide (CTAB) ((c) in Figure 1) reveals the displacement of the position of the diffraction peak (001) of stevensite towards the low values of $2\theta$. This shows an expansion of the Rhassoul interface space due to the insertion of the CTAB cationic surfactant. In Table 1, we give the positions in Å of the diffraction peak (001) for the starting compound and that treated by CTAB.

The baseline distance $d_{001}$ increases by 16.24 Å for the purified Rhassoul at 19 Å for the Rh-P intercalated by CTAB. This indicates that the increase in the spacing $d_{001}$ is attributed to the exchange of $Na^+$ by the cationic surfactant in the interspace.

### 3.1.2. FTIR Analysis.
Figure 2 shows the infrared spectra of the two clays studied. The adsorption bands appearing in the 3700 to 3620 cm$^{-1}$ region correspond to the vibrations of the structural hydroxyl groups characteristic of the Rh-P and to the elongation vibrations of the OH group of the adsorbed water. The exact position of these bands and their intensities vary according to the nature of the molecule. They appear in the Rh-P at 3439 cm$^{-1}$ and the Rh-CTAB at 3416 cm$^{-1}$. The band corresponding to the stretching vibration of N–H groups appears around 3680 cm$^{-1}$, and those corresponding to the vibration of symmetrical and asymmetrical stretching of the C–H bond in $CH_2$ and $CH_3$ appear, respectively, at 2927 cm$^{-1}$ and 2855 cm$^{-1}$ (Figure 2(b)). The water molecules of the bending vibration of H–OH bands appear around 1632 cm$^{-1}$, while the bands characteristic of carbonates are detected in the purified and the modified Rhassoul at 1446 cm$^{-1}$, 1464 cm$^{-1}$, and 880 cm$^{-1}$. The characteristic

bands of vibration deformation of the Si–O bond of quartz manifest at 676 cm$^{-1}$ and 468 cm$^{-1}$ for the purified Rhassoul and 672 cm$^{-1}$ and 471 cm$^{-1}$ for the modified one by CTAB. The infrared spectra of these solids also show the bands corresponding to the stretching vibration of the group Si–O–Si quartz at 1024 cm$^{-1}$ for both purified and modified clays.

The functions of the main vibration bands observed in the spectrum of the Rh-P and Rh-CTAB are shown in Table 2.

The results obtained by infrared are in good agreement with those revealed by X-ray diffraction. Both clays contain quartz.

### 3.1.3. Scanning Electron Microscopy and Energy-Dispersive X-Ray Spectroscopy (SEM/EDX).
The SEM shows that the Rh-P ((a) in Figure 3) and Rh-CTAB ((a) in Figure 4) have an outer surface with more or less irregular form of platelets and heterogeneous structure ((a) in Figure 4).

On the contrary, the EDX spectrum of the Rh-P ((b) in Figure 3) shows the presence of chemical elements in the purified Rhassoul (Si, Al, Mg, Fe, K, P, S, O, and Ca). Table 3 shows a very high percentage of Si and Mg mainly due to the predominant presence of quartz and magnesium oxide in the clay studied [19]. These results confirm the validity of the X-ray diffraction analysis. The EDX spectrum of the Rh-CTAB ((b) in Figure 4) shows the presence of the same chemical elements as the purified Rhassoul with the appearance of the carbon element, which confirms the presence of the CTAB surfactant (Table 4) in agreement with the FTIR and the XRD which showed, respectively, the bands characteristics of C–H and N–H groups and a shift of the diffraction peak (001). The results of the analysis are summarized in Tables 3 and 4 for the two clays.

### 3.1.4. DTA/TGA.
The DTA/TGA thermogram of the Rh-P (Figure 5) reveals the presence of an endothermic peak, with a maximum around 84°C, accompanied by a 7% loss of mass, which is attributed to the adsorbed water in the surface of the clay, and an exothermic peak whose maximum appears around 332°C accompanied by a loss of mass equal to 4% corresponding to the allotropic transformation of stevensite into enstatite [20].

The DTA/TGA thermogram of the Rh-CTAB (Figure 6) shows the presence of (i) an endothermic peak around 56°C with a weight loss of about 2%, which corresponds to the removal of water adsorbed on the surface, (ii) an endothermic peak around 290°C corresponding to the loss of the intercalated water molecules, and (iii) an exothermic peak whose maximum occurs at 346°C accompanied by a loss of mass equal to 20%, corresponding to the destruction of the cationic surfactant
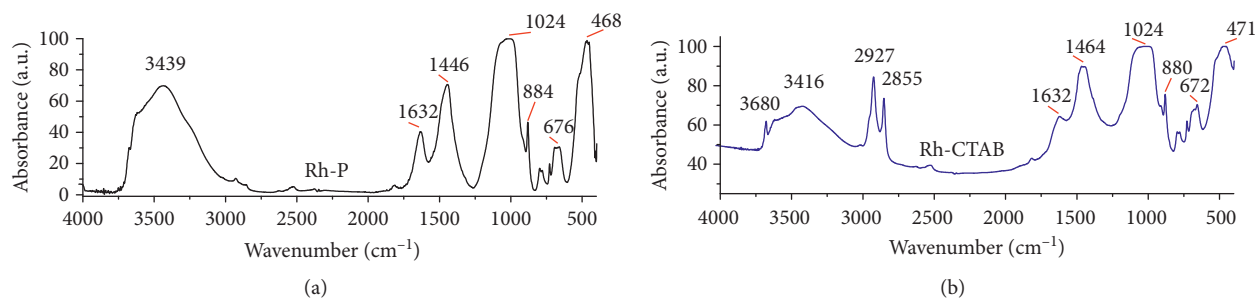
Figure 2: Infrared spectra of the Rh-P (a) and Rh-CTAB (b).

Table 2: Vibration bands of the Rh-P and Rh-CTAB.

| Vibration frequencies (cm$^{-1}$) | | Functions |
|---|---|---|
| Rh-P | Rh-CTAB | |
| — | 3680 | Stretching vibration of N–H groups |
| 3439 | 3416 | Stretching vibration of hydroxyl O–H |
| — | 2927 and 2855 | Symmetric and asymmetric stretching vibrations of C–H in CH$_2$ and CH$_3$ |
| 1632 | 1632 | Vibration deformation of the H–OH water molecules |
| 1446 | 1464 | Vibrations due to the presence of carbonates and C–H deformation vibration of Rhassoul modified |
| 1024 | 1024 | Stretching vibration of silica Si–O–Si |
| 884 | 880 | Bending vibration (CO$_3$) and Al$_2$OH |
| 676 and 468 | 672 and 471 | Vibration deformation of Si–O–Si |



Lsec: 30.0  0 Cnts 0.000 keV det: octane plus det
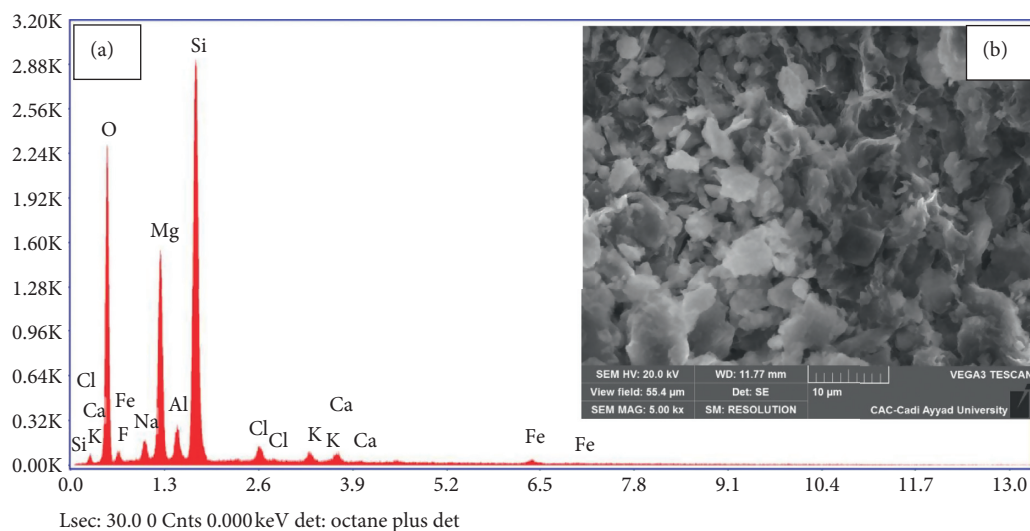
Figure 3: SEM-EDX micrograph of the Rh-P.

CTAB intercalated into the interlayer space and the allotropic transformation of stevensite into enstatite.

## 3.2. Adsorption Studies

### 3.2.1. Adsorption Kinetics.
From Figure 7, it is seen that the adsorbed amount of thymol increases with contact time and equilibrium is reached near the end of 60 minutes for both the clays with a retention capacity $q_e \approx 16$ mg/g of the modified Rhassoul and $q_e \approx 6$ mg/g of the purified Rhassoul.

The curves represent the adsorption kinetics of thymol (Figure 7) makes it possible to highlight two phases; at first,

the rapid and maximum adsorption is reached after about thirty minutes and corresponds to the external mass transfer. The second phase is slow and is related to the diffusion phenomenon as it has been obtained by Ziyat et al. in adsorption of thymol onto hydrotalcite Mg–Al–CO$_3$ [21]. This is related to the availability of free clay active sites at the beginning of the experiment and decreases gradually as we advance in time.

The results of the adsorption kinetics show that the amount of thymol adsorbed is greater for the Rh-CTAB compared to the Rh-P because the purified Rhassoul is initially hydrophilic and becomes organophilic after treatment with CTAB; subsequently, the affinity of the latter to

Lsec: 30.0 0 Cnts 0.000 keV det: octane plus det
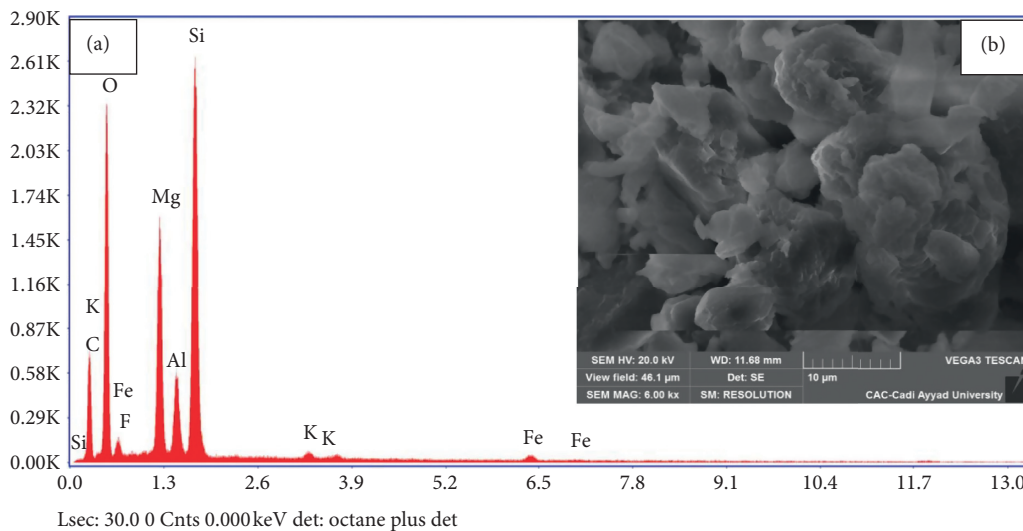
FIGURE 4: SEM-EDX micrograph of the Rh-CTAB.

TABLE 3: Chemical elements of the Rh-P in %.

| Elements | O | F | Na | Mg | Al | Si | Cl | K | Ca | Fe |
|---|---|---|---|---|---|---|---|---|---|---|
| Weight % | 44.6 | 2.7 | 2.0 | 14.9 | 2.4 | 29.4 | 1.3 | 0.8 | 1.0 | 0.9 |

TABLE 4: Chemical elements of the Rh-CTAB in %.

| Elements | C | O | F | Mg | Al | Si | K | Fe |
|---|---|---|---|---|---|---|---|---|
| Weight % | 27.7 | 39.9 | 3.6 | 9.2 | 3.6 | 14.6 | 0.4 | 0.9 |
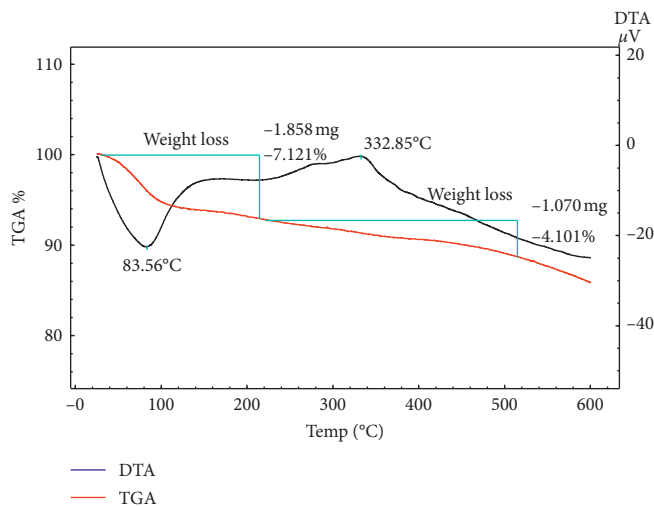


FIGURE 5: DTA/TGA thermogram of the Rh-P.



FIGURE 6: DTA/TGA thermogram of the Rh-CTAB.
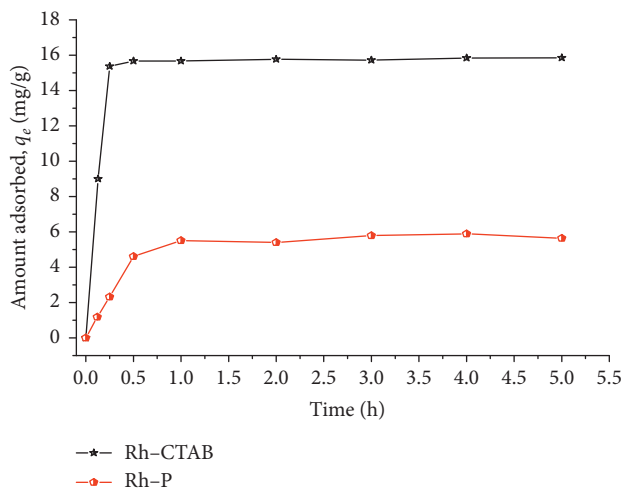


FIGURE 7: Adsorption kinetics of thymol onto the Rh-P and Rh-CTAB.

thymol increases, and the adsorbed quantity also increases. Similar results were obtained for Cr(VI) adsorption onto Al-montmorillonite and CTA-montmorillonite [22] and for Cr(VI) adsorption onto CTA-stevensite [10].

To understand the behavior of the adsorbent and examine the control mechanism of the adsorption process, the pseudo-first-order models, pseudo-second-order models,

and intraparticle diffusion were applied to the experimental data.

The pseudo-first-order kinetic model [23–25] is given by

$$\ln(q_e - q_t) = \ln q_e - k_1 \cdot t, \tag{2}$$

where $q_e$ is the amount adsorbed at equilibrium per gram of the adsorbent ($\text{mg·g}^{-1}$), $q_t$ represents the quantity adsorbed at a given instant $t$ ($\text{mg·g}^{-1}$), $t$ is the contact time (min), and $k_1$ is the adsorption rate constant for the first order ($\text{min}^{-1}$). By plotting $\ln(q_e - q_t)$ versus the time $t$, the adsorption rate constant $k_1$ and the equilibrium adsorbed quantity $q_e$ can be determined.

The pseudo-second-order kinetic model [24, 26] is expressed as

$$\frac{t}{q_t} = \frac{1}{k_2 \cdot q_e^2} + \frac{t}{q_e}, \tag{3}$$

where $k_2$ is the adsorption rate constant for the pseudo-second-order ($\text{g·mg}^{-1}\cdot\text{min}^{-1}$) and $q_e$ is the amount of the adsorbate at equilibrium per gram of the adsorbent ($\text{mg·g}^{-1}$).

The equilibrium adsorbed quantity ($q_e$) and the constant $k_2$ can be determined experimentally from the slope and ordinate at the origin of the line as $t/q_t$, a function of $t$.

It is noticed from Figure 8 that the pseudo-second-order model describes better the results of the adsorption of thymol onto the two clays. The adsorbed quantity values found in this model are very close to those determined experimentally (Table 5).

The values of the correlation coefficient $R^2$ of the second-order model are close to 1 ($R^2 \geq 0.99$) than those of the first-order model. The pseudo-second-order model is the most reliable for determining the order of adsorption kinetics of thymol on both clays and gives a 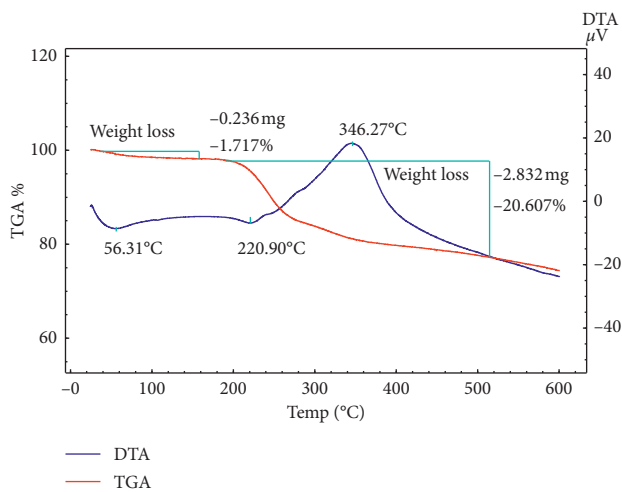better description of the adsorption kinetics compared to the pseudo-first-order model. This model was based on the assumption that the rate-limiting step might be chemical sorption or chemisorption involving valence forces through sharing or exchange of electrons between the adsorbent and the adsorbate [27, 28]. Similar results have been reported in the study of the adsorption of thymol onto clay-based adsorbents [14, 29], the adsorption of the basic yellow cationic dye onto Moroccan stevensite [5], and the adsorption of methyl violet onto rich clay stevensite from Morocco [6].

The intraparticle diffusion model proposed by Weber and Morris [30] is given by

$$q_t = k_d \cdot t^{1/2} + C, \tag{4}$$

where $k_d$ is the constant of intraparticle diffusion ($\text{mg·g}^{-1}\cdot\text{h}^{-1/2}$) and $C$ is a constant which characterizes the diffusion of the solute in the liquid phase.

The plot of the adsorbed quantity $q_t$ versus $t^{1/2}$ shows two separate linear steps (Figure 9): a fast step at the beginning followed by a slow evolution towards the equilibrium state of adsorption for whatever adsorbent. The first step can be attributed to the external diffusion of the adsorbate to the surface of the adsorbent and the second step corresponds to the intraparticle diffusion due

to the adsorbent-adsorbent interaction [31], confirming the results obtained from the pseudo-second-order kinetic model.

From Table 6, it is remarked that the values of $C$, the diffuse layer thickness constant, are different from 0, suggesting that intraparticle scattering is not the only factor controlling the adsorption rate of thymol on both clays. Wu et al. observed similar results in the study of the characteristics of the pseudo-second-order kinetic model for liquid-phase adsorption [32]. The surface properties including the number of adsorption sites also have an effect on the adsorption.

### 3.2.2. Adsorption Isotherms.
The results of the study of thymol isothermal adsorption of the two samples are represented by the adsorbed amount based on the residual concentration of thymol. The obtained experimental isotherms are shown in Figure 10. These isotherms were compared with models of Langmuir and Freundlich, whose equations are given below.

Langmuir model [33]: it assumes that there is no interaction between the adsorbate molecules, and the maximum adsorption corresponds to the monolayer coverage given by

$$\frac{q_e}{q_{\max}} = \frac{(k_L \cdot C_e)}{(1 + k_L \cdot C_e)}. \tag{5}$$

The linear form of Langmuir (5) is

$$\frac{1}{q_e} = \frac{1}{C_e} \cdot \frac{1}{(q_{\max} \cdot K_L)} + \frac{1}{q_{\max}}, \tag{6}$$

where $q_e$ is the adsorbed amount at equilibrium (mg/g), $C_e$ is the equilibrium concentration (mg/L), $K_L$ is the equilibrium constant of Langmuir (L/mg), and $q_{\max}$ is the maximum adsorption amount (mg/g). The separation factor ($R_L$) is a dimensionless parameter whose expression is given by

$$R_L = \frac{1}{1 + K_L \cdot C_0}, \tag{7}$$

where $C_0$ is the initial concentration of the adsorbate (mg/L) and $K_L$ (L/mg) is the constant of Langmuir. When the separation factor ($R_L$) is between 0 and 1, the adsorption process is considered favorable [34, 35].

Freundlich model [36]: it is usually applied to the adsorption on heterogeneous solid surfaces it is represented by the following empirical formula:

$$q_e = k_F \cdot C_e^{1/n}. \tag{8}$$

The commonly used form is the linear form given by

(a)

(b)
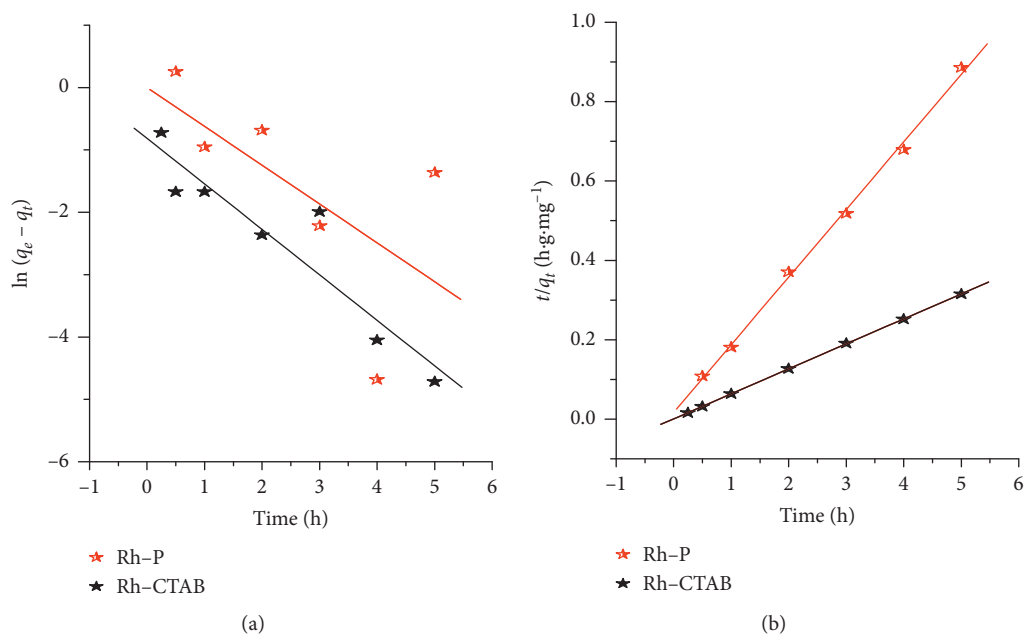
Figure 8: Linear representation of the kinetic model: (a) pseudo-first-order and (b) pseudo-second-order models for adsorption of thymol onto the Rh-P and Rh-CTAB.

Table 5: Pseudo-first-order and pseudo-second-order kinetic parameters for the adsorption of thymol onto the Rh-P and Rh-CTAB.

| Sample | | Pseudo-first-order model | | | | Pseudo-second-order model | |
| | $q_{exp}$ (mg/g) | $q_e$ (mg/g) | $K_1$ (h$^{-1}$) | $R^2$ | $q_e$ (mg/g) | $K_2$ (g·mg$^{-1}$·h$^{-1}$) | $R^2$ |
| --- | --- | --- | --- | --- | --- | --- | --- |
| Rh-P | 5.89 | 1.001 | 0.623 | 0.636 | 5.870 | 1.700 | 0.998 |
| Rh-CTAB | 15.85 | 0.443 | 0.730 | 0.935 | 15.891 | 4.747 | 0.999 |
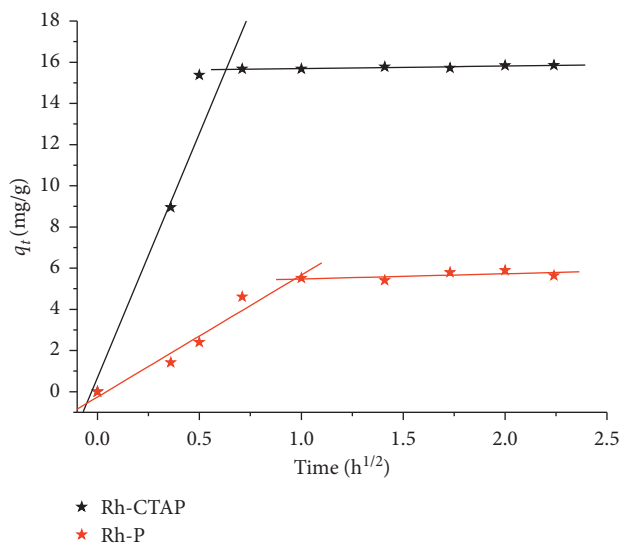


Figure 9: Model of intraparticle diffusion of thymol onto the Rh-P and Rh-CTAB.

Table 6: Intraparticle diffusion parameters of thymol onto the Rh-P and Rh-CTAB.

| Samples | | 1st line | | | 2nd line | |
| | $C$ | $K_{d1}$ (mg·g$^{-1}$·h$^{-1/2}$) | $R^2$ | $C$ | $K_{d2}$ (mg·g$^{-1}$·h$^{-1/2}$) | $R^2$ |
| --- | --- | --- | --- | --- | --- | --- |
| Rh-P | 0.25 | 5.91 | 0.98 | 5.22 | 0.25 | 0.62 |
| Rh-CTAB | 0.7 | 23.69 | 0.96 | 15.57 | 0.12 | 0.90 |

(a)



(b)
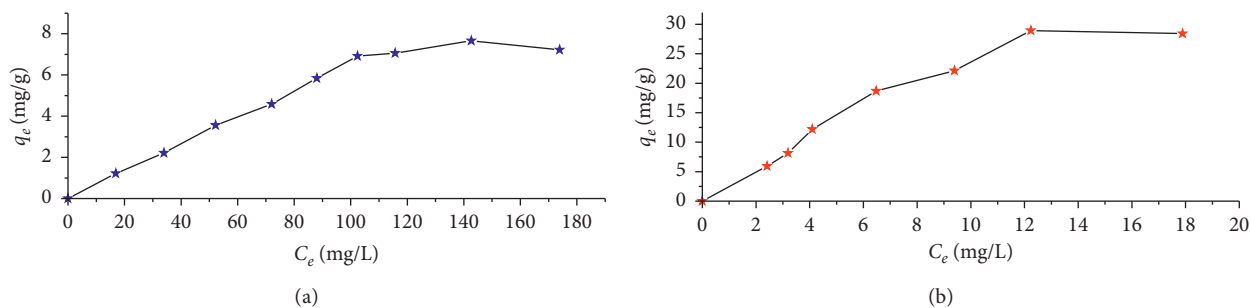
FIGURE 10: Adsorption isotherms of thymol onto the Rh-P (a) and Rh-CTAB (b).



★ Rh–P
★ Rh–CTAB

(a)



★ Rh–P
★ Rh–CTAB

(b)
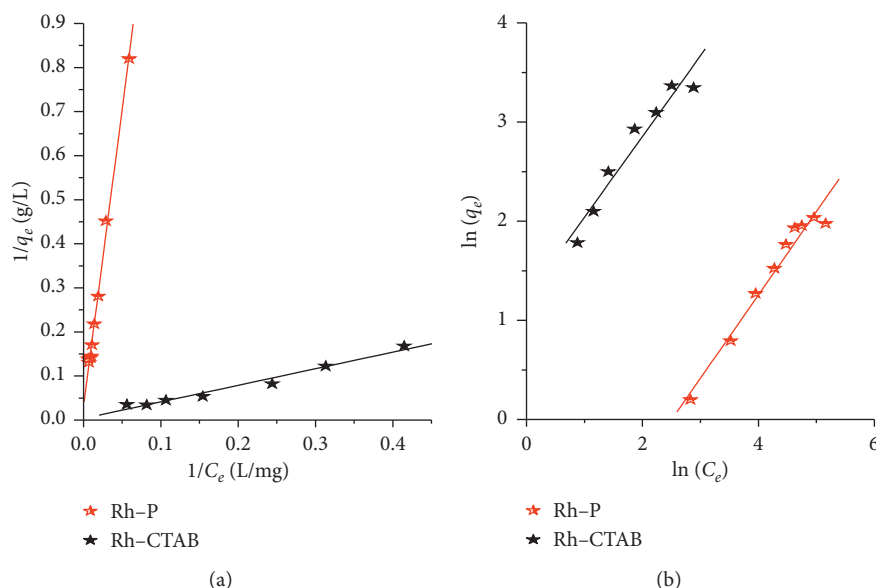
FIGURE 11: Linear representation of thymol adsorption isotherms onto the Rh-P and Rh-CTAB: Langmuir (a) and Freundlich (b).

TABLE 7: Langmuir and Freundlich fitting parameters for the adsorption of thymol onto the Rh-P and Rh-CTAB.

| Samples | Langmuir | | | | Freundlich | | |
|---|---|---|---|---|---|---|---|
| | $q_{max}$ (mg/g) | $K_L$ (mg/g) | $R_L$ | $R^2$ | $n$ | $K_F$ (mg g$^{-1}$) | $R^2$ |
| Rh-P | 31.221 | 0.0024 | 0.912–0.675 | 0.997 | 1.190 | 0.122 | 0.982 |
| Rh-CTAB | 277.01 | 0.010 | 0.33–0.714 | 0.986 | 1.228 | 3.404 | 0.970 |

$$\ln q_e = \ln K_F + \frac{1}{n} \ln C_e, \qquad (9)$$

where $q_e$ is the concentration of the adsorbate (mg/g), often expressed in mg/L, $K_F$ is a constant of the adsorption capacity, and $n$ is a constant relative to the affinity between the adsorbate and the surface. The values of $n > 1$ represent favorable adsorption conditions [37].

The curves of linear transforms obtained by Langmuir and Freundlich models are shown in Figure 11, and different parameters of the two models are summarized in Table 7.

From the results of Table 7, it is remarked that the correlation coefficients $R^2$ of both models (Langmuir and Freundlich) show a good correlation with experimental data for both clays ($R^2 \geq 0.97$). However, the amounts adsorbed $q_{max}$ calculated from the Langmuir model are much different from those found experimentally for both clays, which means that the Langmuir model is not valid to describe the adsorption.

In addition, the values of $n$ from the Freundlich model (Table 7) are greater than 1 for both clays studied, indicating that the adsorption is favorable and the values of $K_F$ are large. Therefore, the Freundlich model is most likely to characterize the adsorption of thymol onto both adsorbents. Similar results have been observed for the adsorption of

thymol onto various adsorbents [14], for the removal of the basic yellow cationic dye by Moroccan stevensite [5], and for the adsorption of thymol onto hydrotalcite Mg–Al–CO$_3$ and onto its counterpart enabled at 500°C [21]. In conclusion, the model which adequately expresses the experimental data of the adsorption of thymol onto the two clays is that of Freundlich.

## 4. Conclusion

Interesting results are found in this study as follows.

Rhassoul used in this study has a majority stevensite phase characteristic of the clay from Morocco. This treated with CTAB has an expansion space interfolliaire, indicating the insertion of the surfactant as it was observed by XRD and FTIR. The study of the adsorption of thymol onto Rhassoul shows that there is affinity of thymol to Rhassoul. The results of the adsorption kinetics show that the adsorption of thymol onto the purified Rhassoul and modified one by CTAB is fast and the maximum quantity is reached after 40 min of adsorption. The modeling of the adsorption kinetics revealed its conformity to the pseudo-second-order model for the purified Rhassoul and also for its counterpart modified by CTAB. The experimental results are favorable for adsorption by the Freundlich model than by the Langmuir model for both clays. The modification of Rhassoul by CTAB greatly improves its adsorption capacity. It goes from almost 6 mg/g for the purified Rhassoul to a value of about 16 mg/g for the modified Rhassoul (Rh-CTAB).

## Data Availability

The authors confirm that all data underlying the findings of this study are fully available without restriction.

## Conflicts of Interest

The authors declare no conflicts of interest.

## Acknowledgments

## References

[1] N. Trauth, *Argiles Évaporitiques Dans la Sédimentation Carbonateé Continentale et Épicontinentale Tertiaire*, Bassins de Paris, de Mormoiron et de Salinelles (France) et du Jbel Ghassoul (Maroc), Paris, France, 1974.

[2] S. Azarkan, A. Peña, K. Draoui, and C. I. Sainz-Díaz, "Adsorption of two fungicides on natural clays of Morocco," *Applied Clay Science*, vol. 123, pp. 37–46, 2016.

[3] K. Elass, A. Laachach, A. Alaoui, and M. Azzi, "Removal of methylene blue from aqueous solution using ghassoul, a low-cost adsorbent," *Applied Ecology and Environmental Research*, vol. 8, no. 2, pp. 153–163, 2010.

[4] Y. El Mouzdahir, A. Elmchaouri, R. Mahboub, A. Gil, and S. A. Korili, "Adsorption of methylene blue from aqueous solutions on a moroccan clay," *Journal of Chemical & Engineering Data*, vol. 52, no. 5, pp. 1621–1625, 2007.

[5] M. Ajbary, A. Santos, V. Morales-Flórez, and L. Esquivias, "Removal of basic yellow cationic dye by an aqueous dispersion of Moroccan stevensite," *Applied Clay Science*, vol. 80-81, pp. 46–51, 2013.

[6] K. Elass, A. Laachach, A. Alaoui, and M. Azzi, "Removal of methyl violet from aqueous solution using a stevensite-rich clay from Morocco," *Applied Clay Science*, vol. 54, no. 1, pp. 90–96, 2011.

[7] Y. El Mouzdahir, A. Elmchaouri, R. Mahboub et al., "Interaction of stevensite with Cd$^{2+}$ and Pb$^{2+}$ in aqueous dispersions," *Applied Clay Science*, vol. 35, no. 1-2, pp. 47–58, 2007.

[8] Y. Bentahar, C. Hurel, K. Draoui, S. Khairoun, and N. Marmier, "Adsorptive properties of Moroccan clays for the removal of arsenic (V) from aqueous solution," *Applied Clay Science*, vol. 119, pp. 385–392, 2016.

[9] L. Bouna, B. Rhouta, M. Amjoud et al., "Correlation between eletrokinetic mobility and ionic dyes adsorption of Moroccan stevensite," *Applied Clay Science*, vol. 48, no. 3, pp. 527–530, 2010.

[10] A. Benhammou, A. Yaacoubi, L. Nibou, and B. Tanouti, "Chromium (VI) adsorption from aqueous solution onto Moroccan Al-pillared and cationic surfactant stevensite," *Journal of Hazardous Materials*, vol. 140, no. 1-2, pp. 104–109, 2007.

[11] A. Benhammou, A. Yaacoubi, L. Nibou, and B. Tanouti, "Study of the removal of mercury(II) and chromium(VI) from aqueous solutions by Moroccan stevensite," *Journal of Hazardous Materials*, vol. 117, no. 2-3, pp. 243–249, 2005.

[12] Y. Li, A.-S. Fabiano-Tixier, and F. Chemat, "Essential oils: from conventional to green extraction," in *Essential Oils as Reagents in Green Chemistry*, pp. 9–21, Springer, Cham, Switzerland, 2014.

[13] M. M. G. Nguemtchouin, M. B. Ngassoum, L. S. T. Ngamo, X. Gaudu, and M. Cretin, "Insecticidal formulation based on *Xylopia aethiopica* essential oil and kaolinite clay for maize protection," *Crop Protection*, vol. 29, no. 9, pp. 985–991, 2010.

[14] M. G. M. Nguemtchouin, M. B. Ngassoum, R. Kamga et al., "Characterization of inorganic and organic clay modified materials: an approach for adsorption of an insecticidal terpenic compound," *Applied Clay Science*, vol. 104, pp. 110–118, 2015.

[15] L. A. Tapondjou, C. Adler, H. Bouda, and D. A. Fontem, "Efficacy of powder and essential oil from *Chenopodium ambrosioides* leaves as post-harvest grain protectants against six-stored product beetles," *Journal of Stored Products Research*, vol. 38, no. 4, pp. 395–402, 2002.

[16] M. M. G. Nguemtchouin, M. B. Ngassoum, L. S. T. Ngamo et al., "Adsorption of essential oil components of *Xylopia aethiopica* (Annonaceae) by kaolin from Wak, Adamawa province (Cameroon)," *Applied Clay Science*, vol. 44, no. 1-2, pp. 1–6, 2009.

[17] Y. Huang, X. Ma, G. Liang, and H. Yan, "Adsorption of phenol with modified rectorite from aqueous solution," *Chemical Engineering Journal*, vol. 141, no. 1-3, pp. 1–8, 2008.

[18] A. Benhammou, A. Yaacoubi, L. Nibou, and B. Tanouti, "Adsorption of metal ions onto Moroccan stevensite: kinetic and isotherm studies," *Journal of Colloid and Interface Science*, vol. 282, no. 2, pp. 320–326, 2005.

[19] A. Benhammou, *Valorisation de la stevensite du jbel rhassoul: application à l'adsorption des métaux lourds*, Ph.D. thesis, Cadi Ayyad University, Marrakesh, Morocco, 2005.

[20] G. T. Faust, K. J. Murata, and Stevensite, "Redefined as a member of the montmorillonite group," *American Mineralogist*, vol. 38, pp. 973–987, 1953.

[21] H. Ziyat, M. Naciri Bennani, H. Hajjaj, S. Mekdad, and O. Qabaqous, "Synthesis and characterization of crude hydrotalcite Mg-Al-CO$_3$: study of thymol adsorption," *Research on Chemical Intermediates*, vol. 44, no. 7, pp. 4163–4177, 2018.

[22] B. S. Krishna, D. S. R. Murty, and B. S. Jai Prakash, "Surfactant-modified clay as adsorbent for chromate," *Applied Clay Science*, vol. 20, no. 1-2, pp. 65–71, 2001.

[23] S. Lagergren, "Zur theories der sogenannten adsorption gelöster stoffe," *Kungliga Svenska Vetenskapsakademiens Handlingar*, vol. 4, pp. 1–39, 1898.

[24] Y. S. Ho and G. McKay, "Sorption of dye from aqueous solution by peat," *Chemical Engineering Journal*, vol. 70, no. 2, pp. 115–124, 1998.

[25] Y.-S. Ho, "Citation review of lagergren kinetic rate equation on adsorption reactions," *Scientometrics*, vol. 59, no. 1, pp. 171–177, 2004.

[26] Y. S. Ho and G. McKay, "Pseudo-second order model for sorption processes," *Process Biochemistry*, vol. 34, no. 5, pp. 451–465, 1999.

[27] F. Jia, Q. Wang, J. Wu, Y. Li, and S. Song, "Two-dimensional molybdenum disulfide as a superb adsorbent for removing Hg$^{2+}$ from water," *ACS Sustainable Chemistry & Engineering*, vol. 5, no. 8, pp. 7410–7419, 2017.

[28] Y. Ho and G. Mckay, "The kinetics of sorption of divalent metal ions onto sphagnum moss peat," *Water Research*, vol. 34, no. 3, pp. 735–742, 2000.

[29] M. EL Miz, S. Salhi, I. Chraibi, A. El Bachiri, M. Fauconnier, and A. Tahani, "Characterization and adsorption study of thymol on pillared bentonite," *The Journal of Physical Chemistry*, vol. 4, no. 2, pp. 98–116, 2013.

[30] J. C. Weber and W. J. Morris, "Kinetics of adsorption of carbon from solutions," *Journal of the Sanitary Engineering Division American Society*, vol. 89, pp. 31–63, 1963.

[31] G. Mckay, "The adsorption of dyestuffs from aqueous solutions using activated carbon: an external mass transfer and homogeneous surface diffusion model," *AIChE Journal*, vol. 31, no. 2, pp. 335–339, 1985.

[32] F.-C. Wu, R.-L. Tseng, S.-C. Huang, and R.-S. Juang, "Characteristics of pseudo-second-order kinetic model for liquid-phase adsorption: a mini-review," *Chemical Engineering Journal*, vol. 151, no. 1–3, pp. 1–9, 2009.

[33] I. Langmuir, "The adsorption of gases on plane surfaces of glass, mica and platinum," *Journal of the American Chemical Society*, vol. 40, no. 9, pp. 1361–1403, 1918.

[34] K. R. Hall, L. C. Eagleton, A. Acrivos, and T. Vermeulen, "Pore- and solid-diffusion kinetics in fixed-bed adsorption under constant-pattern conditions," *Industrial & Engineering Chemistry Fundamentals*, vol. 5, no. 2, pp. 212–223, 1966.

[35] W. Weber and R. K. Chakravorti, "Pore and solid diffusion models for fixed bed adsorbers," *American Institute of Chemical Engineers*, vol. 20, no. 2, pp. 229–238, 1974.

[36] Freundlich, "Over the adsorption in solution," *The Journal of Physical Chemistry*, vol. 57, pp. 385–470, 1906.

[37] L. Wang, J. Zhang, R. Zhao, C. Li, Y. Li, and C. Zhang, "Adsorption of basic dyes on activated carbon prepared from *Polygonum orientale* Linn: equilibrium, kinetic and thermodynamic studies," *Desalination*, vol. 254, no. 1–3, pp. 68–74, 2010.

*Review Article*

# A Brief Review of Pulp and Froth Rheology in Mineral Flotation

**Lei Wang** [iD][1] **and Chao Li** [iD][2]

[1]*National Engineering Research Centre of Coal Preparation and Purification, China University of Mining and Technology, Xuzhou, China*
[2]*Henan Province Industrial Technology Research Institute of Resources and Materials, Zhengzhou University, Zhengzhou, China*

Correspondence should be addressed to Chao Li; c.li@zzu.edu.cn

In mineral flotation, rheological problems have limited the efficient upgrading of low-grade and complex ores. Since pulp and froth rheology are deemed to play different roles in influencing the separation performance, in this paper, a brief review on pulp and froth rheology in flotation is provided, with an objective of developing a basic understanding of rheology in flotation. The essential variables that affect the rheology of a flotation pulp and froth are discussed. The methods for measuring pulp and froth rheology are presented. The correlations of pulp and froth rheological properties to flotation performance are reviewed. Strategies that are currently used to mitigate the deleterious effects of problematic ores in flotation are also provided for flotation optimization. Research gaps are also proposed to highlight the need of further exploration of flotation rheology in future.

## 1. Introduction

Rheology is a science related to the deformation and flow of a material under applied stress, and it is widely applied to industrial, geological, and biological materials [1]. In mineral processing industries, it has witnessed a dramatic influence of the rheological behaviour of mineral particles in mineral slurry transportation, ore grinding, and mineral separation such as dewatering and flotation [2, 3]. In the past, investigations on the rheological effect of mineral particles mainly focused on slurry transportation and ore grinding [4]. As low-grade and complex ores such as clayey and fibrous ores in large quantities are being processed due to the depletion of high-grade ores (both metallic and nonmetallic) on a world scale, the fine/ultrafine grinding for the liberation of valuable minerals often leads to rheological difficulties and complexities in the subsequent separation process, namely, flotation [5, 6]. Thus, attention has been increasingly aroused as to the importance of flotation rheology.

Flotation is a useful technique for ore upgrading by exploiting differences in surface properties to separate valuable minerals from gangue, which is typically carried out in a flotation cell that contains both a pulp and froth zone

(see Figure 1). Flotation pulp and froth zone are well known to play different roles in determining flotation performance due to their different compositions and characteristics [8]. In the pulp zone, hydrophobic particles collide with air bubbles to form particle-bubble aggregates moving upwards against gravity to the froth zone while most hydrophilic gangue mineral particles report to the tailings. The froth zone further concentrates the collected particles by reducing the recovery of entrained gangue mineral particles to the concentrate stream, leading to an improved selectivity and recovery of the flotation process. In general, variations in flotation conditions could result in different rheological behaviours of mineral particles in the pulp and froth, thereby influencing the separation performance.

In the literature, Boger [9] has provided a review on the significance of rheology in mineral processing with detailed rheological behaviours of nonsettling mineral slurries and the relevant measuring methods. Farrokhpay [4] has reviewed the importance of rheology in mineral flotation with a focus on the correlation of flotation rheology to froth stability and flotation recovery. Cruz and Peng [10] and Cruz et al. [3] also offered reviews on flotation rheology particularly associated with rheology measurements of flotation
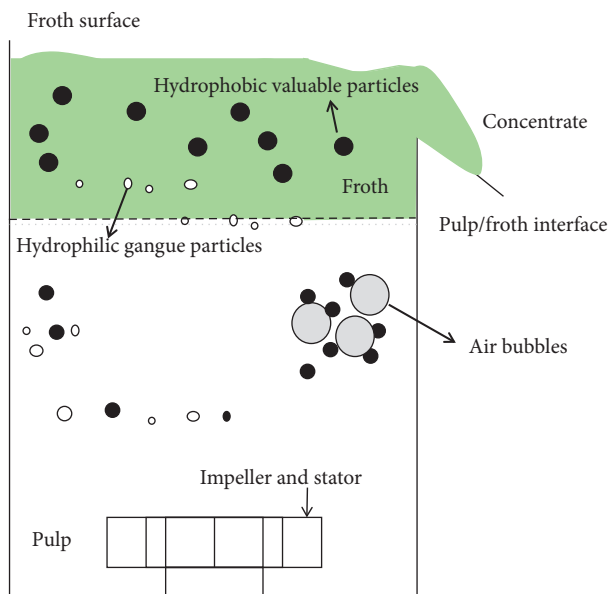
FIGURE 1: Processes of true flotation and entrainment in a flotation cell (after [7]).



FIGURE 2: Flow curves or rheograms representing the rheological behaviour of different flow types (after [11]).

pulps with a high clay content. In general, in mineral flotation, studies on flotation rheology have been detailed in many aspects including rheological effects on flotation response, influencing variables and rheological measurement techniques, in both the pulp and froth zone. In recent years, progress in flotation rheological investigations, especially the froth rheology, has been greatly advanced. However, no work is available yet that updates this progress to improve the understanding of rheology in mineral flotation.

In this paper, flotation pulp and froth rheology are reviewed in brief. The essential variables that affect flotation rheological behaviours, the techniques for rheology measurements, and the correlation of rheological characteristics to flotation performance are reviewed with respect to the pulp and the froth zone. Strategies that are currently attempted to mitigate the deleterious effects of problematic ores in flotation are also presented. Research gaps are also proposed to highlight the need of further exploration of flotation rheological effects in the future.

## 2. Rheology in Froth Flotation

The rheological behaviour of a material is often presented by a "flow curve" or "rheogram" obtained by plotting the shear stress against the shear rate obtained from a rheometer. Figure 2 shows five typical rheograms representing the Newtonian and the non-Newtonian behaviours including dilatant, plastic, pseudoplastic, and Bingham that a material could exhibit [11]. Yield stress and apparent viscosity are two important rheological parameters, of which the former represents the stress at which a material begins to deform plastically and the latter measures the resistance of a material to gradual deformation by shear stress. In flotation, mineral slurries made of good quality ores often display a Newtonian behaviour, whereas complex and low-grade ore slurries
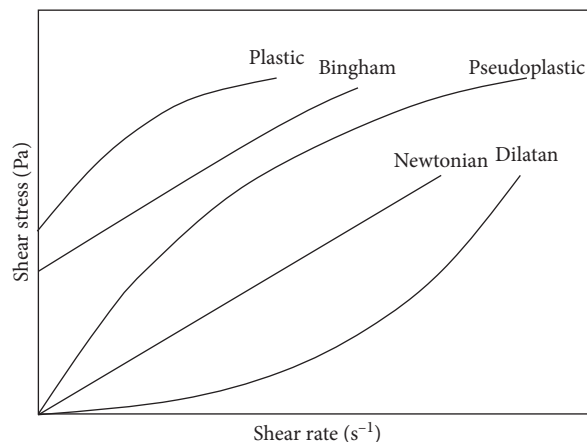
normally exhibit a pseudoplastic or Bingham behaviour [4]. Flotation froths, as indicated from the literature, exhibit pseudoplastic characteristics, similar to air-liquid foams [12–14].

The information regarding the rheological behaviour of flotation pulps and froths as exhibited in Figure 2 is usually incorporated in relationships between yield stress and viscosity using rheological models such as the Bingham, the Casson, and the Herschel–Bulkley model [15]. Among these models, the Herschel–Bulkley model is the most widely used one in flotation rheology characterisation, which is given as [15]

$$\tau = \tau_0 + K\dot{\gamma}^n, \tag{1}$$

where $\tau$ is the shear stress, $\tau_o$ is the yield stress, $\dot{\gamma}$ represents the shear rate, and $n$ and $K$ are the parameters representing the flow index and consistency index, respectively. When flow index is lower than 1, the fluid material behaves as pseudoplastic or plastic flow; if flow index is greater than 1, the material is dilatant flow. When $n$ is 1, the viscosity of the fluid material is constant, suggesting a Newtonian flow or Bingham flow. When the consistency index is high, the fluid material is more viscous.

## 3. Rheology of Flotation Pulp

*3.1. Variables Affecting Pulp Rheology.* The rheology of flotation pulp is a complex function of the physical properties of the continuous and discrete phases as well as of processes that occur at the scale of mineral particles. The principal factors affecting pulp rheology mainly include solids volume fraction, particle characteristics, and interaction between particles and its associated influencing variables such as shear rate and pulp chemistry. These influencing factors often combine to determine the rheological behaviour of flotation pulps.

*3.1.1. Solids Volume Fraction.* Solids volume fraction is one of the essential variables that dominate the rheology of mineral suspensions in mineral processing [16–18]. In

flotation, pulp apparent viscosity generally increases with increasing solid concentration of pulp slurries. Figure 3 shows the apparent viscosity of flotation samples with different solids concentrations obtained from processing two different platinum ores (UG2 ore and Great Dyke ore) [19]. Clearly, pulp solid concentration significantly affects the slurry rheological behaviour. And this effect of solid concentration on the pulp apparent viscosity has been widely attributed to the significant energy dissipation resulting from the friction between particles [15, 20].

In most flotation pulps, a low solid concentration is generally used. The more dilute the pulp, the cleaner the separation [21]. As can be seen in Figure 3, when the UG2 and Great Dyke feed solid concentration exceeds 25 vol.%, a discernible increase in the apparent viscosity of the feed samples could be detected, which would result in rheological complexities in the separation process. In mineral flotation, it has been reported that pulp solid concentration generally falls at 5–40 wt.% (11–20 vol.%), with an upper-bound concentration of about 50 wt.% (approximately 27 vol.%) [21, 22]. In this case, flotation pulps with good-quality ores are Newtonian or very close to Newtonian with a low viscosity, but those made of low-grade and complex ores are typically non-Newtonian exhibiting a pseudoplastic or Bingham behaviour, which could cause deleterious rheological effect on flotation, as evidenced in a number of studies [6, 23–25].

### 3.1.2. Particle Characteristics.

Flotation is often employed to float mineral particles with certain size, depending on the floatability of the particles within relevant limits of flotation conditions [26]. Particle size is well known to significantly affect the pulp rheological behaviour, and generally, the apparent viscosity of the pulp slurries increases as particle size decreases. Figure 4 shows the apparent viscosity of a gold ore slurry with high clay contents as a function of particle size [27]. Particle size effect became notable when the pulp solids concentration exceeded 25 wt.%, and the apparent viscosity of the mineral suspension increased with decreasing particle size (P80 of $125\,\mu m < 106\,\mu m < 53\,\mu m$). This clearly shows that the apparent viscosity is affected by particle size, and the interaction of particle size effect with pulp solid concentration is also indicated. In general, a decrease in particle size could result in a more complex rheological property such as shear thickening and aggregation of network structures, which inevitably entails a difficulty in the separation process [17, 27–29].

Pulp rheology is also affected by particle shape, although this effect has never been well studied in flotation [30]. Studies have shown that the rheology of mineral suspensions is associated with particle shape [10, 17, 31–34]. At the same particle volume fraction, the degree of frictions among irregular particles is greater than that among spherical particles [17]. For example, it has been found in the dense medium separation that the suspension of spherical particles of ferrosilicon exhibited lower viscosity than the irregular particles of ground magnetite for a given slurry density and particle size [35].
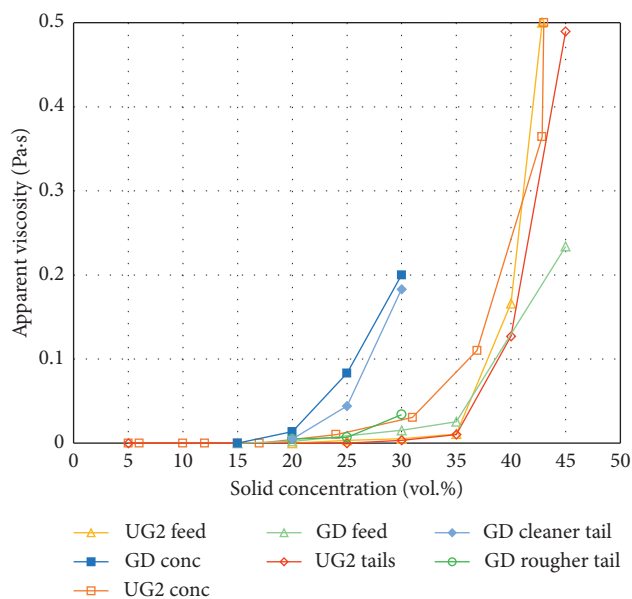


FIGURE 3: The comparison of the apparent viscosity (at $160\,s^{-1}$) of the UG2 and Great Dyke flotation samples at different solid concentrations (after [19]).
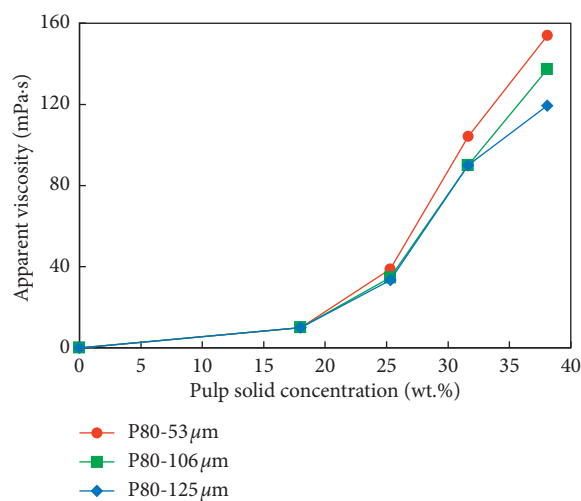


FIGURE 4: Apparent viscosity of the ore as a function of pulp density for different P80 values (after [27]).

Rheological complexities in flotation pulps also originate from the minerals themselves such as mineral surface charge distribution and morphologies. Studies on the correlation of rheological response and mineralogical content have shown that mineral type can significantly vary pulp rheological behaviour [6, 19, 25, 27, 34, 36–39]. Figure 5 shows the difference in the Bingham viscosity of mineral suspensions composed of different clay minerals that usually exist in real ores [6]. Clearly, the rheological behaviour of flotation pulps is closely associated with mineral type, and phyllosilicate minerals, particularly swelling clays and serpentine minerals, can result in higher viscosities compared with non-phyllosilicate minerals such as quartz.
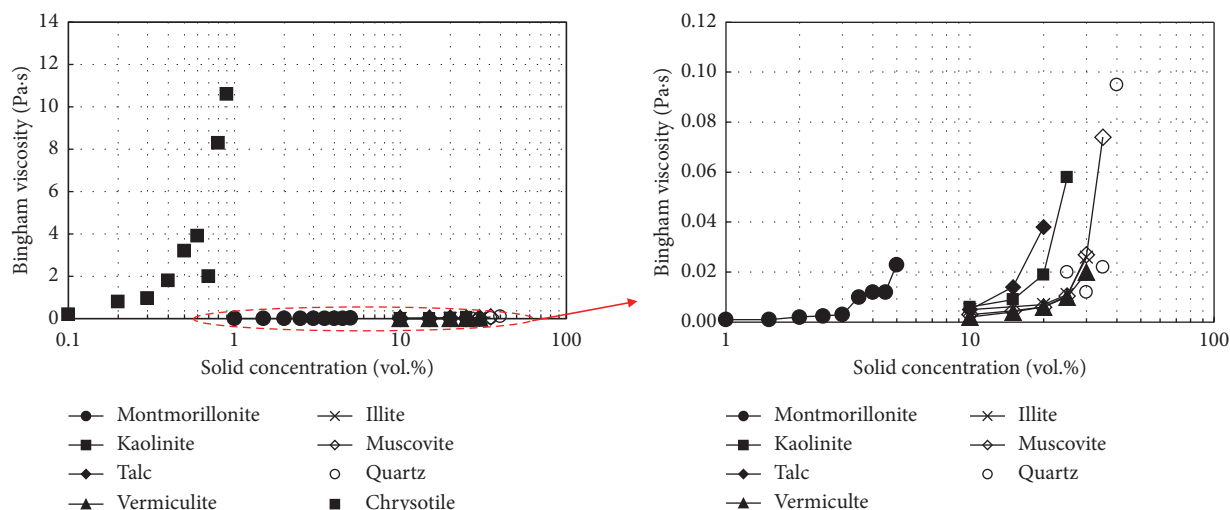
FIGURE 5: Comparison of the Bingham viscosities of different minerals (after [6]).

*3.1.3. Interparticle Interaction.* Since the presence of numerous fine/ultrafine particles (colloidal particles and clays) is a characteristic of pulps comprising low-grade and complex ores, interparticle interaction force becomes one of the most important aspects to determine the rheological properties of flotation pulps [10, 40]. Various mineral particles with different surface properties and a broad size distribution commonly exist in this type of flotation pulps, and therefore, many interactions can occur. Hard-sphere interaction, electrostatic interaction, steric interaction, and van der Waals attractions have been reported to govern the rheology of flotation pulps [15]. Depending on the complexity of particle surfaces, these interaction forces can be DLVO or non-DLVO [10].

It is known that interparticle interactions can be attractive or repulsive, but they are also susceptible to the shear rate and to pulp chemistry such as medium conditions (ionic strength and pH) and chemical reagents. For non-Newtonian flotation pulps, rheology is strongly dependent on the shear rate in a flotation cell [41, 42]. In several studies on pulp viscosity measurement (e.g., [19, 39, 43, 44]), apparent viscosity was obtained at $100 \, s^{-1}$ or $160 \, s^{-1}$ which are claimed to represent a typical shear rate in a mechanical flotation cell [19, 45]. Actually, a wide range of apparent viscosities can be displayed for non-Newtonian pulps in a flotation cell as the shear rate varies from high values close to the impeller to very low ones near the froth phase or in the pulp quiescence zone (see Figure 6). Thus, the rheological behaviour of these pulps also varies at different locations in the flotation cell. Since the collecting zone and quiescence zone in the pulp play different roles in the flotation process, it is advisable to obtain the rheological data from both areas to understand the pulp rheological effects.

In mineral flotation, various reagents can be added to facilitate the separation, and these reagents include collector, frother, promoter, depressant, dispersant, and pH modifier [21]. In some operations, seawater is used in regions where fresh water is in shortage [47]. Chemical additives and salt ions could change pulp chemistry, which in turn affect interparticle interactions and pulp rheology. For example, Cruz et al. [43] studied the effect of flotation reagents including pH modifiers (NaOH, lime, and $Na_2CO_3$), collector (potassium amyl xanthate), and frother (Interfroth 6500), which are normally used in copper-gold flotation, on the rheological behaviour of kaolinite and bentonite suspensions. All these reagents were found to alter the rheological behaviour of the kaolinite and bentonite suspensions, which was ascribed to the variation in the interparticle interactions in the presence of these reagents. In a different study by Farrokhpay and Zanin [48] where the effect of water quality on froth stability was investigated, the pulp viscosity increased as the concentration of $Al^{3+}$, $Ca^{2+}$, and $Na^+$ in a zinc ore pulp increased (see Figure 7). This change was believed as a result from these salt ions changing the particle interaction to form aggregates.

In summary, pulp rheology is affected by a number of variables in the pulp including solids concentration and particle attributes. Given the nature of flotation pulps made of low-grade and complex ores, the interactions between particles in the pulp also dominate the rheological properties of a flotation pulp. These interactions are not only subject to solids concentration and particle characteristics but also susceptible to shear rate at local regions of a flotation cell, as well as to pulp chemistry such as medium conditions and chemical reagents.

*3.2. Pulp Rheology Measurements.* Although flotation pulps are a three-phase regime consisting of air bubbles, water, and mineral particles, the viscosity of flotation slurries (water and mineral particles) is generally the subject investigated. It is known that bubbles disperse in the liquid phase without becoming attached when the air volume fraction (air holdup) is less than the critical air holdup point (73%) [49]. In flotation pulps, air holdup was found to range from 2.5% to 15% in laboratory flotation cells and from 6% to 21% in industrial machines, which is far below 73% [50]. In these cases, energy dissipations during pulp flow are thought not

(a)



(b)
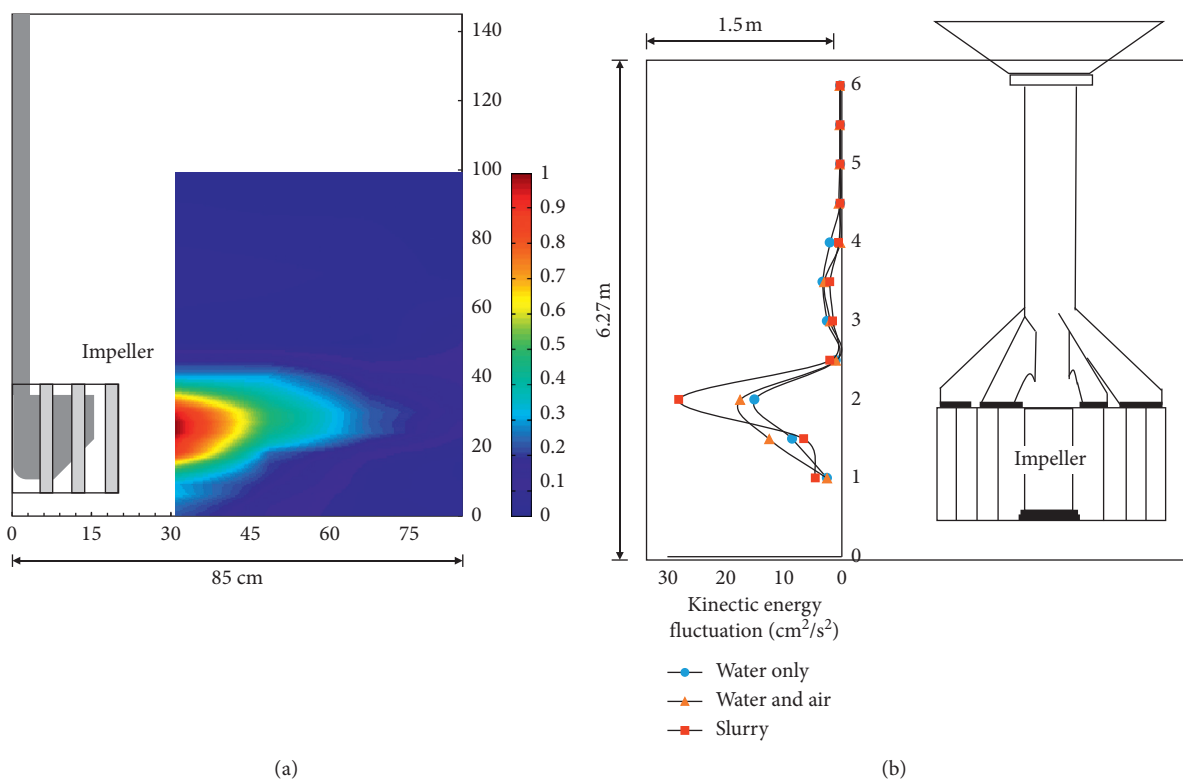
FIGURE 6: Turbulence distribution indicating shear rate distribution in a (a) 3 m³ flotation cell operating with slurry and (b) 300 m³ flotation cell operating with water, water and air, and slurry [46].
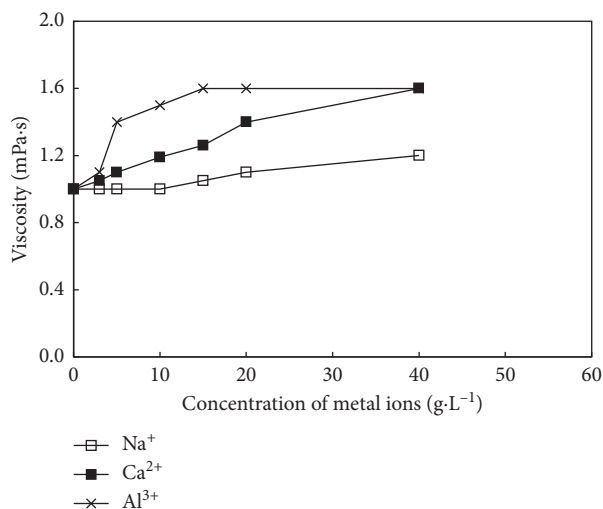


FIGURE 7: Effect of metal ions addition ($Al^{3+}$ (×), $Ca^{2+}$ (■), and $Na^{+}$ (□)) on the viscosity of a zinc ore slurry (after [48]).

associated with bubble deformation or frictions between bubbles. Thus, it is reasonable to use mineral slurry to represent the pulp in rheology measurements.

To measure pulp rheology, various setups including capillary viscometers, vibrating sphere viscometers, and rotational rheometers have been used, but the rotational rheometer prevails over the others since it can be operated at a specific shear rate in addition to the ease of completing measurements and data analysis [51–53]. Rotational rheometers generally involve the relative rotation about a common axis of one of three geometries: concentric cylinder, cone and plate, or parallel plates (see Figure 8). The one with the concentric cylinder geometry (also known as the bob and cup style, Figure 8(a)) has been widely applied for pulp rheology measurements. This is because rheometer geometries including the cone and plate and the parallel plate have trouble in holding samples during measurements [15].

The rheology measurement for pulps made of good-quality ores has been a challenge. This type of pulps is generally of low viscosity, being Newtonian or very close to Newtonian. Wall slip often occurs as mineral particles do not always adhere perfectly to the smooth surface of the rheometer tools such as the cylinder in the Couette geometry during the measurement, causing an erroneously low viscosity and yield value [54, 55]. In the literature, modifications to the surface of bobs or using vane-style viscometers could be found to address this problem [56, 57]. More importantly, mineral particles in this type of pulps tend to experience fast settling during rheology measurement. This settlement of particles may also cause shear-induced particle migration along the rotation shaft of a rheometer [58, 59]. To avoid particle settlement, methods including slurry mixing and recirculation have been tried to keep the slurry in suspension for measurement, but these methods are generally limited by the interference of slurry flow created purposely for suspension such as Taylor vortices and
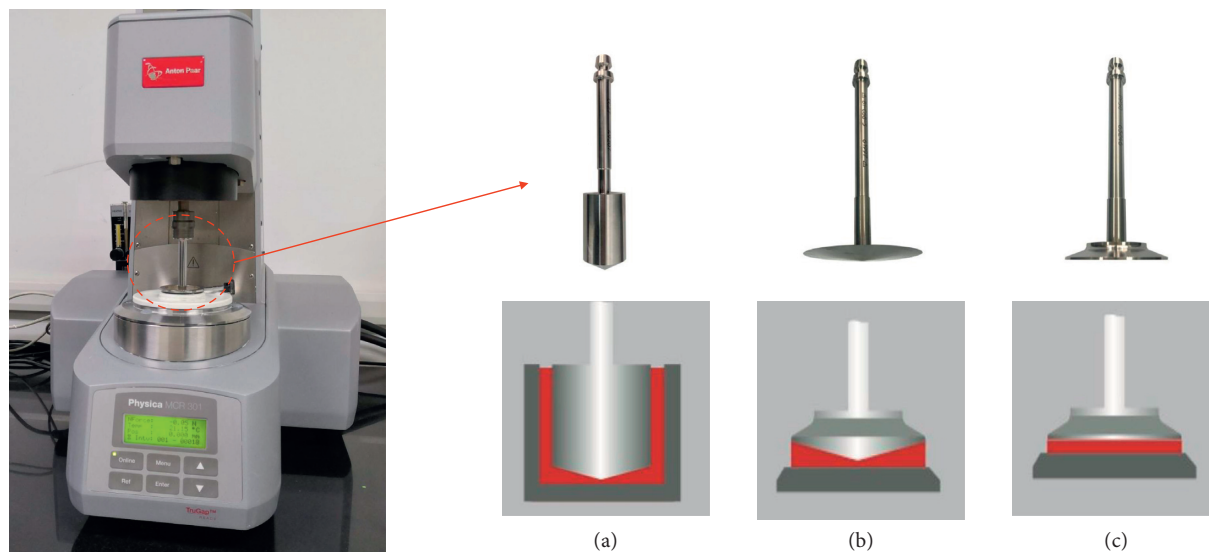
Figure 8: Basic geometries for the rotational rheometer: (a) concentric cylinder; (b) cone and plate; (c) parallel plate.

turbulent flow, leading to severe deviations in rheometer readings [9, 10, 51, 60]. Other approaches have also been provided such as using capillary viscometers or making use of zone settling properties of coarse particle suspensions for measurement [61, 62], but these methods also have disadvantages which have been detailed in the review by Cruz and Peng [10]. At the current stage, there has not been a promising technique for measuring the flotation pulp with fast settling solids.

It is worth noting that, however, in most flotation operations, pulps made of high-quality ores are not thought to cause detrimental rheological effects on flotation performance. In this sense, pulp rheology measurement becomes particularly critical when processing low-grade and complex ores which can produce a highly viscous pulp. Researchers have demonstrated that consistent measurement for this type of pulps can be obtained using the bob and cup style rheometer [10, 24, 43, 63, 64]. All concerns over rheology measurement of high-quality ore slurries can be minimal as to problematic ore slurries with high viscosity. The rheology measurement includes a preshear for 15 s at $1000 \, \text{s}^{-1}$ followed by 3 s of resting period before the measurement that lasts for 35 s. Besides, at the low shear rate, yield stress for the non-Newtonian flotation pulp may occur. Boger [9] has suggested using the rheometer with a vane head to detect yield stress. Air bearing with high sensitivity is also recommended to apply very low torques [15].

Also, Cruz and Peng [10] suggested performing viscoelastic measurements such as dynamic oscillatory rheology measurement in the linear viscoelasticity region as a supplement to analyse rheological properties of non-Newtonian flotation pulps. In practice, there are few studies on oscillatory rheology in mineral pulps, but these have shown to be a good strategy to understand more about particle interactions. Viscoelastic modules are known to have physical sense only when a flotation pulp presents a linear viscoelastic response [15, 65, 66]. In some flotation operations, however,

the deformation is large and rapid [67]. Thus, the oscillatory rheology must necessarily be analysed under large amplitude oscillatory shear (LAOS) deformation. In this sense, considering deformation only under small amplitude oscillatory shear (SAOS) flow will be insufficient to interpret interparticle interactions in the pulp.

### 3.3. Impact of Pulp Rheology on Flotation Performance

*3.3.1. True Flotation.* The impact of pulp rheology on true flotation recovery is basically associated with bubble-particle interactions and the transport of formed bubble-particle aggregates [22, 37, 68, 69]. For example, Patra et al. [69] carried out flotation tests using a copper ore in the absence and presence of two fibers, namely, fibrous Ni ore (1–6 wt.% chrysotile fibers) and nylon fibers (1–2 wt.%), and found that a viscous pulp was the key underlying reason for the poor flotation recovery of valuable mineral. High viscosity of pulp was caused by the entanglement of fibers, which prevented air dispersion and bubble transport, resulting in decreased copper recovery. This clearly shows the detrimental rheological effect that fibrous minerals would potentially have on the flotation recovery. As in ultramafic Ni ore beneficiation processes, slime coating of serpentines on the Ni sulphide minerals to deteriorate the flotation has been widely acknowledged. The findings by Patra et al. [69] evidently suggest that pulp rheological behaviour plays a critical role in the effective separation of ore containing fibrous minerals.

In a copper-gold flotation in the presence of bentonite (a swelling clay) and kaolinite (Q38 and Snobrite, nonswelling clays), Zhang and Peng [37] also observed a strong correlation between pulp viscosity and flotation recovery (see Figure 9). Clay minerals of different mineral types in the flotation pulp exhibit different rheological behaviours, leading to different effects on the true flotation recovery. Bentonite exhibited a more profound influence than Q38
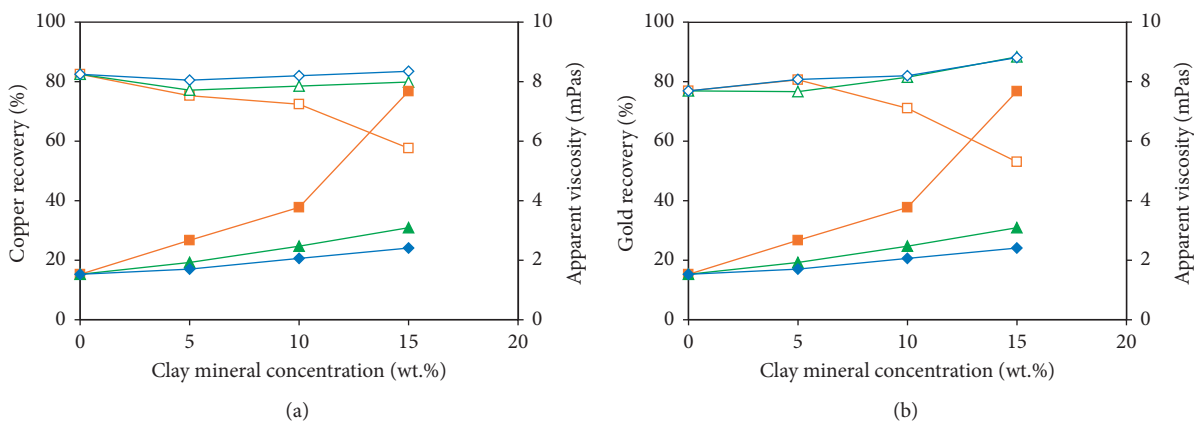
Figure 9: Effect of clay minerals on (a) copper recovery and (b) gold recovery (hollow points) and apparent viscosity (solid points) of flotation slurries: Snobrite (◊); Q38 (△); and bentonite (□) (after [37]).

and Snobrite in the pulp viscosity and flotation recovery when increasing the solid concentration. In general, a high pulp viscosity corresponded to low copper recovery (see Figure 9(a)), as these clay minerals would increase pulp viscosity that interferes with flotation hydrodynamics and prevented the probability of particle-bubble collision. Gold flotation showed some similarities to copper flotation in response to the addition of bentonite, as evidenced by that the addition of bentonite at greater than 5% concentration corresponding to higher apparent viscosity decreased gold recovery (see Figure 9(b)).

Not all the true flotation recovery decreases with an increase in pulp viscosity, as demonstrated by Zhang and Peng [37] that a slight increase in the pulp viscosity by Q38 (15 wt.% concentration) and bentonite (5 wt.% concentration) enhanced the gold recovery. This was attributed to a reduced detachment of gold particle from bubbles in the pulp as pulp viscosity increased. It is known that high bubble-particle detachment probability is the main reason for the poor recovery by true flotation in some flotation operations [70, 71]. Turbulent flow in the pulp is beneficial to bubble-particle collision and attachment, but the turbulent effect can also cause particles with high inertia to detach from bubbles, thus decreasing the flotation efficiency [70, 72, 73]. Thus, it can be seen that a proper pulp viscosity would stabilize bubble-particle aggregates that enhance the flotation of heavy metal minerals.

Similarly, a slightly viscous pulp is also beneficial to coarse particle flotation. Xu et al. [74] observed an increased recovery of coarse hydrophobic quartz particles when adding glycerol to increase the medium viscosity. In their study, a discernible change was found in the pulp viscosity, from 0.9 mPa·s in water to 7.6 mPa·s in a 50% glycerol/water mixture. When pulp viscosity increased, a more stable bubble-particle aggregate was formed as analysed by a novel electro-acoustic technique used for detachment experiments, leading to the increase in the quartz recovery. Therefore, using a proper viscous pulp is recommended for the flotation of either coarse particles or precious metals.

In addition, the pulp rheological effects on true flotation have also been extensively reported with respect to other flotation variables such as particle size and flotation reagents including rheology modifiers, pH modifiers, and metal ions except for mineralogy and solid concentration [27, 44, 75, 76]. Fine/ultrafine particles are well known to decrease true flotation recovery by increasing the pulp viscosity and slime coating of fine gangue mineral particles onto the surface of the valuables [77]. In mineral flotation, various flotation reagents can be added to facilitate the separation. Farrokhpay et al. [27] have shown that different flotation pH modifiers and rheological modifiers have different effects on the pulp apparent viscosity and flotation performance. For example, in their study, the gold recovery and grade increased due to a low flotation pulp viscosity when the pH was adjusted by $Na_2CO_3$, while NaOH was less influential. In general, due to the rheological complexities of low-grade and complex ores, different chemical additives would often result in different rheological effects on flotation by affecting the interactions between particles in the pulp. This basic understanding of pulp rheological effects offers essential insights into to the methods used to mitigate the deleterious impact of pulp rheology on flotation, which will be presented in Section 5.

### 3.3.2. Entrainment.
Apart from true flotation, gangue entrainment is also associated with pulp rheology. It is known that entrainment mechanism mainly accounts for the recovery of gangue mineral particles in flotation, and it is directly related to the ultimate water recovered to the concentrate and the entrainment factor for particles [7]. Since a large amount of fine/ultrafine particles such as colloidal particles and clays exist in pulps with low-grade and complex ores, pulp viscosity is very likely to change pulp flow patterns, which subsequently changes the water transferred to the froth from the pulp, and the degree of sedimentation of particles in the pulp (i.e., entrainment factor). Although there is no common agreement on how entrainment responds in the pulps with different degrees of pulp viscosity, the literature suggests a nonignorable impact of pulp rheology on entrainment in flotation [36, 39, 78, 79].

Kirjavainen [78] studied the entrainment of hydrophilic particles by performing flotation tests in a circulating system with granular quartz and flaky phlogopite at different slurry densities using only frother. Pulp viscosity was found to control particle entrainment, especially in the flotation of very fine materials. Chen et al. [39] also studied the correlation between pulp rheological property and gangue entrainment in flotation of a mixture of chalcopyrite (a particle size of P80 $38\,\mu$m), quartz (a particle size of $38$–$75\,\mu$m), and amorphous silica (a particle size of $38$–$75\,\mu$m). It was observed that gangue recovery increased with a slight increase in pulp viscosity, but further increasing viscosity would reduce gangue entrainment. Note that the gangue particles with the size of $38$–$75\,\mu$m may have settled during the rheology measurement in their study, but using a preshear at $100\,\text{s}^{-1}$ to avoid particle settlement would also be likely to make a turbulent flow which is not a valid measurement. In this sense, whether the observed trend can be transversal for all flotation systems is still unknown.

In a copper flotation reported by Farrokhpay et al. [36], a significant decrease in the copper grade was also found in the presence of muscovite. The copper recovery remained unchanged irrespective of the presence of muscovite. A maximum copper grade of 19% was observed without muscovite approximately, but it decreased to 2% in the presence of 30% muscovite. This decrease was a result of muscovite increasing the pulp viscosity that increased the gangue entrainment into the concentrate. Clearly, this observation also indicates the ignorable impact of pulp rheology on entrainment in flotation. In addition, it is worth mentioning that the rheograms obtained in their study may be unreliable, as extremely fast rheograms were made using a vane rheometer, i.e., measurement with an upward and downward ramp within the range $0$–$400\,\text{s}^{-1}$ over a $60\,\text{s}$ period. There may not be enough time for the pulps to stabilize at each shear rate, so the influence of the thixotropy cannot be appreciated, although the vane geometry is reported to result in less sample disturbance and thixotropic breakdown during rheology measurements [80–82].

In general, both the true flotation and gangue entrainment are closely associated with the pulp rheology. Table 1 summarizes some implications of correlation between flotation response and pulp rheological property mentioned above. As can be seen that no common agreement has been reached as to how flotation recovery and grade respond to pulp rheological property at different flotation conditions. These complex pulp rheological effects on flotation recovery and grade warrant further investigations in this topic.

## 4. Rheology of Flotation Froth

*4.1. Variables Affecting Froth Rheology.* Foam is an air-bubble dispersion in an aqueous solution with a packing fraction above 73% [49, 83]. In a foam, air volume fraction is normally high, and the packed bubbles are separated by thin watery films (lamellae) which form plateau borders and vertices [84, 85]. As indicated by Princen and Kiss [49], the rheological behaviour of a foam is affected by a number of variables including bulk liquid viscosity, foam quality, and bubble size, and a model was developed to predict the apparent viscosity of foams that demonstrates how these variables affect foam rheology:

$$\eta = \frac{\tau_0}{\gamma} + 32.0\left(\varepsilon_f - 0.73\right)\left(\frac{R_{32}\gamma}{\eta_0\sigma}\right)^{-0.5} \qquad (2)$$

where $\eta$ is the apparent viscosity, $\gamma$ is the shear rate, $\tau_0$ is the yield stress, $\varepsilon_f$ is the air volume fraction, $\eta_0$ is the viscosity of the Newtonian continuous phase, $R_{32}$ is the Sauter mean bubble radius, and $\sigma$ is the interfacial tension.

A flotation froth has a structure similar to a foam, but is a three-phase regime which has hydrophobic particles attached to liquid films of air bubbles, and both hydrophobic and hydrophilic particles in the plateau borders and vertices [85]. Although the literature suggests that flotation froths are non-Newtonian showing pseudoplastic characteristics which are similar to foams, the presence of solid particles makes froths' rheological behaviour more complicated [12, 13, 86–88].

Froth flow is also an irreversible process, which involves the rearrangement of bubbles and changes in bubble surface area [13]. In a series of flotation tests, in both pilot and industrial scale, conducted by [87–90]; the measured froths showed pseudoplastic behaviour. In their flotation tests, flotation variables including frother dosage, feed grade, air rate, froth depth, impeller speed, and valuable mineral particle size were investigated with respect to froth rheology [88, 89]. Table 2 shows the variables that significantly affected froth rheology [89]. Feed grade and froth height were positively correlated with froth apparent viscosity, whereas particle size and impeller speed were negatively correlated with froth apparent viscosity. Air rate was found to affect froth viscosity in a nonlinear way. Some of these variables were also observed to interact with each other to affect froth rheology, as shown in Figure 10. Frother dosage in a range of $10$–$15\,$ppm did not appear to result in any significant effect on froth rheology [88].

Furthermore, the mechanisms underpinning the effects of these significant variables reported in Table 2 were also explored, and it was found that froth characteristics including bubble size and bubble loading are primary determinants for froth rheology [87]. The variations in flotation variables could result in a change in these primary determinants, which significantly altered the froth rheology. In their studies, bubble size was found to negatively affect the froth viscosity while bubble loading had a reverse effect. In froths, viscous dissipation of energy is largely due to the relative motion of neighbouring bubbles and bubble deformation. As in their study a very low solids concentration was found in the plateau borders and vertices of the froth, solids volume fraction in the plateau borders and vertices determining froth rheology has not been identified.

In addition, a froth rheology model as a function of the primary determinants identified in their study was proposed (see equation (3)), by assuming that bulk viscosity remains unchanged due to a low solids concentration in the plateau borders and vertices of the froth as well as that the interfacial tension is associated with the fraction of the lamella covered

TABLE 1: Literature (part) related to pulp rheological effects on flotation recovery and grade.

| Ore type | Froth rheological effect on recovery and grade | References |
| --- | --- | --- |
| Copper flotation | Fibrous minerals increased pulp viscosity and decreased copper recovery | Patra et al. [69] |
| Quartz flotation | A slight increase in pulp viscosity by glycerol increased the recovery of coarse hydrophobic quartz particles | Xu et al. [74] |
| Gold flotation | Different pH modifiers and rheology modifiers had different effects on pulp viscosity, resulting in different gold recoveries and grades | Farrokhpay et al. [27] |
| Copper-gold flotation | Clay minerals increased pulp viscosity; copper recovery decreased as pulp viscosity increased; a slight increase in pulp viscosity increased gold recovery but further increasing the pulp viscosity reduced gold recovery | Zhang and Peng [37] |
| Copper flotation | Swelling clays increased pulp viscosity and reduced both copper recovery and grade, but nonswelling clays were less influential | Farrokhpay et al. [25] |
| Copper-gold flotation | Copper recovery and grade decreased with increasing pulp viscosity by bentonite; seawater (salt ions) reduced pulp viscosity in the presence of bentonite and improved copper and gold recoveries but further reduced copper and gold grade | Zhang et al. [27] |
| Copper flotation | Cations ($Na^+$, $K^+$, $Mg^{2+}$, and $Ca^{2+}$) reduced pulp viscosity and increased copper recovery | Wang et al. [44] |
| Copper flotation | Copper recovery remained unchanged first and then decreased with increasing pulp viscosity by amorphous silica, while copper grade decreased; gangue entrainment increased first and then decreased with increasing pulp viscosity | Chen et al. [39] |
| Gold flotation | Lignosulfonate-based biopolymer (DP-1777) increased gold recovery and grade through reducing pulp viscosity; gangue entrainment decreased with decreasing pulp viscosity | Liu et al. [76] |
| Copper flotation | Copper recovery remained unchanged with increasing pulp viscosity by muscovite, but copper grade decreased as pulp viscosity increased; gangue entrainment increased with increasing pulp viscosity | Farrokhpay et al. [36] |

TABLE 2: Significance of flotation variables on froth apparent viscosity at different shear rates.

| Flotation variables | Shear rate ($s^{-1}$) | | | |
| --- | --- | --- | --- | --- |
| | 1 | 2 | 3 | 4 |
| | Significance (%) | | | |
| Froth height (FH) | 98.9 | 99.2 | 98.9 | 98.4 |
| Superficial gas velocity ($J_g$) | 84.5 | 22.6 | 52.0 | 86.5 |
| Impeller speed (IS) | 100.0 | 100.0 | 100.0 | 100.0 |
| Chalcopyrite size (CS) | 100.0 | 100.0 | 100.0 | 100.0 |
| Copper grade (CG) | 99.8 | 100.0 | 100.0 | 100.0 |
| $J_g \cdot J_g$ | 99.9 | 99.9 | 99.9 | 99.9 |

by solids [87]. The model was found successful in predicting the rheological behaviours of froths generated in a copper flotation operated at different flotation conditions including frother dosage and feed grade [88]:

$$\eta = \left( \varepsilon_f - 0.73 \right) \left( \frac{R_{32}\gamma}{k_0 \alpha} \right)^{-0.5}, \tag{3}$$

where $k_0$ is the constant representing those parameters of the system that should not change between the experiments and $\alpha$ is the fraction of the lamella covered by solids.

Despite that concerns remain over the variables determining froth rheology. For example, for heavily entrained froths, a high solid content in plateau borders and vertices may distort the flow field and could presumably increase the energy dissipation during flow to increase froth viscosity [91]. Another example is that in a copper flotation performed by Li et al. [88], an increase in Dowfroth 250 dosage from 10 ppm to 15 ppm exhibited no effect on the froth viscosity. It is well known that frother could strongly affect bubble surface tension, air holdup, bubble size, and thus the fraction of the lamellae covered by solid particles [92–95],

which should have affected froth viscosity. In this respect, more work is still required to identify the variables determining the rheology of froths and to correlate flotation conditions including particle attributes such as clay minerals, operational variables, and flotation reagents with these primary determinants to elucidate the significant variables influencing froth rheology.

*4.2. Froth Rheology Measurements.* For decades, two-phase systems (air-liquid foam and solid-liquid emulsions) have been the subject of many studies on rheology and restricted information is available about the rheological behaviour of flotation froths, due mainly to the difficulty in the measurement of froth rheology [13, 86]. As stated previously, bob and cup style rheometers have been useful for pulp rheology measurement. However, the small clearance between the cup and the bob would result in a change in froth structure with no prevailing froth rheology properties obtained [13]. Due to the similarity between flotation froths and foams, rheometers and purpose-built setups, for example, parallel-plate rheometers and capillary viscometers, for determining foam rheological behaviour should have been useful in measuring froth rheology, but wall slip effect and froth degradation during froth sample transfer to the setups would cause deviations from genuine froth rheological properties.

To measure froth rheology, an initial attempt was made by Moudgil [96] who used a Brookfield viscometer in a laboratory flotation cell. The measurement was only taken at a constant rotational rate of 6 rpm, and no rheogram of the froth was generated due to the limitations of the viscometer. After that, Shi and Zheng [13] introduced an in situ measurement method that involves a direct immersion of a vane head into the flowing froth to perform measurement, with
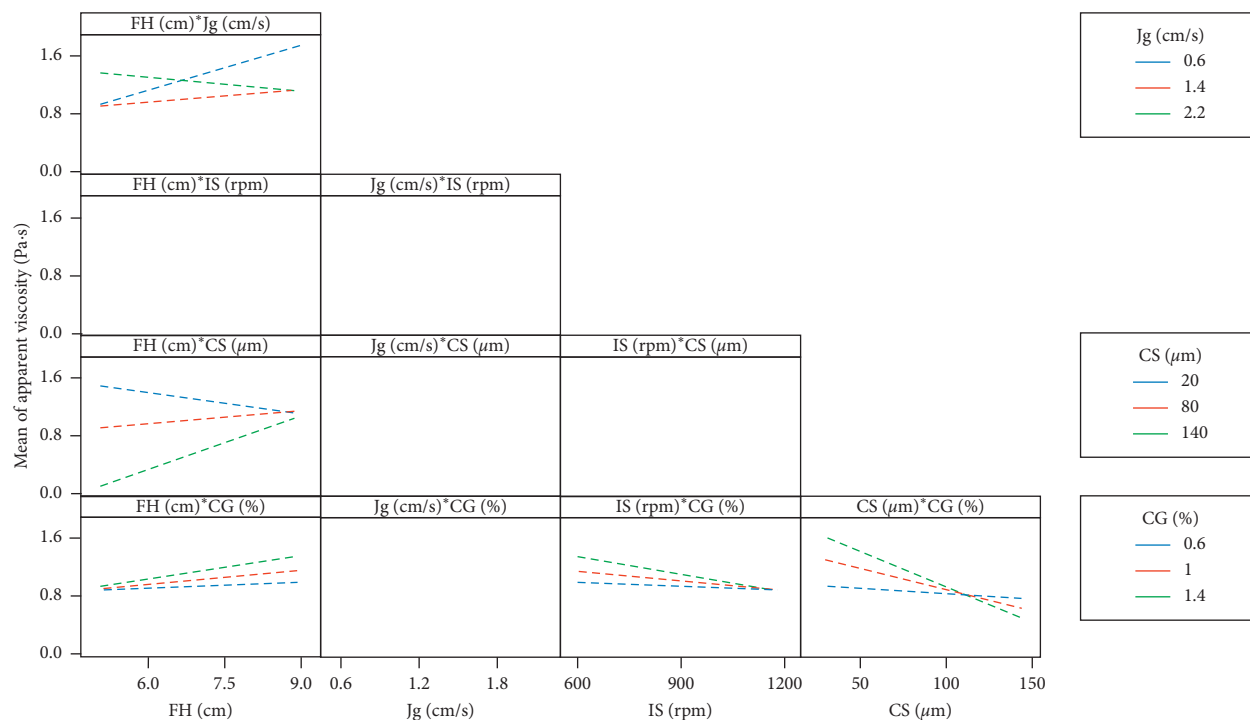
FIGURE 10: Interactions between flotation variables in determining froth rheology (after [89]).

the advantage of minimum disturbance caused by the vane and no apparent slip effect or filling influences [80, 97].

However, Li et al. [86] found that horizontal flow in the froth could significantly affect the torque readings and consequently influence rheology measurement results. Besides, the rheometer used by Shi and Zheng [13] was found to be suitable for measurement only in the shear rate range above $2.5 \, \mathrm{s}^{-1}$ due to the mechanical bearing of the rheometer. Based on these concerns, Li et al. [86] modified the vane method for froth rheology measurement by encircling the vane using a tube with geometrically designed diameter in a vane rheometer with an air bearing, as shown in Figure 11. They evaluated the rheometer with a Newtonian silicone oil of known viscosity and claimed that it was capable of producing true flow curves. It should be noted that, as the vane is rotated in the horizontal direction during measurement, the effect of vertical froth velocity on the measurement has been assumed to be negligible in their study, which remains to be evaluated. Also, since the vane geometry is not a standard device to create rheograms, the acquired raw data (vane rotating speed and torque) are required to be converted to rheological parameters (shear rate and shear stress). The mathematical expressions used by Li et al. [86] to obtain the rheograms are based on the assumption that the deformation profile of the froth sample within the distance between tube and vane is linear. Whether this linearity could be preserved at different gaps is still unknown, which requires further investigation. Despite that the appliance has been applied to various flotation froths, showing that the shear rate of the flotation froth was less than $4 \, \mathrm{s}^{-1}$, much less than that in pulp phase of which the average has been believed to be around 100 or $160 \, \mathrm{s}^{-1}$,

quantitatively confirming that flotation froth provides a much more tranquil environment (i.e., less turbulence) than the pulp phase for further product concentration.

Besides, Zhang et al. [98] have introduced a steady-state method for froth rheology measurement recently when investigating the effect of froth rheology on the dewatering of fine coals. Oscillatory rheology of froth was measured using a vane-in-cup system. Rather than measuring the froth rheology in situ, the measurement was conducted on the froth that was produced in the cup to avoid its degradation during transfer. The froth was generated by introducing air into a preconditioned coal slurry in the cup, and air injection was terminated when the coal froth was believed to be sufficiently high. The vane head was then placed into the froth to perform the measurement. Note that the froth regenerated in the cup is highly unlikely to reproduce the flowing froth in flotation, as bubbles in the froth tend to collapse or coalesce during froth transportation, leading to continuous changes in the froth structure and the content of air, liquid, and both hydrophobic and hydrophilic particles in the local froth. This may result in deviations from genuine froth rheological properties. Since oscillatory rheology measurement on flotation froths could provide complementary information about flotation rheological properties, delicate experiments should be designed for such measurements.

### 4.3. Impact of Froth Rheology on Flotation Performance

*4.3.1. Flotation Recovery and Grade.* The impact of froth rheology on flotation recovery and grade has long been recognised, and high viscosity can result in no froth

(a)                                            (b)                                            (c)
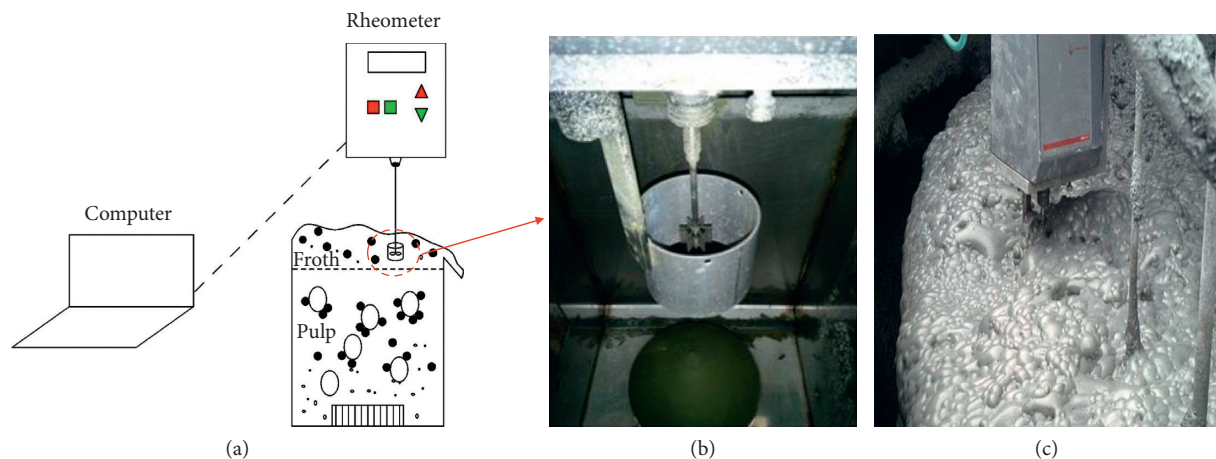
FIGURE 11: Froth rheology measurement device (the Anton Paar DSR 301 rheometer) by Li et al. [86]: (a) schematic diagram; (b) modified vane system; (c) setup of the rheometer in an industrial cell.

generated, and few valuable minerals loaded on the top of the froth [44]. To date, however, no consensus has been reached with respect to the correlations between froth rheology and flotation recovery or grade, as shown in Table 3. In the phosphate flotation reported by Moudgil [96], a higher solid loading of the froth led to a higher froth viscosity, which slowed the drainage of entrained particles in the froth. As a result, a decrease in the concentrate grade was observed as froth viscosity increased. In the copper flotation, however, Shi and Zheng [13] found that the grade of hydrophobic chalcopyrite was positively correlated with froth viscosity, while the grade of hydrophilic quartz was negatively correlated with froth viscosity. Interestingly, the recent study by Li et al. [90] showed that the entrainment recovery of hydrophilic quartz in a copper flotation was strongly correlated with froth rheology in a nonlinear way, as shown in Figure 12. An increase in froth viscosity (consistency index) would enhance quartz recovery at low froth viscosity, while at high froth viscosity, the recovery of quartz deteriorated when froth became more viscous.

*4.3.2. Other Flotation Performance Indicators.* Apart from flotation recovery and grade, froth rheology has also been correlated to other flotation performance measures including froth recovery, air recovery, and froth height. In a copper flotation, Li et al. [90] observed that froth height above the lip increased as froth viscosity increased, resulting in a prolonged froth residence time that determines froth drainage and froth recovery. Air recovery was also associated with froth rheology: at low froth viscosity, air recovery increased as froth viscosity increased, while at high froth viscosity, the opposite was found.

Farrokhpay [4] and Li et al. [90] have proposed that froth viscosity affects flotation performance through its effect on both froth mobility and froth stability. When froth is less viscous, froth stability dominates froth transportation. Increasing froth viscosity will result in a more stable froth where less bubble bursting and detachment of valuable minerals occur and considerably increases the flotation

recovery of valuables. When the froth becomes excessively viscous, froth transportation would be retarded due to poor froth mobility, and thus, flotation deteriorates. In general, a requirement for a froth is that the froth should not be too stable with low coalescence or of too low viscosity with high coalescence, which is targeted to achieve a balance between optimal recovery and minimal mechanical entrainment [99].

Note that froth mobility and froth stability are two aspects of froth characteristics that determine the flotation recoveries such as froth recovery and air recovery in mineral flotation. Froth rheological parameters such as yield stress and apparent viscosity are generally a measure of the degree of froth mobility. A positive correlation of froth rheology (froth mobility) and froth stability has been suggested from rheological investigations on the froth in a chalcopyrite flotation by Li et al. [90]. However, whether the observed trend can be transversal for all flotation systems is still unknown. Since the correlation between froth rheology and froth stability would be conducive to improving the current flotation recovery models for process predication and optimization, more work is needed.

## 5. Mitigating Rheological Problems in Flotation

Rheology can be a useful tool for flotation optimization. Many approaches have been tried to mitigate the deleterious effects caused by rheology in flotation, but these methods mainly focus on the pulp zone [40, 77]. In mineral flotation, it is known that the nature of pulp and froth determines their rheological behaviour. When the nature is altered, either by the addition of chemical additives or by changing the proportion of each component material (i.e., liquid, air bubble, and particle), viscosity is also quite likely to change.

In flotation, the chemicals of many types have been tried to control the rheological properties of flotation pulps. The literature shows that rheology modifiers (dispersants) can be used to reduce the negative rheological impact of problematic ores with clay minerals in flotation [40, 76, 77]. For example, in studies by Seaman et al. [100] and Wei et al. [101] where biopolymers such as lignosulfonate-based polymers

TABLE 3: Literature related to froth rheological effects on flotation recovery and grade.

| Ore type | Froth rheological effect on recovery and grade | References |
|---|---|---|
| Phosphate flotation | Concentrate grade decreased as froth viscosity increased | Moudgil [96] |
| Copper flotation | Concentrate copper grade increased as froth viscosity increased; concentrate quartz grade increased as froth viscosity decreased | Shi and Zheng [13] |
| Copper flotation | At low viscosity: air recovery and gangue recovery increased with froth viscosity increased; at high viscosity, air recovery and gangue recovery decreased as froth viscosity increased | Li et al. [90] |
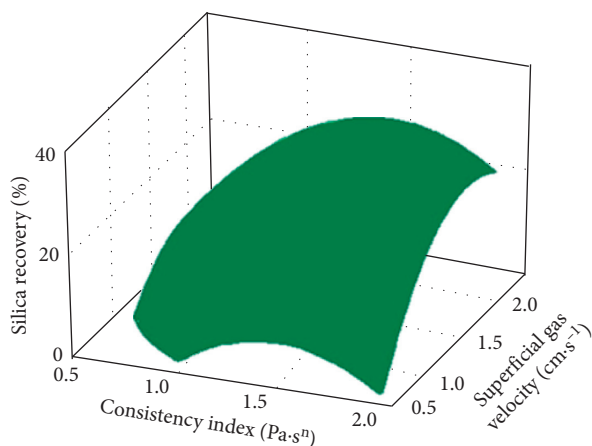


FIGURE 12: Surface plot of hydrophilic quartz recovery versus consistency index and superficial gas velocity (after [90]).

were used as effective clay dispersants to improve the flotation performance, the possible role of reduced pulp viscosity in the improved flotation was addressed by Chen and Peng [10] in addition to the effect of reduced slime coating of clays onto the valuables. In a different study where the effect of different commercial rheology modifiers on flotation performance of a gold ore with high clay contents from Carlin Trend was investigated, Cyquest 40E (a modified polymer) decreased the pulp apparent viscosity significantly and increased the gold recovery by about ten percent at a rheology-modifier dosage of 600 g/t and a pulp density of 32% [27]. As pulp rheology can strongly affect the dispersion of particles and air bubbles as well as the bubble-particle collision, this improvement in the gold recovery is highly likely to be related with the reduced pulp viscosity. In their study, BorreFlo D-919 (a lignosulfonate-based polymer) also decreased the pulp viscosity, but a reverse effect was observed on both the gold recovery and grade. This implies the difficulty in selecting the rheology modifiers to improve the flotation of various low-grade and complex ores.

The literature also suggests using salt ions to manipulate pulp viscosity to improve flotation recovery [44, 75, 77]. For example, Zhang et al. [75] found that the deleterious effect of bentonite could be mitigated in seawater containing the salt ions of $Na^+$, $K^+$, $Mg^{2+}$, $Ca^{2+}$, $Cl^-$, and $SO_4^{2-}$. The salt ions reduced the swelling capacity of bentonite, modified the network structures of bentonite in flotation pulp, reduced the pulp viscosity, and improved both the copper and gold recoveries. In a different study, Wang et al. [44] examined the effect of different cations ($Na^+$, $K^+$, $Mg^{2+}$, and $Ca^{2+}$) on

pulp viscosity and copper flotation behaviour and found that these cations could effectively decrease the pulp viscosity, which contributed to an improved copper flotation recovery. These studies have experimentally confirmed the beneficial effect of some salt ions in reducing the pulp viscosity and improving flotation performance.

It should be stated that lack of froth rheological investigations in mineral flotation has led to no conclusion on whether froth rheology also changes with changing pulp rheology when using the abovementioned approaches. In addition to the incomplete understanding of the effect that froth rheology has on flotation recovery and grade, few techniques are developed targeting at manipulating the froth rheology to improve the flotation performance at the current stage. However, as can be seen in most industrial flotation columns, washing water is added at the top of the columns to facilitate the drainage of gangue particles in the plateau borders and vertices out of the froth zone. This added washing water is expected to result in a wetter froth of which the viscosity should be lower. Therefore, introducing washing water into the froth zone may be a feasible way for plant operators to mitigate the deleterious froth rheological effect on flotation.

It should also be stated that pulp rheology and froth rheology act as a whole to influence the flotation performance, and thus, to comprehend the correlation between pulp and froth rheology becomes particularly necessary in respect of adjusting flotation variables to achieve a better flotation result. To date, however, no studies on this correlation have been conducted yet due to its complexity. For example, the presence of different types of clays in flotation may result in different impacts on pulp and froth rheology. Increasing the content of clays in pulp would increase pulp viscosity regardless of clay type, while it may not be the case for froth rheology. The hydrophobicity and the swelling characteristics of clays could affect froth viscosity in addition to the contents [25, 87].

As a matter of fact, adjusting flotation operational variables can be a possible alternative, but caution must still be taken even if the correlation between pulp rheology and froth rheology is established. This is because operational variables themselves may also impose an undesired effect on flotation performance. For example, one of the most common ways to treat problematic ores in flotation plants is to process them at a lower solids concentration. Low solids concentrations can reduce both the pulp and froth viscosity [39, 87, 102], but this method would also inevitably lead to a reduced the flotation productivity [40]. As Wang et al. [44] argued, at present, no reliable and effective ways are available

in the case of manipulating rheology to improve the flotation efficiency of problematic ores.

## 6. Conclusions and Future Work

This paper reviews the pulp and froth rheology in mineral flotation. It reveals the rheological complexities encountered when processing problematic ores by the flotation technique, and analysis of pulp and froth rheology still has a long way to go before becoming a dependable tool for process control that would consistently produce an efficient performance in flotation plants. Although a few rheological investigations show some significant correlations between flotation recovery and grade and the rheological behaviours of flotation pulps and froths, no general agreement has been reached due to the complex nature of various flotation feeds. The essential flotation variables that affect pulp and froth rheology show similarities as well as differences, which indicates that these variables are interrelated to some extent to affect flotation rheology and flotation response. However, concerns remain over the principle variables affecting flotation rheology especially in the froth zone, and also no work has been done towards the intercorrelation between pulp rheology and froth rheology. This results in the difficulty in the mitigation of deleterious rheological effects on flotation by manipulating the influencing variables in both the pulp and froth zones. At the current stage, only some polymeric dispersants and metal ions are found effective with respect to reducing pulp viscosity and improving flotation in some applications. For rheology measurements, it is revealed that progress has been advanced in measuring the rheological behaviour of both flotation pulps and froths with a focus on rheological parameters yield stress and apparent viscosity and other techniques such as oscillatory rheology measurements are being introduced to the field to properly interpret interparticle interactions in mineral flotation. But caution must be taken when analysing the rheological data reported by rheology measurement devices, as a rheometer always reports data which are not always associated with rheology.

To better understand the rheological effects in mineral flotation, the following topics are recommended to investigate in future:

(i) To develop sound techniques (measuring device and methodology) to characterise the complex flotation rheological behaviours based on the recognition of flow types and shear rate of flotation pulps and froths and to adapt froth rheology measuring technique by Li et al. [86] to various mineral flotation systems through experimental validation and mechanical modification.

(ii) To classify the main gangue mineral components into groups to facilitate the rheological investigations based on the mineralogical understanding of various low-grade and complex ores.

(iii) To identify the essential flotation variables that influence the rheological behaviours of flotation pulps and froths, to elucidate the effects of these variables on pulp and froth rheology and overall flotation performance, and to propose approaches combined properly to mitigate the deleterious rheological effects in flotation of different groups of mineral systems.

(iv) To clarify the correlation between pulp rheology and froth rheology and the correlation between froth rheology and froth stability so as to allow flotation rheology to be a useful tool for process prediction and optimization.

## Conflicts of Interest

The authors declare that they have no conflicts of interest.

## Acknowledgments

## References

[1] A. Y. Malkin and A. I. Isayev, *Rheology: Concepts, Methods, and Applications*, Elsevier Science, London, UK, 3rd edition, 2017.

[2] T. H. Muster and C. A. Prestidge, "Rheological investigations of sulphide mineral slurries," *Minerals Engineering*, vol. 8, no. 12, pp. 1541–1555, 1995.

[3] N. Cruz, J. Forster, and E. R. Bobicki, "Slurry rheology in mineral processing unit operations: a critical review," *The Canadian Journal of Chemical Engineering*, vol. 97, no. 7, pp. 2102–2120, 2019.

[4] S. Farrokhpay, "The importance of rheology in mineral flotation: a review," *Minerals Engineering*, vol. 36–38, pp. 272–278, 2012.

[5] B. Ndlovu, M. Becker, E. Forbes, D. Deglon, and J.-P. Franzidis, "The influence of phyllosilicate mineralogy on the rheology of mineral slurries," *Minerals Engineering*, vol. 24, no. 12, pp. 1314–1322, 2011.

[6] B. Ndlovu, E. Forbes, S. Farrokhpay, M. Becker, D. Bradshaw, and D. Deglon, "A preliminary rheological classification of phyllosilicate group minerals," *Minerals Engineering*, vol. 55, pp. 190–200, 2014.

[7] L. Wang, Y. Peng, K. Runge, and D. Bradshaw, "A review of entrainment: mechanisms, contributing factors and modelling in flotation," *Minerals Engineering*, vol. 70, pp. 77–91, 2015.

[8] W. Zhang and J. A. Finch, "Effect of solids on pulp and froth properties in flotation," *Journal of Central South University*, vol. 21, no. 4, pp. 1461–1469, 2014.

[9] D. V. Boger, "Rheology and the minerals industry," *Mineral Processing and Extractive Metallurgy Review*, vol. 20, no. 1, pp. 1–25, 2000.

[10] N. Cruz and Y. Peng, "Rheology measurements for flotation slurries with high clay contents—a critical review," *Minerals Engineering*, vol. 98, pp. 137–150, 2016.

[11] J. Mewis and N. J. Wagner, *Colloidal Suspension Rheology*, Cambridge University Press, New York, NY, USA, 2012.

[12] J. R. Calvert and K. Nezhati, "A rheological model for a liquid-gas foam," *International Journal of Heat and Fluid Flow*, vol. 7, no. 3, pp. 164–168, 1986.

[13] F. N. Shi and X. F. Zheng, "The rheology of flotation froths," *International Journal of Mineral Processing*, vol. 69, no. 1–4, pp. 115–128, 2003.

[14] C. Li, *An Investigation of Flotation rheology PhD Thesis*, The University of Queensland, Brisbane, Australia, 2016.

[15] T. F. Tadros, *Rheology of Dispersions: Principles and Applications*, Wiley VCH, Weinheim, Germany, 1st edition, 2010.

[16] Z. Zhou, P. J. Scales, and D. V. Boger, "Chemical and physical control of the rheology of concentrated metal oxide suspensions," *Chemical Engineering Science*, vol. 56, no. 9, pp. 2901–2920, 2001.

[17] S. Mueller, E. W. Llewellin, and H. M. Mader, "The rheology of suspensions of solid particles," *Proceedings of the Royal Society A: Mathematical, Physical and Engineering Sciences*, vol. 466, no. 2116, pp. 1201–1228, 2010.

[18] D. B. Genovese, "Shear rheology of hard-sphere, dispersed, and aggregated suspensions, and filler-matrix composites," *Advances in Colloid and Interface Science*, vol. 171-172, pp. 1–16, 2012.

[19] M. Becker, G. Yorath, B. Ndlovu, M. Harris, D. Deglon, and J.-P. Franzidis, "A rheological investigation of the behaviour of two Southern African platinum ores," *Minerals Engineering*, vol. 49, pp. 92–97, 2013.

[20] P. A. Kralchevsky and K. D. Danov, "Chemical physics of colloid systems and interfaces," in *Handbook of Surface and Colloid Chemistry*, K. S. Birdi, Ed., Taylor & Francis, Boca Raton, FL, USA, 4th edition, 2015.

[21] B. A. Wills and T. J. Napier-Munn, *Mineral Processing Technology*, Elsevier Science & Technology, New York, NY, USA, 6th edition, 2006.

[22] C. W. Bakker, C. J. Meyer, and D. A. Deglon, "Numerical modelling of non-Newtonian slurry in a mechanical flotation cell," *Minerals Engineering*, vol. 22, no. 11, pp. 944–950, 2009.

[23] E. Forbes, K. J. Davey, and L. Smith, "Decoupling rehology and slime coatings effect on the natural flotability of chalcopyrite in a clay-rich flotation pulp," *Minerals Engineering*, vol. 56, pp. 136–144, 2014.

[24] N. Cruz, Y. Peng, E. Wightman, and N. Xu, "The interaction of clay minerals with gypsum and its effects on copper-gold flotation," *Minerals Engineering*, vol. 77, pp. 121–130, 2015b.

[25] S. Farrokhpay, B. Ndlovu, and D. Bradshaw, "Behaviour of swelling clays versus non-swelling clays in flotation," *Minerals Engineering*, vol. 96-97, pp. 59–66, 2016.

[26] C. Li, L. Dong, and L. Wang, "Improvement of flotation recovery using oscillatory air supply," *Minerals Engineering*, vol. 131, pp. 321–324, 2019.

[27] S. Farrokhpay, D. Bradshaw, and R. Dunne, "Rheological investigation of the flotation performance of a high clay containing gold ore from Carlin trend," in *Proceedings of the World Gold Conference*, Brisbane, Australia, September 2013.

[28] D. V. Boger, "Rheology and the resource industries," *Chemical Engineering Science*, vol. 64, no. 22, pp. 4525–4536, 2009.

[29] W. Chen, F. Chen, X. Bu, G. Zhang, C. Zhang, and Y. Song, "A significant improvement of fine scheelite flotation through rheological control of flotation pulp by using garnet," *Minerals Engineering*, vol. 138, pp. 257–266, 2019.

[30] P. Patra, P. Somasundaran, and D. R. Nagaraj, "The impact of shape and morphology of gangue minerals on pulp rheology and selective value mineral separation," in *Proceedings of the XXVI International Mineral Processing Congress*, New Delhi, India, September 2012.

[31] R. M. Turian, T. W. Ma, F. L. G. Hsu, and D. J. Sung, "Characterization, settling, and rheology of concentrated fine particulate mineral slurries," *Powder Technology*, vol. 93, no. 3, pp. 219–233, 1997.

[32] J. Du, R. A. Pushkarova, and R. S. C. Smart, "A cryo-SEM study of aggregate and floc structure changes during clay settling and raking processes," *International Journal of Mineral Processing*, vol. 93, no. 1, pp. 66–72, 2009.

[33] J. Du, G. Morris, R. A. Pushkarova, and St. C. Smart R., "Effect of surface structure of kaolinite on aggregation, settling rate, and bed density," *Langmuir*, vol. 26, no. 16, pp. 13227–13235, 2010.

[34] A. M. Genc, I. Kilickaplan, and J. S. Laskowski, "Effect of pulp rheology on flotation of nickel sulphide ore with fibrous gangue particles," *Canadian Metallurgical Quarterly*, vol. 51, pp. 368–375, 2012.

[35] B. Collins, T. J. Napier-Munn, and M. Sciarone, "The production, properties, and selection of ferrosilicon powders for heavy-medium separation," *Journal-South African Institute of Mining and Metallurgy*, vol. 75, pp. 103–119, 1974.

[36] S. Farrokhpay, B. Ndlovu, and D. Bradshaw, "Behavior of talc and mica in copper ore flotation," *Applied Clay Science*, vol. 160, pp. 270–275, 2018.

[37] M. Zhang and Y. Peng, "Effect of clay minerals on pulp rheology and the flotation of copper and gold minerals," *Minerals Engineering*, vol. 70, pp. 8–13, 2015.

[38] L. Basnayaka, N. Subasinghe, and B. Albijanic, "Influence of clays on the slurry rheology and flotation of a pyritic gold ore," *Applied Clay Science*, vol. 136, pp. 230–238, 2017.

[39] X. Chen, E. Hadde, S. Liu, and Y. Peng, "The effect of amorphous silica on pulp rheology and copper flotation," *Minerals Engineering*, vol. 113, pp. 41–46, 2017.

[40] R. I. Jeldres, L. Uribe, L. A. Cisternas, L. Gutierrez, W. H. Leiva, and J. Valenzuela, "The effect of clay minerals on the process of flotation of copper ores—a critical review," *Applied Clay Science*, vol. 170, pp. 57–69, 2019.

[41] C. A. Prestidge, "Rheological investigations of ultrafine galena particle slurries under flotation-related conditions," *International Journal of Mineral Processing*, vol. 51, no. 1–4, pp. 241–254, 1997.

[42] S. Farrokhpay, G. E. Morris, D. Fornasiero, and P. Self, "Stabilisation of titania pigment particles with anionic polymeric dispersants," *Powder Technology*, vol. 202, no. 1–3, pp. 143–150, 2010.

[43] N. Cruz, Y. Peng, S. Farrokhpay, and D. Bradshaw, "Interactions of clay minerals in copper-gold flotation: Part 1 - rheological properties of clay mineral suspensions in the presence of flotation reagents," *Minerals Engineering*, vol. 50-51, pp. 30–37, 2013.

[44] Y. Wang, Y. Peng, T. Nicholson, and R. A. Lauten, "The role of cations in copper flotation in the presence of bentonite," *Minerals Engineering*, vol. 96-97, pp. 108–112, 2016b.

[45] J. Ralston, D. Fornasiero, S. Grano, J. Duan, and T. Akroyd, "Reducing uncertainty in mineral flotation-flotation rate constant prediction for particles in an operating plant ore," *International Journal of Mineral Processing*, vol. 84, no. 1–4, pp. 89–98, 2007.

[46] J. Meng, E. Tabosa, W. Xie, K. Runge, D. Bradshaw, and E. Manlapig, "A review of turbulence measurement techniques for flotation," *Minerals Engineering*, vol. 95, pp. 79–95, 2016.

[47] B. Wang and Y. Peng, "The effect of saline water on mineral flotation—a critical review," *Minerals Engineering*, vol. 66–68, pp. 13–24, 2014.

[48] S. Farrokhpay and M. Zanin, "An investigation into the effect of water quality on froth stability," *Advanced Powder Technology*, vol. 23, no. 4, pp. 493–497, 2012.

[49] H. M. Princen and A. D. Kiss, "Rheology of foams and highly concentrated emulsions," *Journal of Colloid and Interface Science*, vol. 128, no. 1, pp. 176–187, 1989.

[50] L. Vinnett, T. Ledezma, M. Alvarez-Silva, and K. Waters, "Gas holdup estimation in flotation machines using image techniques and superficial gas velocity," *Minerals Engineering*, vol. 96-97, pp. 26–32, 2016.

[51] S. K. Kawatra and A. K. Bakshi, "On-line measurement of viscosity and determination of flow types for mineral suspensions," *International Journal of Mineral Processing*, vol. 47, no. 3-4, pp. 275–283, 1996.

[52] D. T. Fisher, S. A. Clayton, D. V. Boger, and P. J. Scales, "The bucket rheometer for shear stress-shear rate measurement of industrial suspensions," *Journal of Rheology*, vol. 51, no. 5, pp. 821–831, 2007.

[53] J. Kim, H. Lee, and S. Shin, "Advances in the measurement of red blood cell deformability: a brief review," *Journal of Cellular Biotechnology*, vol. 1, no. 1, pp. 63–79, 2015.

[54] R. Buscall, "Letter to the Editor: wall slip in dispersion rheometry," *Journal of Rheology*, vol. 54, no. 6, pp. 1177–1183, 2010.

[55] V. C. Kelessidis, V. Hatzistamou, and R. Maglione, "Wall slip phenomenon assessment of yield stress pseudoplastic fluids in Couette geometry," *Applied Rheology*, vol. 20, pp. 52651–52656, 2010.

[56] I. Kilickaplan, *Effect of Pulp Rheology on Flotation: The Nickel Sulfide Ore with Asbestos Gangue system Master Thesis*, The University of British Columbia, Vancouver, Canada, 2009.

[57] R. Goh, Y.-K. Leong, and B. Lehane, "Bentonite slurries-zeta potential, yield stress, adsorbed additive and time-dependent behaviour," *Rheologica Acta*, vol. 50, no. 1, pp. 29–38, 2010.

[58] A. W. Chow, S. W. Sinton, J. H. Iwamiya, and T. S. Stephens, "Shear-induced particle migration in Couette and parallel-plate viscometers: NMR imaging and stress measurements," *Physics of Fluids*, vol. 6, no. 8, pp. 2561–2576, 1994.

[59] C. F. Ihle, A. Tamburrino, and P. Vivero, "Effect of sample manipulation on the Couette rheometry of copper concentrates," *Powder Technology*, vol. 239, pp. 78–85, 2014.

[60] F. Shi, "Determination of ferrosilicon medium rheology and stability," *Minerals Engineering*, vol. 98, pp. 60–70, 2016.

[61] G. Sarmiento, P. G. Crabbe, D. V. Boger, and P. H. T. Uhlherr, "Measurement of the rheological characteristics of slowly settling flocculated suspensions," *Industrial and Engineering Chemistry Process Design and Development*, vol. 18, no. 4, pp. 746–751, 1979.

[62] B. Klein, J. S. Laskowski, and S. J. Partridge, "A new viscometer for rheological measurements on settling suspensions," *Journal of Rheology*, vol. 39, no. 5, pp. 827–840, 1995.

[63] N. Cruz, Y. Peng, and E. Wightman, "Interactions of clay minerals in copper-gold flotation: part 2—influence of some calcium bearing gangue minerals on the rheological behaviour," *International Journal of Mineral Processing*, vol. 141, pp. 51–60, 2015.

[64] N. Cruz, Y. Peng, E. Wightman, and N. Xu, "The interaction of pH modifiers with kaolinite in copper-gold flotation," *Minerals Engineering*, vol. 84, pp. 27–33, 2015.

[65] J. W. Goodwin and R. W. Hughes, "Linear viscoelasticity I—phenomenological approach," in *Rheology for Chemist—An Introduction*, The Royal Society of Chemistry, Cambridge, UK, 2008.

[66] A. P. Deshpande, J. M. Krishnan, and P. B. S. Kumar, *Rheology of Complex Fluids*, Springer, New York, NY, USA, 2010.

[67] Y. Gao, G. Zhang, M. Wang, and D. Liu, "The critical role of pulp density on flotation separation of nickel-copper sulfide from fine serpentine," *Minerals*, vol. 8, no. 8, pp. 317–326, 2018.

[68] N. Z. P. Shabalala, M. Harris, L. S. Leal Filho, and D. A. Deglon, "Effect of slurry rheology on gas dispersion in a pilot-scale mechanical flotation cell," *Minerals Engineering*, vol. 24, no. 13, pp. 1448–1453, 2011.

[69] P. Patra, T. Bhambhani, D. R. Nagaraj, and P. Somasundaran, "Impact of pulp rheological behavior on selective separation of Ni minerals from fibrous serpentine ores," *Colloids and Surfaces A: Physicochemical and Engineering Aspects*, vol. 411, pp. 24–26, 2012.

[70] B. Pyke, D. Fornasiero, and J. Ralston, "Bubble particle heterocoagulation under turbulent conditions," *Journal of Colloid and Interface Science*, vol. 265, no. 1, pp. 141–151, 2003.

[71] X. You, L. Li, J. Liu, L. Wu, M. He, and X. Lyu, "Investigation of particle collection and flotation kinetics within the Jameson cell downcomer," *Powder Technology*, vol. 310, pp. 221–227, 2017.

[72] T. Kitano, T. Kataoka, and T. Shirota, "An empirical equation of the relative viscosity of polymer melts filled with various inorganic fillers," *Rheologica Acta*, vol. 20, no. 2, pp. 207–209, 1981.

[73] C. T. O'Connor, E. W. Randall, and C. M. Goodall, "Measurement of the effects of physical and chemical variables on bubble size," *International Journal of Mineral Processing*, vol. 28, pp. 139–149, 1990.

[74] D. Xu, I. Ametov, and S. R. Grano, "Quantifying rheological and fine particle attachment contributions to coarse particle recovery in flotation," *Minerals Engineering*, vol. 39, pp. 89–98, 2012.

[75] M. Zhang, Y. Peng, and N. Xu, "The effect of sea water on copper and gold flotation in the presence of bentonite," *Minerals Engineering*, vol. 77, pp. 93–98, 2015.

[76] S. Liu, X. Chen, R. A. Lauten, Y. Peng, and Q. Liu, "Mitigating the negative effects of clay minerals on gold flotation by a lignosulfonate-based biopolymer," *Minerals Engineering*, vol. 126, pp. 9–15, 2018.

[77] X. Chen and Y. Peng, "Managing clay minerals in froth flotation—a critical review," *Mineral Processing and Extractive Metallurgy Review*, vol. 39, no. 2, pp. 1–19, 2018.

[78] V. M. Kirjavainen, "Mathematical model for the entrainment of hydrophilic particles in froth flotation," *International Journal of Mineral Processing*, vol. 35, no. 1-2, pp. 1–11, 1992.

[79] M. Zhang, N. Xu, and Y. Peng, "The entrainment of kaolinite particles in copper and gold flotation using fresh water and sea water," *Powder Technology*, vol. 286, pp. 431–437, 2015.

[80] H. A. Barnes and Q. D. Nguyen, "Rotating vane rheometry—a review," *Journal of Non-newtonian Fluid Mechanics*, vol. 98, no. 1, pp. 1–14, 2001.

[81] G. Ovarlez, F. Mahaut, F. Bertrand, and X. Chateau, "Flows and heterogeneities with a vane tool: magnetic resonance imaging measurements," *Journal of Rheology*, vol. 55, no. 2, pp. 197–223, 2011.

[82] G. Ovarlez, S. Cohen-Addad, K. Krishan, J. Goyon, and P. Coussot, "On the existence of a simple yield stress fluid behavior," *Journal of Non-newtonian Fluid Mechanics*, vol. 193, pp. 68–79, 2013.

[83] S. Cohen-Addad and R. Höhler, "Rheology of foams and highly concentrated emulsions," *Current Opinion in Colloid and Interface Science*, vol. 19, no. 6, pp. 536–548, 2014.

[84] B. Herzhaft, "Rheology of aqueous foams: a literature review of some experimental works," *Oil and Gas Science and Technology*, vol. 54, no. 5, pp. 587–596, 1999.

[85] S. J. Neethling and J. J. Cilliers, "Modelling flotation froths," *International Journal of Mineral Processing*, vol. 72, no. 1–4, pp. 267–287, 2003.

[86] C. Li, S. Farrokhpay, F. Shi, and K. Runge, "A novel approach to measure froth rheology in flotation," *Minerals Engineering*, vol. 71, pp. 89–96, 2015.

[87] C. Li, K. Runge, F. Shi, and S. Farrokhpay, "Effect of flotation froth properties on froth rheology," *Powder Technology*, vol. 294, pp. 55–65, 2016.

[88] C. Li, K. Runge, F. Shi, and S. Farrokhpay, "Effect of flotation conditions on froth rheology," *Powder Technology*, vol. 340, pp. 537–542, 2018.

[89] C. Li, S. Farrokhpay, K. Runge, and F. Shi, "Determining the significance of flotation variables on froth rheology using a central composite rotatable design," *Powder Technology*, vol. 287, pp. 216–225, 2016.

[90] C. Li, K. Runge, F. Shi, and S. Farrokhpay, "Effect of froth rheology on froth and flotation performance," *Minerals Engineering*, vol. 115, pp. 4–12, 2018.

[91] L. Wang, *Entrainment of fine particles in froth flotation*, Ph.D. thesis, The University of Queensland, Brisbane, Australia, 2017.

[92] Y. S. Cho and J. S. Laskowski, "Effect of flotation frothers on bubble size and foam stability," *International Journal of Mineral Processing*, vol. 64, no. 2-3, pp. 69–80, 2002.

[93] F. Azgomi, C. O. Gomez, and J. A. Finch, "Characterizing frothers using gas hold-up," *Canadian Metallurgical Quarterly*, vol. 46, no. 3, pp. 237–242, 2007.

[94] X. Zhou, A. Jordens, F. Cappuccitti, J. A. Finch, and K. E. Waters, "Gas dispersion properties of collector/frother blends," *Minerals Engineering*, vol. 96-97, pp. 20–25, 2016.

[95] L. Wang, Y. Peng, and K. Runge, "The mechanism responsible for the effect of frothers on the degree of entrainment in laboratory batch flotation," *Minerals Engineering*, vol. 100, pp. 124–131, 2017.

[96] B. M. Moudgil, "Correlation between froth viscosity and flotation efficiency," *Mining, Metallurgy and Exploration*, vol. 10, no. 2, pp. 100-101, 1993.

[97] Q. D. Nguyen and D. V. Boger, "Yield stress measurement for concentrated suspensions," *Journal of Rheology*, vol. 27, pp. 321–349, 1983.

[98] N. Zhang, X. Chen, T. Nicholson, and Y. Peng, "The effect of froth on the dewatering of coals—an oscillatory rheology study," *Fuel*, vol. 222, pp. 362–369, 2018.

[99] Y. Wang, R. A. Lauten, and Y. Peng, "The effect of biopolymer dispersants on copper flotation in the presence of kaolinite," *Minerals Engineering*, vol. 96-97, pp. 123–129, 2016.

[100] D. R. Seaman, R. A. Lauten, G. Kluck, and N. Stoitis, "Usage of anionic dispersants to reduce the impact of clay particles in flotation of copper and gold at the Telfer mine," in *Proceedings of the 11th Mill Operators' Conference 2012*, The Australasian Institute of Mining and Metallurgy, Hobart, Tasmania, October 2012.

[101] R. Wei, Y. Peng, and D. Seaman, "The interaction of lignosulfonate dispersants and grinding media in copper-gold flotation from a high clay ore," *Minerals Engineering*, vol. 50-51, pp. 93–98, 2013.

[102] D. J. Bradshaw and C. T. Connor, "Measurement of the subprocess of bubble loadin in flotation," *Minerals Engineering*, vol. 9, no. 4, pp. 443–448, 1996.